

*A UBV Study of the Field  
of NGC 7790*

© *John Michael Takala*

*A thesis submitted in partial fulfillment of the  
requirements for the degree of  
Master of Science*

Saint Mary's University  
Halifax, Nova Scotia  
August 1988

© John M. Takala 1988

Permission has been granted to the National Library of Canada to microfilm this thesis and to lend or sell copies of the film.

The author (copyright owner) has reserved other publication rights, and neither the thesis nor extensive extracts from it may be printed or otherwise reproduced without his/her written permission.

L'autorisation a été accordée à la Bibliothèque nationale du Canada de microfilmer cette thèse et de prêter ou de vendre des exemplaires du film.

L'auteur (titulaire du droit d'auteur) se réserve les autres droits de publication; ni la thèse ni de longs extraits de celle-ci ne doivent être imprimés ou autrement reproduits sans son autorisation écrite.

ISBN 0-315-48187-0

## Table of Contents

Signature Page .....	i
Acknowledgements .....	ii
Abstract .....	iii
List of Figures .....	iv
List of Tables .....	vi
Chapter One	
Introduction .....	1
Chapter Two      Observational Data and Their Reduction	
Data .....	10
Reduction Process .....	13
Secondary Images .....	26
Calibration Results .....	34
Chapter Three      Analysis of Results	
Dereddening .....	45
ZAMS Fitting .....	73
Proper Motion Study .....	87
Chapter Four      Discussion and Conclusions	
Discussion .....	89
Age of Cepheids .....	95
Conclusions .....	98
References .....	102
Curriculum Vitae .....	106

Signatures of the Examining Committee

*George F. Mitchell*

---

Dr. G.F. Mitchell  
Professor of Astronomy  
St. Mary's University

*David G. Turner*

---

Dr. D.G. Turner (Thesis Supervisor)  
Associate Professor of Astronomy  
St. Mary's University

*Gary A. Welch*

---

Dr. G.A. Welch  
Associate Professor of Astronomy  
St. Mary's University

*Mario Pedreros*

---

Dr. M. Pedreros  
Department of Astronomy  
St. Mary's University

## Acknowledgements

I would like to thank each member of the Astronomy Department at Saint Mary's for helping to provide a challenging and stimulating atmosphere, which made the last two years a rewarding experience. My thesis supervisor, Dr. Turner, gave many insightful suggestions which added to my understanding of my thesis topic. I also benefited on many occasions from the advice, assistance and words of encouragement offered by Cameron Reed, Mario Pedreros and Randall Brooks.

I would like to thank Dr. Kruse for providing access to T<sub>E</sub>X which greatly aided in the production of an aesthetically pleasing document. Dave and Steve get the nod for their general advice on T<sub>E</sub>X and some very useful macros.

My fellow classmates deserve credit for sharing their opinions, thoughts and ideas. Bob's carefully chosen words, Ken's less carefully chosen words, and debates with Dave all helped make my stay at Saint Mary's an enjoyable experience. I also owe a debt of gratitude to my new found friends from the Maritimes for giving me a new home.

Finally I would like to thank my parents for nurturing my early interest in astronomy. My father deserves special acknowledgement for taking me to many late and often cold observing sessions at various RASC events. The support of my family has been and continues to be greatly appreciated.

## Abstract

### A UBV Study of the Field of NGC 7790

John M. Takala

August 1988

This thesis presents a UBV study of the field of the open cluster NGC 7790, which has three Cepheids within its boundaries. Photographic plates taken at CFHT were measured on an Astromechanics Iris Photometer. The distance modulus of the cluster was found to be  $12.25 \pm 0.10$ . A trend in reddening with spectral type was detected;  $\langle E_{B-V} \rangle = 0.40 \pm 0.06$  s.d. for stars with  $(B - V)_0 > 0.10$  and  $\langle E_{B-V} \rangle = 0.57 \pm 0.07$  s.d. for stars with  $(B - V)_0 < 0.10$ . The implied luminosities of the Cepheids in NGC 7790 from the calculated cluster distance are in agreement with recent calibrations of the period-luminosity and period-luminosity-colour relations.

## List of Figures

Figure 1	Finder Chart for NGC 7790 .....	12
Figures 2a-g	Plate Calibration Relations .....	19
Figure 3	Microdensitometer Tracing .....	30
Figures 4a-c	Secondary Images .....	31
Figure 5	Plate Comparison Plot .....	36
Figures 6a-b	U Plate Comparison Plots .....	37
Figures 7a-b	B Plate Comparison Plots .....	39
Figure 8	V Plate Comparison Plot .....	41
Figures 9a-c	Colour Transformation Plots .....	42
Figure 10	Two Colour Plot .....	54
Figure 11	Colour Magnitude Diagram .....	55
Figure 12	Colour Magnitude Diagram Large Reddening Solution .....	56
Figure 13	Colour Magnitude Diagram Small Reddening Solution .....	57
Figure 14	Intrinsic Colour vs Reddening Plot .....	58
Figures 15a-b	Colour Magnitude Diagrams from Pedreros <i>et al.</i> (1984) .....	63
Figure 16a	Two Colour Diagram from Mateo and Madore (1988) .....	64
Figure 16b	Two Colour Diagram this study .....	65
Figure 17	Field Reddening Chart for NGC 7790 .....	67

## List of Figures

Figures 18a-b	Variable Extinction Analysis Plots.....	71
Figure 19	Intrinsic Colour Magnitude Diagram.....	83
Figure 20	Intrinsic Colour Magnitude Diagram with ZAMS Relation.....	84
Figure 21	Distance Moduli versus Intrinsic Colour.....	86
Figure 22	Proper Motion Plot.....	88
Figure 23	Period-Luminosity Relation.....	96
Figure 24	Intrinsic Colour Magnitude Relation.....	97

## List of Tables

Table I	Summary of Distance and Reddening Determinations for NGC 7790 .....	8
Table II	Photoelectric Standards of NGC 7790 .....	11
Table III	Stars Rejected from Calibration Relations .....	18
Table IV	Parameters for Colour Equations .....	44
Table V	UBV Data and Reddening Determinations .....	48
Table VI	$(V - M_V) - E_{B-V}$ Data .....	70
Table VII	$R_V$ Determinations .....	72
Table VIII	Intrinsic Magnitudes, Colours and Cluster Membership Information .....	76
Table IX	Reddening Determinations of CF Cas .....	92
Table X	Cepheid Data .....	94
Table XI	$M_V$ Determinations for CF Cas, CE Cas a and CE Cas b .....	94

## Chapter One

### Introduction

A fundamental problem astronomers grapple with is the distance scale of the universe. Astronomers rely on the ability to accurately determine the distances of nearby objects to calculate the distances to progressively more remote ones. Objects that are used to calibrate the distance scale in this fashion are often called "standard candles." Cepheid variables constitute a class of objects which make excellent standard candles. They are bright variable stars that obey a relationship between their luminosities and periods of variability. Thus, by observing the period and magnitude of a Cepheid its distance can be inferred. A full review of the work done on Cepheids would not be appropriate for a thesis. However, a brief review of their history will be given. I would direct the reader to an excellent review of the subject by Fernie (1969) for a much more complete history.

The history of Cepheids dates back to the turn of the century. Miss Henrietta Leavitt catalogued 1777 variable stars in the Small Magellanic Cloud (SMC) between 1893 and 1906. She determined periods for 16 of these variables and noticed that the brightest ones had the longest periods. Although the distance to the SMC had not been determined, it was obvious that these variables were members of the SMC, and thus at a common distance. These stars interested her enough that she had expanded the list of Cepheids to 25 by 1912. In a paper with

Pickering (1912) she noted that the "apparent magnitude decreases almost linearly with the logarithm of their periods." The years subsequent to this statement have seen much work devoted to finding the constants for this particular relationship, now known as the period-luminosity, or PL relation.

One of the first calibrations of the PL relation was done by Hertzsprung (1913). He applied a statistical parallax analysis of thirteen galactic Cepheids to determine the zero-point, adopting the slope determined by Leavitt from SMC Cepheids. Hertzsprung, like other investigators of the time, did not incorporate the effects of interstellar absorption into his calculations; definite proof for the existence of interstellar absorption was not established until 1930. This factor affected the first thirty years of work on Cepheids.

Some of the early errors in the calibration of the PL relation persisted for many years. The most famous example of this can be found in the work of Shapley (1918). He used the same data set of population I Cepheids as Hertzsprung and arrived at a value for the zero-point that is  $\sim 1^m5$  fainter than the modern value. This discrepancy in the zero-point, present in this early study, persisted for over thirty years. The cause of this discrepancy in Shapley's study was the result of several factors, namely (1) the neglect of interstellar absorption, (2) poor and insufficient proper motion data, and (3) the unknown effects of galactic rotation on proper motions (Ferne 1969). This last effect became more important in later

work as fainter and more distant objects were included in such calibrations.

Great confidence was placed in Shapley's zero-point value as a consequence of several unfortunate coincidences. The calibrating Cepheids in Shapley's initial study were all Population I objects, and he noted that long period Cepheids in the star clusters  $\omega$  Centauri, M5, and M3 (now recognized as Population II Cepheids), plus the RR Lyrae variables obeyed a similar relationship to the Cepheids in the SMC. Shapley therefore extended his period-luminosity relation to include these Population II objects. A  $1^m4$  error in the original statistical parallax study made this luminosity scale systematically too faint, and was almost exactly compensated for by the fact that Population II Cepheids are  $\sim 1^m5$  fainter than Population I Cepheids of a similar period. Thus, the absolute magnitudes of RR Lyrae type variables were predicted to be approximately  $\langle M_v \rangle \simeq 0.0$ , which is close to the actual value. Subsequent work on field RR Lyraes confirmed the prediction of  $\langle M_v \rangle \simeq 0.0$  for these stars, and served to increase confidence in Shapley's determination of the zero-point for the PL relation, despite its inherent error.

During the next few decades a variety of astronomers published results that generally confirmed the work of Shapley. A common error in the work of this era was the neglect of the effects of interstellar absorption, the existence of which became firmly established through the work of Trumpler (1930). Although it was some years before the exact significance of interstellar absorption for the absolute

magnitude determination of Cepheids was realized, some researchers were quick to point out the need for a revision of the zero-point. Lundemark (1931) noted that Shapley's zero-point should be made brighter by  $1^m2$  if the galactic absorption rates of Bottlinger and Schneller (1930) were valid. However, he concluded that, since evidence had been published arguing for a fainter zero-point, Shapley was essentially correct. Kukarkin (1937, 1949) appears to be the first to have demonstrated that classical Cepheids and RR Lyraes do not lie on the same relationship. Furthermore, he stated that the zero-point of Cepheids in external galaxies was  $0^m5$  brighter than Shapley's value. Mineur (1944) showed that the value of the zero-point determined by statistical parallax is strongly dependent on interstellar absorption. He concluded that the zero-point should be decreased by  $0^m75$ . These and other arguments that called for a brighter zero-point were not generally accepted until new observational evidence became available.

The new observational evidence which confirmed the need for a zero-point revision of the PL relation came soon after the commissioning of the 5-m telescope at the Mt. Palomar Observatory. The extension of existing photographic limiting magnitudes resulting from the large aperture of this telescope made it possible to search for RR Lyrae variables in M31. The RR Lyraes were found, but were  $1^m5$  fainter than expected. This led Baade (1952) to conclude that the zero-point for the PL relation must be  $1^m5$  brighter. Baade's claim was soon confirmed by other researchers. Thackeray (Fernie 1969) reported at the same time that three RR

Lyraes had been found in the SMC at  $m_{pg} = 19.0$ , 1<sup>m5</sup> fainter than predicted by Shapley's relation. This 1<sup>m5</sup> change in the zero-point resulted in an immediate doubling of the estimated size of the universe. Revisions to the period-luminosity relationship have continued to the present day, but none as large or dramatic as that announced by Baade in 1952.

Since the 1950's attempts have been made to use Cepheids in open clusters for a more strongly-defined zero-point calibration of the PL relation for galactic Cepheids. Several people appear to have noted the potential membership of Cepheids in galactic clusters virtually simultaneously. Kholopov (1956) listed 16 Cepheids spatially coincident with 13 open clusters. However, it is Irwin (1955) who is attributed with the modern-day discovery of two Cepheids associated with galactic clusters. Doig (1925, 1926) was previously aware of the same Cepheid cluster associations noted by Irwin, but distance determinations for clusters were very uncertain at that time so these associations were not recognized to be of any importance. By the 1950's the situation had improved due to the development of the Johnson UBV system. The accurate determination of open cluster distances and reddenings available with UBV photometry, and the recognition that some Cepheids were cluster members, gave astronomers a reliable method for calibrating the period-luminosity relation.

The importance of independent distance determinations for Cepheids led

to several immediate searches that revealed a number of Cepheids spatially coincident with open clusters. The work of determining reliable distances to those clusters containing Cepheids has continued to the present day. Caldwell and Coulson (1987) list 27 possible cluster or association Cepheids, although the cluster membership of several of these seems doubtful (Caldwell and Coulson 1987). Systematic studies of these and other Cepheids and their associated clusters have been initiated recently in an attempt to obtain more accurate distances and reddenings (Walker 1985, Turner 1986) for these calibrators.

The open cluster NGC 7790 is very important for calibrating the distance scale of Cepheids. Olin Eggen was aware in 1952 that three Cepheids, CF Cas, CE Cas a and CE Cas b, could be physically associated with the cluster (Sandage 1958), which has since been verified by several studies. The cluster is located close to the plane of the Milky Way in the constellation of Cassiopeia ( $l = 116^{\circ}6$ ,  $b = -1^{\circ}0$ ;  $\alpha_{1950.0} = 23^{\text{h}}55^{\text{m}}9$ ,  $\delta_{1950.0} = +60^{\circ}56'$ ). Ruprecht (1966) classifies NGC 7790 on the Trumpler system as III 2 p, which corresponds to a cluster with a uniform distribution of stars, a medium range of brightness and less than 50 members. More recent studies of the cluster (Pedreros *et al.* 1984, Mateo and Madore 1988) indicate that NGC 7790 has  $> 100$  members (i.e. a rich cluster), and recent classifications (Janes and Adler 1982, Turner 1985) denote this fact. Barbaro *et al.* (1969) quote a turn-off point age of  $7.0 \times 10^7$  yr, which is typical of most clusters containing Cepheids. The presence of three Cepheids within the

boundaries of NGC 7790 has therefore resulted in several studies of the cluster.

The first detailed study of NGC 7790 as a calibrating cluster was a photometric investigation by Sandage (1958), in which a combination of photoelectric and photographic observations were obtained in the standard Johnson UBV passbands. Sandage found the cluster distance modulus to be  $12.80 \pm 0.15$  with a reddening of  $E_{B-V} = 0.52 \pm 0.04$ . This particular data set has been reworked frequently by a number of researchers, with very similar results. However, recent observations (Turner and Forbes, unpublished) indicate that Sandage's photoelectric observations contain systematic errors, a not uncommon feature of the equipment he used. Turner and Forbes (unpublished) have found Sandage's data to be too bright and blue by the following amounts,  $\Delta V = +0^m03$ ,  $\Delta(B - V) = +0^m04$  and  $\Delta(U - B) = +0^m06$ . Sandage's analysis of the cluster relied in part on a spectroscopic study of seven stars in the region by Kraft (1958). Regrettably, this has been the only published spectroscopic study of NGC 7790 to date, and the photoelectric standards of Sandage's study have not been systematically remeasured until recently.

Recent reexaminations of NGC 7790 have produced somewhat conflicting results. These are summarized in Table I, where the spread of  $\sim 1^m$  in the cluster distance modulus should be particularly noted. For a complete listing of work done on NGC 7790 prior to 1970 see Alter *et al.* (1970).

Table I

$V_0 - M_V$	$E_{\beta-v}$	Technique	Reference
$12.80 \pm 0.15$	0.52	ZAMS fit	Sandage 1958
$13.10 \pm 0.13$	0.49	MK Spectral Analysis	Kraft 1958
$11.98 \pm 0.10$	0.55	$H\beta$ photometry *	Schmidt 1981
$12.15 \pm 0.10$	—	$H\beta$ photometry *	Balona and Shobbrook (1984)
$12.30 \pm 0.20$	0.64	ZAMS fit	Pedreras <i>et al.</i> 1984
$12.05 \pm 0.13$	0.51	$H\beta$ photometry *	Schmidt 1984
$12.38 \pm 0.19$	0.56	ZAMS fit	Mateo and Madore 1988
$12.25 \pm 0.10$	0.57	ZAMS fit	this study

\* Strömgren and  $H\beta$  photometry

Presently the PL and PLC relations are calibrated with  $\sim 27$  Cepheids in galactic clusters or associations. Since NGC 7790 contains three of these Cepheids, the accurate determination of its distance is very important. There are reasons to be concerned with some of the recent results for NGC 7790. First, the original photoelectric photometry of Sandage (1958) is now known to contain systematic errors. New photoelectric observations were not available at the time of the study by Pedreras *et al.* (1984), although they were aware of the problems with Sandage's data and did apply corrections to his results. They estimated the corrections to be  $\Delta V = 0^m00$ ,  $\Delta(B - V) = +0^m025$ , and  $\Delta(U - B) = +0^m075$ . These corrections are in the same sense as those found by Turner and Forbes (unpublished), but differ quantitatively. The Strömgren and  $H\beta$  photometry results are based on only 16 stars in the field of NGC 7790 measured by Schmidt (1981). Furthermore, Turner (1986) has raised concerns that the  $H\beta$  calibration neglects rotation and can result

in biased estimates of absolute magnitude. Despite the interest generated in NGC 7790 by the Cepheids associated with it, the distance to the cluster is still not firmly established.

The availability of high quality plates taken at CFHT and new photoelectric observations of NGC 7790, along with the need for a better distance determination for the cluster, prompted this present study. An attempt was made by Turner (private communication) to reanalyze the cluster using the new photoelectric data and the original iris measurements of Pedreros *et al.* (1984). However, problems were encountered with the calibration of these measures. Since a reliable methodology has been established for measuring and reducing photographic plate material with the Saint Mary's iris photometer, the decision was made to simply remeasure the plates. The combination of improved photoelectric data and accurate photographic photometry was believed to be capable of generating reliable new estimates for the distance and reddening of stars in NGC 7790.

## Chapter Two

### Data

The plates used to study NGC 7790 were obtained with the CFHT by Barry Madore in 1981. Wide band filters and photographic emulsions were used to reproduce the Johnston UBV system. Three plates in each passband were taken. Ila-0 emulsions were used with plates taken through UG1 and GG395 filters, corresponding to U and B passbands respectively. The visual plates were taken on Ila-D emulsions with a GG495 filter. The plates were taken on two separate nights in seeings of 1" and  $\approx 2 - 3''$  respectively. A Racine wedge was used to produce secondary images on all the plates, nominally about 4.6 magnitudes fainter than the primaries.

Standardization of the photographic observations requires the use of photoelectrically observed stars in the same field. The values quoted here are a homogeneous set constructed from the observations of Sandage (1958), Christian *et al.* (1985), Schmidt (1981, transformed to the UBV system), and Turner and Forbes (unpublished), all adjusted to the Johnson UBV system using new UBV photoelectric observations by Turner and Forbes (unpublished). These data are summarized in Table II. The same identification scheme employed by Pedreros *et al.* (1984) was used for this study (see Fig. 1).

Table II

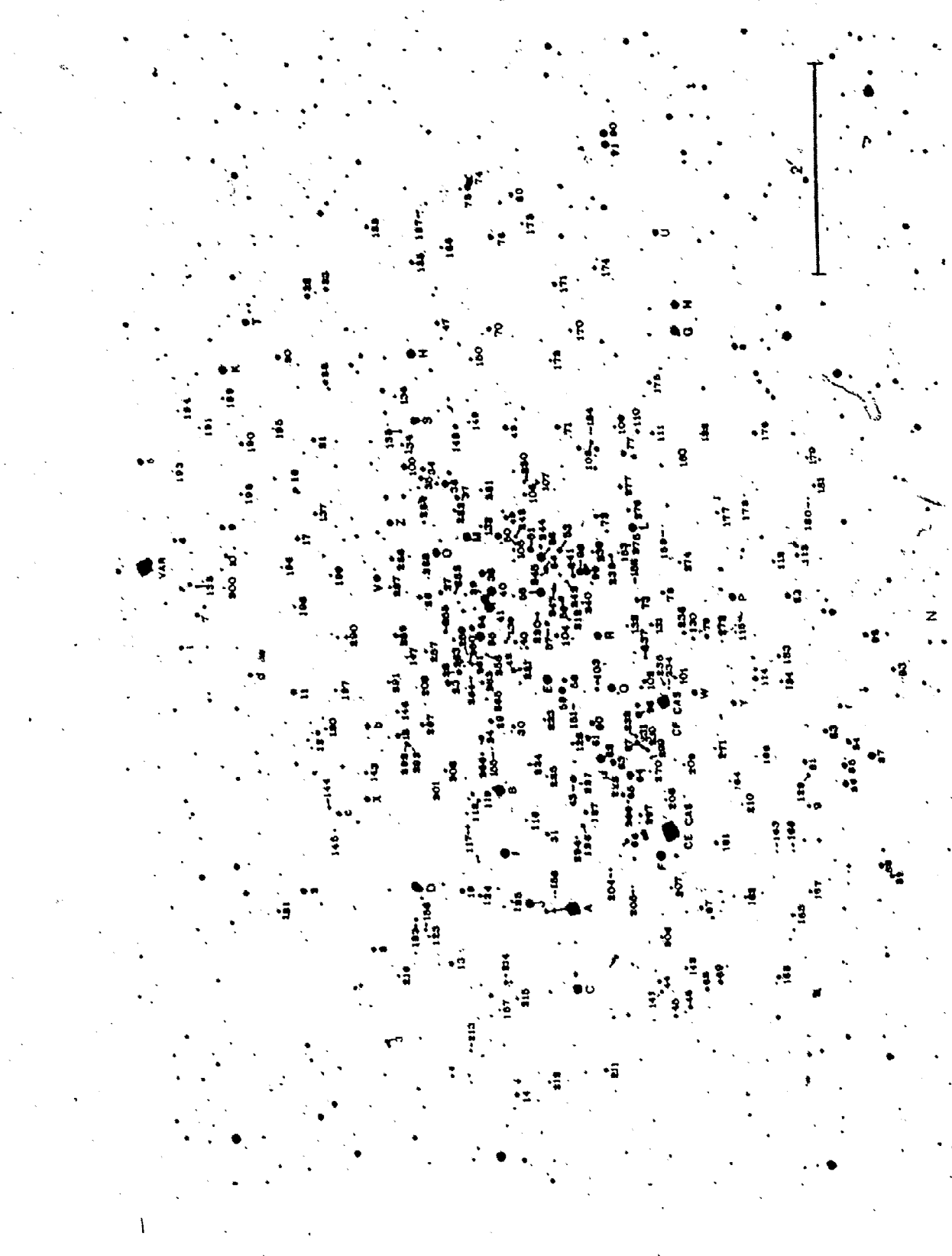
Star	V	B - V	U - B	n <sub>V</sub>	n <sub>B-V</sub>	n <sub>U-B</sub>
A	11.11	0.28	-0.53	40	49	49
B	12.18	0.43	-0.02	5	8	8
C	12.50	0.58	+0.27	9	9	9
D	12.63	0.46	+0.32	4	7	7
E	12.79	0.43	-0.04	3	6	6
F	12.87	2.00	+2.06 :	3	3	2
G	13.18	0.57	+0.38	3	3	3
H	13.19	0.53	+0.35	3	3	3
I	13.22	1.25	+0.85 :	2	2	2
J	13.24	0.56	+0.38	4	4	4
K	13.23	1.53	—	6	6	0
L	13.30	0.73	+0.16	3	3	3
M	13.37	0.39	-0.07	2	5	5
N	13.51	0.47	+0.07	2	6	6
O	13.52 :	0.43	-0.01	2	6	6
P	13.63	0.83	+0.17	3	3	3
Q	13.80 :	0.41	+0.02	2	2	2
R	14.17	0.41	+0.02	2	2	2
S	14.29	0.53	-0.23	5	5	2
T	14.33	0.72	—	1	1	0
U	14.51	0.60	+0.40	1	1	1
V	14.54	0.49	+0.07	2	2	2
W	14.59	1.49	+1.11	4	4	1
X	14.65	0.46	+0.12	2	2	2
Y	14.75	1.39	—	3	3	0
Z	14.79	0.48 :	+0.05 :	2	2	2
a	14.96	0.77	—	1	1	0
b	15.21	0.52	+0.00	1	1	1
c	15.32	0.86	—	1	1	0
d	15.68	0.95	—	3	3	0
e	15.79	0.55	—	1	1	0
f	16.01	0.84	—	1	1	0
g	16.25	0.87	—	1	1	0
9	15.41	1.66	—	5	5	0
10	16.03	0.72	—	5	5	0
16	15.33	0.62	—	4	4	0
17	16.02	0.55	—	4	4	0
20	15.77	1.00	—	3	3	0
21	15.98	0.71	—	4	4	0
25	15.44	0.68	—	3	3	0
100	14.39	0.44	—	3	3	0

Figure 1

Finder chart for the field of NGC 7790 adopted from Pedreros *et al.* (1984). See star A for orientation of secondary images

A

6



## Reduction Process

The plates were measured with the iris photometer system at Saint Mary's University. The system is comprised of an Astro Mechanics Cuffey-type Iris Astrophotometer which is controlled by an IBM PC. Details of the system can be found in an article by Reed *et al.* (1986). Two senior physics students made the measurements, and each plate was measured at least twice. The standards were measured twice each measuring session, at the beginning and end of each session. Several plates were measured by both students and the author to ensure that no systematic differences arising from the measuring technique were present.

The ideal type of broadband observations for a study of this nature would be photoelectric. However, it is not practical to obtain such data for clusters containing several hundred measurable stars. Photographic photometry offers a reasonable compromise between high accuracy and number of observations, and eliminates some of the problems with U-band photometry arising from CCD imaging. Two procedural techniques were used in the measuring of the photographic plates to get accurate results. One of the limits to the accuracy of photographic photometry is the consistency with which the star images can be centred. This limitation was minimized by null-meter centring. This technique involves centring the star and taking a null measurement. Then, the position of the star is fine-tuned to get a minimum reading on the null meter. A new measurement is then

taken of the star, and the process repeated if necessary. This procedure ensures the stars are centred in a consistent fashion with respect to the grain noise. It was found that usually only one adjustment was needed to find the minimum null meter centring position. It has been found that use of a low wedge setting reduces the noise in the calibration relations (Turner, private communication). A low wedge setting results in a relatively wide annulus around each star, but sampling significant amounts of plate grain tends to average out any small plate defects. It will be shown later that such measures also have a high level of internal accuracy.

The nature of the calibration curve is of great importance to this work. Schaeffer (1981) published a study examining the validity of different photographic calibration curves for star images with different profiles. He confirmed earlier predictions that for images with saturated Gaussian profiles (i.e. well exposed images) a linear relationship of the form  $I^2$  vs mag., where  $I$  is the iris reading and mag. the magnitude, is valid. This relationship has been found to work quite well for the iris photometry done at Saint Mary's.

The linear relationship between magnitude and the square of the iris reading is not without complications. Often there is an abrupt change in slope in the relationship, i.e. a kink in the straight line fit. It has been found that sometimes the change in slope occurs less abruptly, with a 1.0 - 1.5 magnitude interval between two longer linear segments. The effect is essentially two long straight lines

connected by a short one, each with a different slope and intercept. At this point some readers may question the validity of imposing straight lines on what essentially looks like a curve, when the relationship (which mimics the characteristic curve for the emulsion) may be better represented by a higher order polynomial.

The system at SMU has produced measures that have been successfully reduced using both second order and higher order polynomials. Reed (private communication) has used polynomials up to fifth order to fit calibration curves to iris photometer data. A program developed by Reed that fits such polynomials to iris measures was tested with the present data. These solutions were compared to linear  $I^2$  vs mag. fits. On an empirical basis both methods produced fits of comparable quality as measured by the rms errors. Although a single relationship describing the calibration curve may be more appealing than two (or three), there are other considerations.

The nature of the secondary images were an important factor in deciding upon the type of fit to be used. Only one secondary image overlapped the magnitude range of the calibration relations. This left the value of the magnitude shift for the Racine prism somewhat uncertain. The utility of a linear fit became apparent when the secondary images were considered in detail. It was easier to determine if the secondaries were obeying the same calibration relation using a linear fit than using a polynomial fit. Magnitude-dependent effects tend to be

hidden in a polynomial fit. Also, when the secondary images were not usable a linear fit could be extrapolated with some care, whereas this was not possible with a polynomial fit. For these reasons linear calibration relations were adopted for the final reductions.

The calibration relations were determined by least squares, where it was assumed the all errors were in the iris readings. First, a plot was made of  $I^2/10^6$  vs magnitude. A visual inspection of the plot revealed the magnitudes at which any kinks existed and a computer program (written by the author) was used to carry out the reduction process. The number of kinks and their magnitude limits had to be supplied to the program. The program would then calculate the fits for the appropriate magnitude intervals. The program would display all the fit information including the rms error and the residuals of each point used in the fit. Any points with residuals greater than 2.5 sigma were discarded. A new solution would then be generated and the residuals checked to see if any other points had unacceptable errors. This iterative procedure would be continued until an acceptable fit was obtained. Typically two to four standards out of ~ 33 were rejected with this procedure.

The procedure outlined above was initially used with a least squares fit that gave equal weight to all the points. The average values calculated from the fits for the visual plates were found to have large standard deviations. The fits were

redone weighing the points according to the number of photoelectric observations, using a weighted least squares fit algorithm adapted from Bevington (1969). The weighted fits revealed that most of the scatter was caused by one specific visual plate. The plot of  $I^2$  vs mag for this plate had the largest scatter. The plate itself appeared to have suffered some light leakage and faint streaking was visible across the emulsion. Since background readings would not be constant in this circumstance (a necessity for the reductions), this plate was rejected from the analysis. A blue plate was rejected from the analysis due to a large crack that caused focus problems across it.

The procedures outlined here generally produced consistent results. Each plate was measured during two independent sessions, and during each session the standards were measured twice. Thus, a total of four calibration relations were produced for each plate. Each calibration relation was used to calculate the magnitudes of the program stars measured in that session. Thus, the two independent program star measuring sessions generated four magnitude estimates of each star. Average plate magnitudes for each colour (U, B, and V) were calculated by averaging all four magnitude determinations. It was noticed that some stars consistently had large residuals and these were therefore rejected from the calibration relations. Some individual plates had one or two stars that were rejected. The reason for rejection could occasionally be attributed to a plate defect, but sometimes the reason was undetermined. Table III lists stars that were rejected from the various

colour calibrations. A cursory glance at the plates immediately reveals star D to be double! Stars B and G also have optical companions visible on the good seeing plates. Other stars were rejected due to the small number of photoelectric observations or to possible optical variability.

Table III

Star	Colour	Comments
B	UBV	optical double
D	UBV	optical double
F	UBV	very red, variable?
G	UBV	optical double
I	V	$n_V = 2$
U	U	$n_U = 1$
Z	U	uncertain U measurement
b	U	$n_U = 1$

A calibration relation for one measuring session of each plate, a plot of the residuals for the fit, and the fit parameters are included on the following pages (Figs. 2a-g). The differences between the calibration relations for the same plate were found to be insignificant. Thus, the plots represent typical results for each plate.

Figure 2a

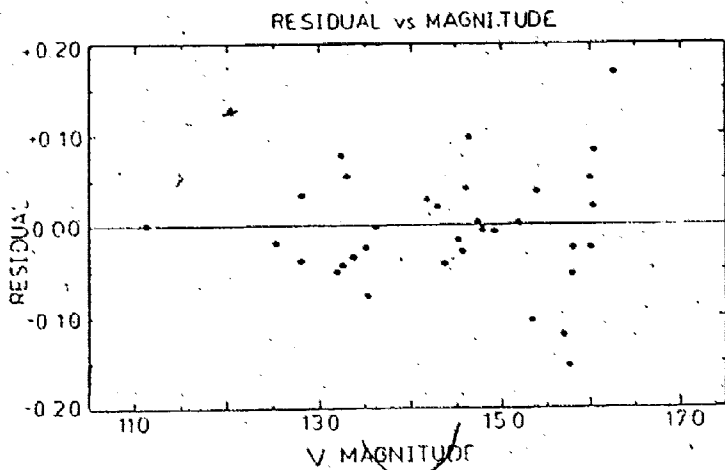
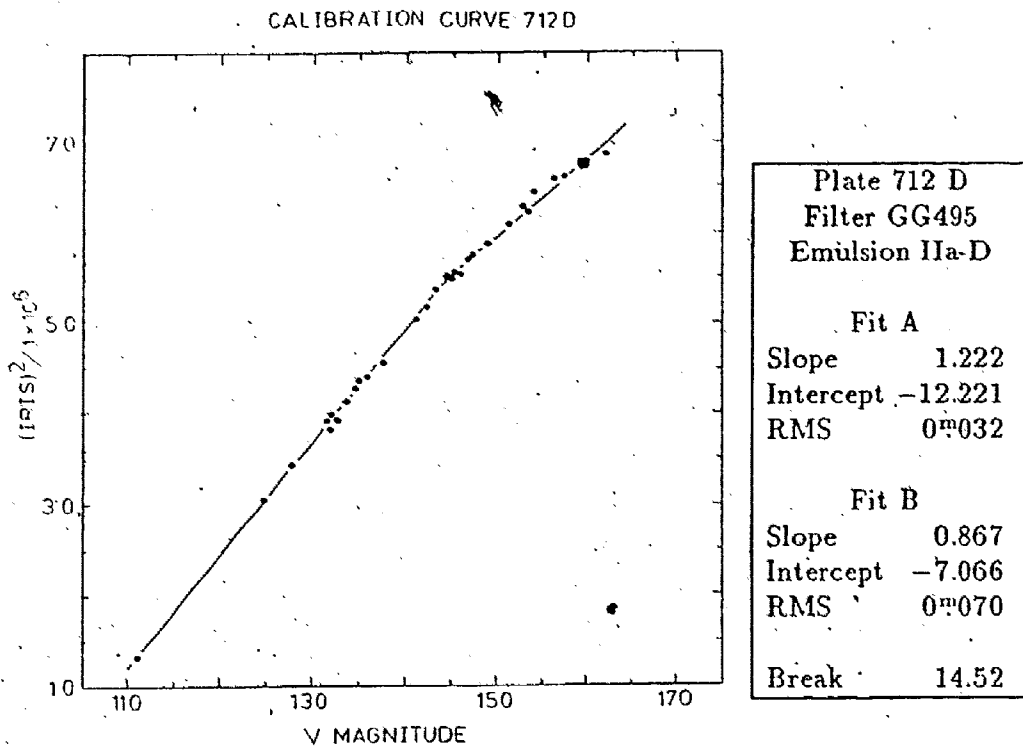


Figure 2b

CALIBRATION CURVE 734 B

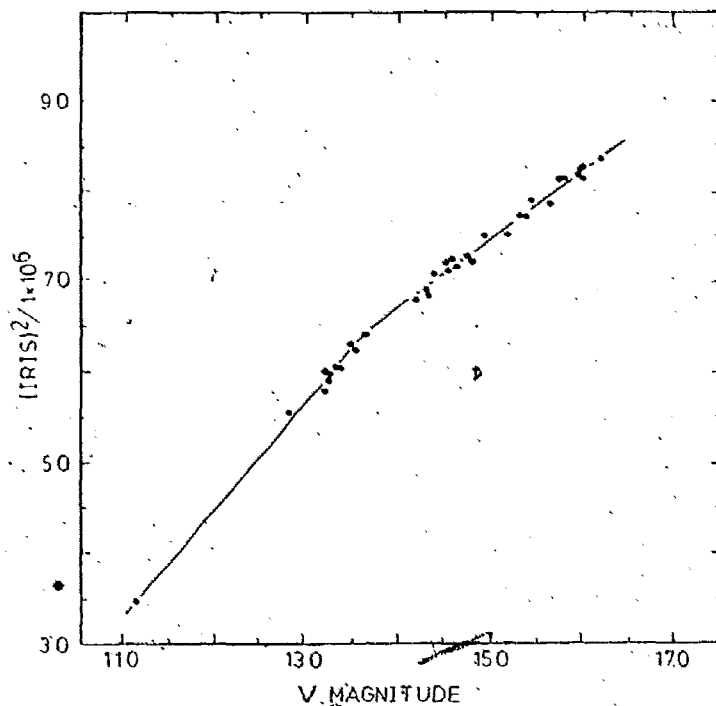


Plate 734 B	
Filter GG495	
Emulsion IIa-D	
Fit A	
Slope	1.177
Intercept	-9.631
RMS	0 <sup>m</sup> 033
Fit B	
Slope	0.742
Intercept	-3.688
RMS	0 <sup>m</sup> 097
Break	13.67

RESIDUAL vs MAGNITUDE

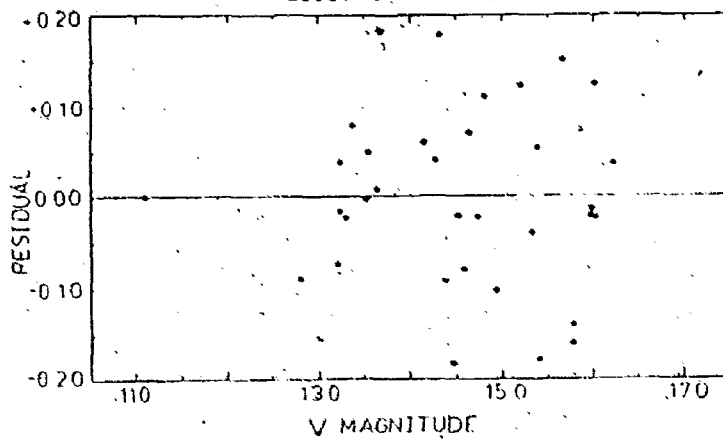


Figure 2c

CALIBRATION CURVE 737A

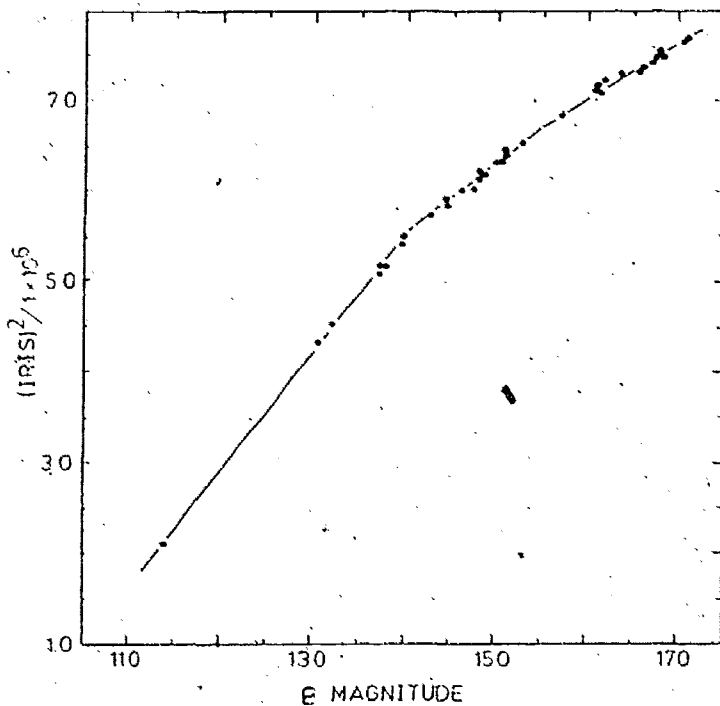


Plate 737 A	
Filter GG395	
Emulsion IIA-O	
Fit A	
Slope	1.294
Intercept	-12.609
RMS	0 <sup>m</sup> 020
Fit B	
Slope	0.791
Intercept	-5.569
RMS	0 <sup>m</sup> 054
Fit C	
Slope	0.594
Intercept	-2.4627
RMS	0 <sup>m</sup> 082
Break 1	14.00
Break 2	15.79

RESIDUAL vs MAGNITUDE

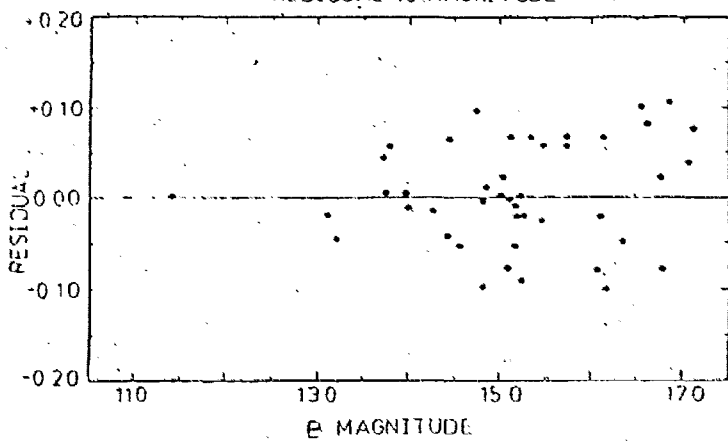


Figure 2d

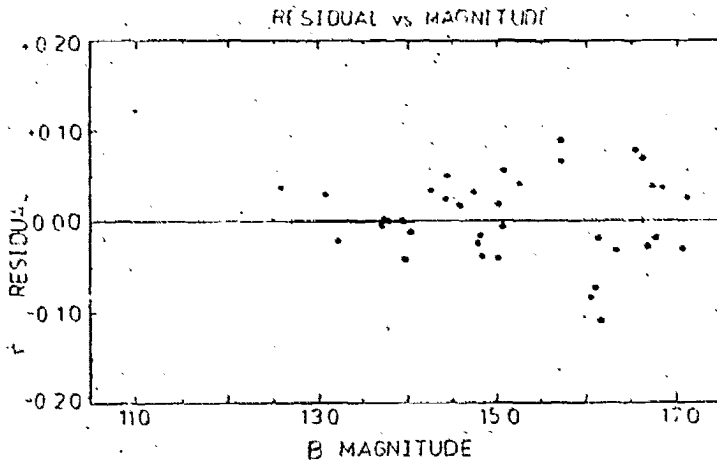
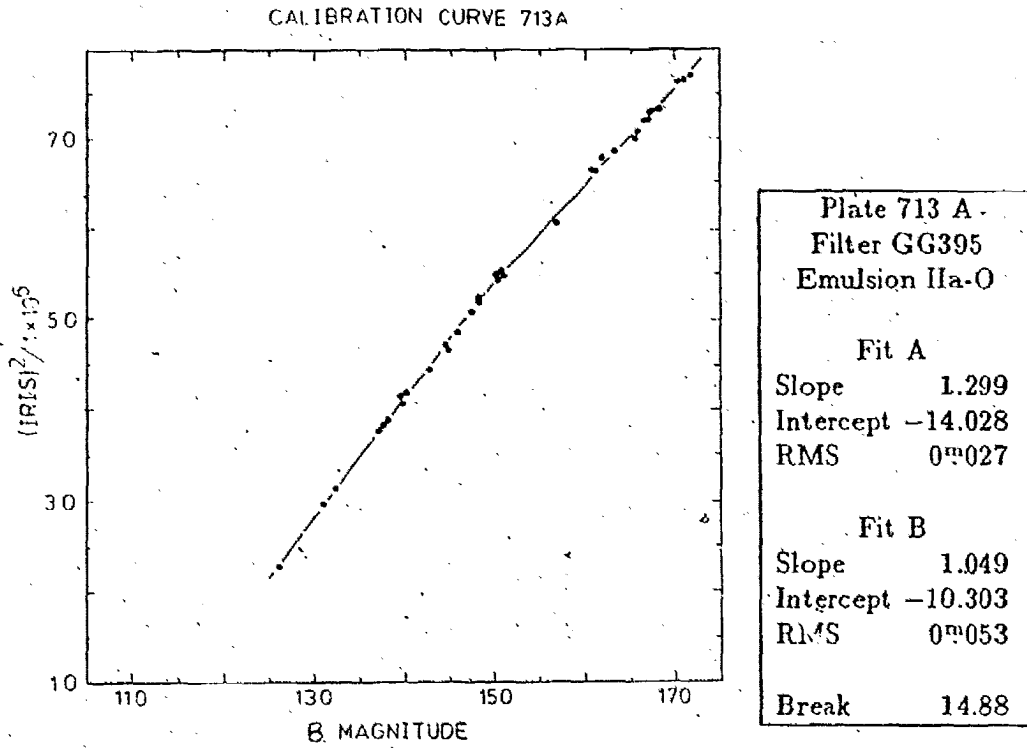


Figure 2e

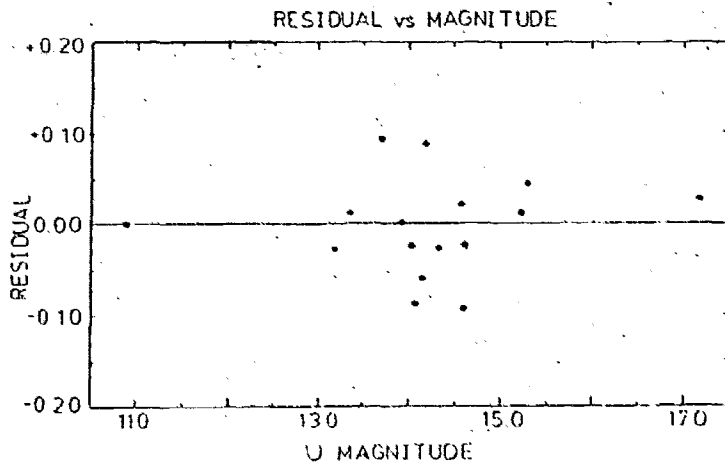
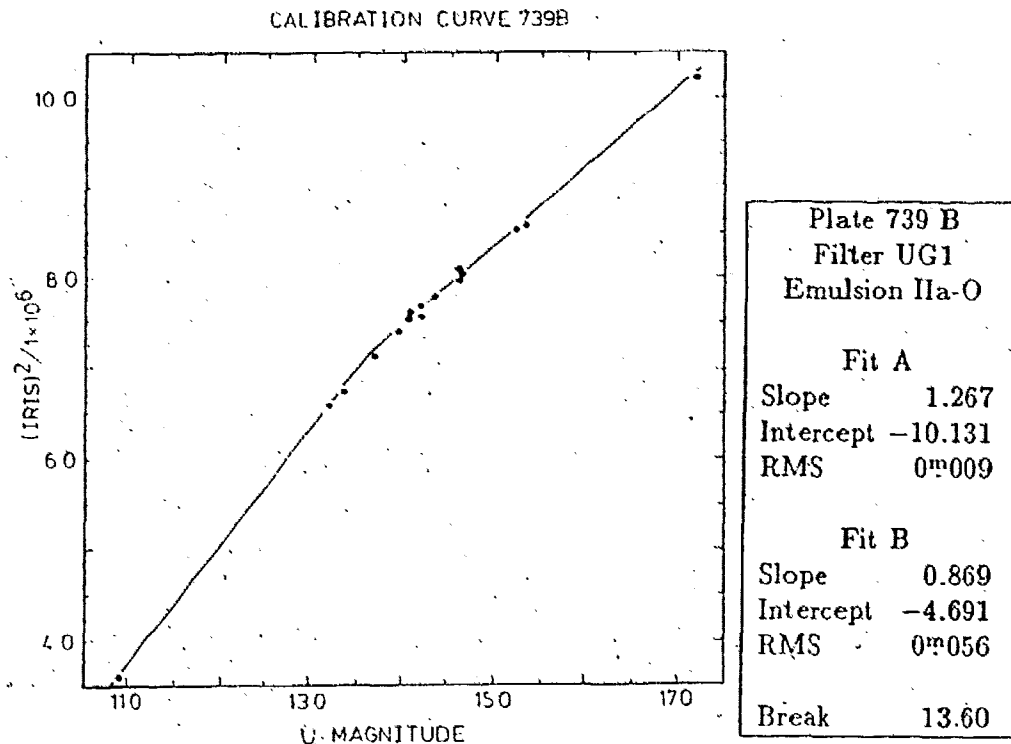


Figure 2f

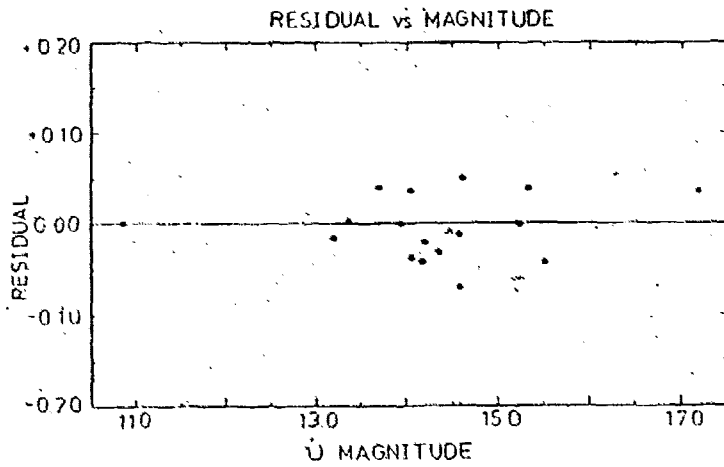
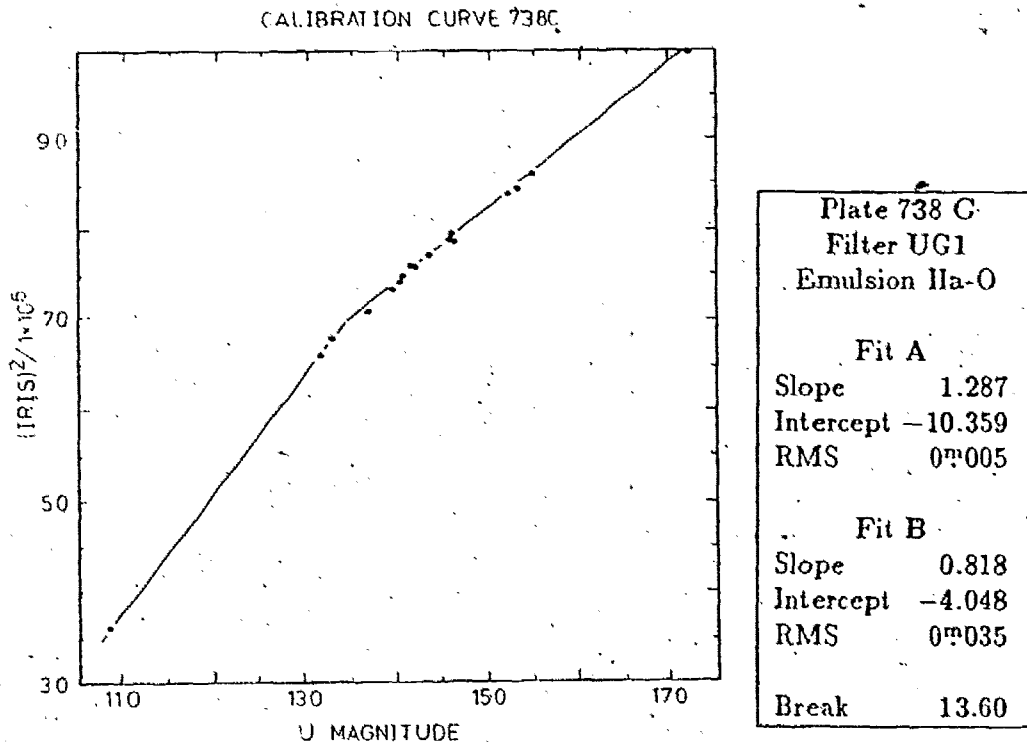
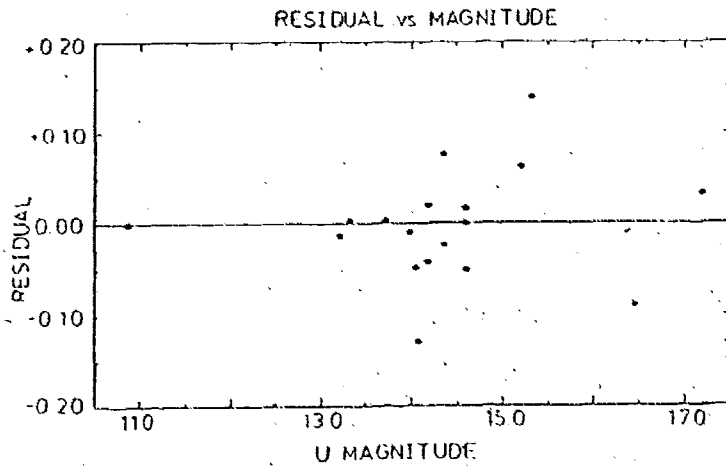
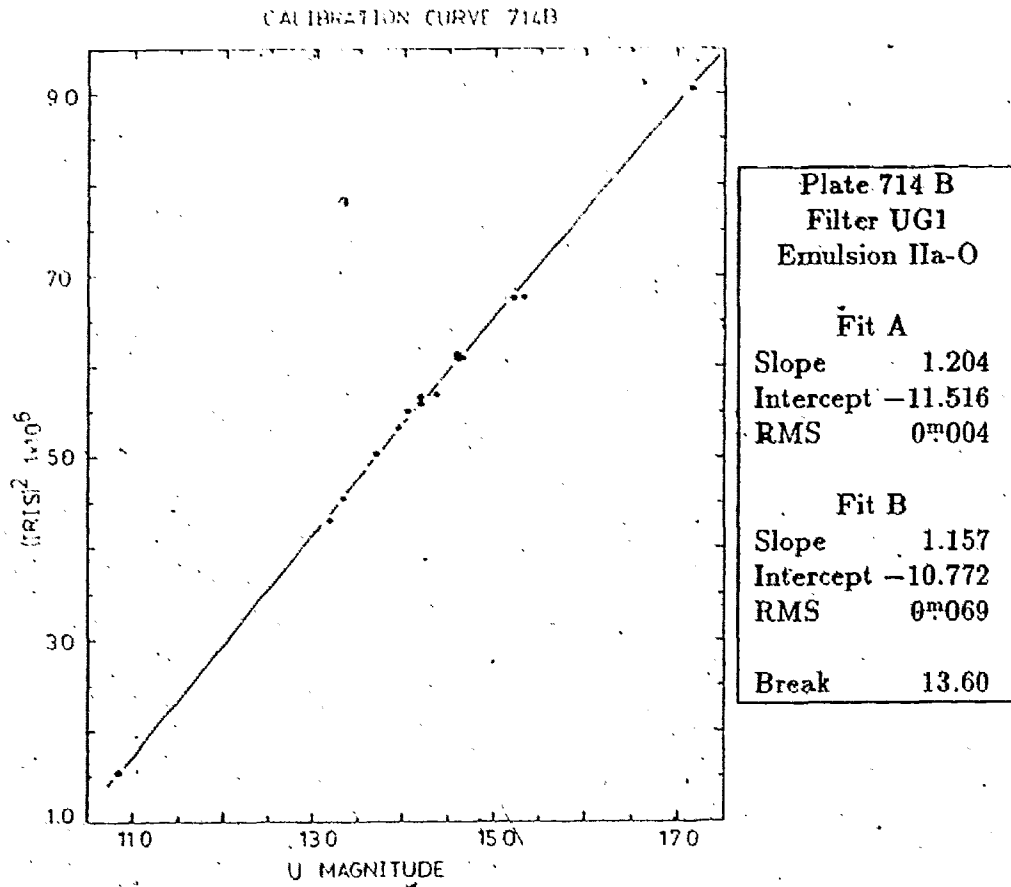


Figure 2g



## Secondary Images

The next phase of the reduction process was to incorporate the secondary images into the calibration relations. The goal of using a Racine prism is to produce double images whose magnitude difference is independent of magnitude. The necessary and sufficient condition to achieve this is that the time-averaged photometric profiles of the secondary and primary images must be the same (Christian and Racine 1983). A variety of factors can conspire to produce images with different density profiles. Blanco (1982) investigated the use of the Racine prism on the CTIO 4m telescope. He found magnitude dependent variations in the magnitude shift,  $\Delta m$ , as large as 0<sup>m</sup>2 per magnitude, which would lead to large systematic errors from the use of secondary images in the plate calibrations. Christian and Racine (1983) noted that the existence of any magnitude-dependent discrepancies in  $\Delta m$  implies that the conditions for the use of the prism have not been met.

Unfortunately, only the secondary of the brightest standard overlapped the faint end of the calibration relations. This image was used to calculate the magnitude shift of the secondaries. All the secondaries were then shifted by this amount and plotted with the calibration relations. A visual culling of the plots was made to remove any obviously erroneous points, and the data for the secondaries were carefully examined to determine if they obeyed the same linear relationships as the primaries. Generally, the secondaries appeared to obey a linear relation for

a range of several magnitudes. Secondaries past this limit (just above the plate limiting magnitudes) were discarded.

The secondaries that remained were assumed to obey the same linear fit as the primaries. The magnitude shift was found by using only the secondary of star A. However, in an attempt to use all the information available, the remaining secondaries were also used to estimate the magnitude shift, as follows. The rms error of the linear fit for the primaries was calculated including the usable secondaries over a range of magnitude shifts. The range was adopted to be  $\pm 0^m35$  centred on the magnitude shift found for the secondary of star A. The rms error was calculated over this range with magnitude shifts increased in increments of  $0^m001$ . The shift adopted was that which minimized the rms error. This method assumes that the secondaries obey the same relationship as the primaries.

The magnitude shift was calculated in this manner for each individual plate. The mean shift was  $4^m74 \pm 0^m09$  s.d., but there was considerable scatter in the results. A similar scatter was also evident for the magnitude shift found with the secondary for star A. The magnitude shift for this case was  $4^m70 \pm 0^m10$  s.d.. No evidence of a wavelength-dependence of  $\Delta m$  was found. A magnitude shift was also calculated by Pedreros *et al.* (1984). The shift in this case was determined using a plot of the iris reading versus magnitude for the standards. A similar plot was done for the secondaries on a separate piece of graph paper, and the

plots were overlain and shifted until a smooth curve was formed (Pedreros, private communication). The magnitude shift,  $\Delta m$ , found by this method was  $4^m73 \pm 0^m02$  s.e.. These results differ slightly from the magnitude shift found for the same Racine prism by Turner *et al.* (1986) and Turner (private communication), who obtained  $\Delta m \simeq 4^m60$  with a slight variation due to colour. The value of the shift found by these authors is quite reliable since there is a significant amount of overlap between primary and secondary sequences in the clusters used. The different value of  $\Delta m$  found here for NGC 7790 from the same Racine prism indicates that it was probably not physically placed in the telescope in the exact same fashion for these observations (which were not contemporaneous with those used by Turner) or that conditions were not appropriate for the use of the prism.

Since the successful use of secondaries requires that their density profiles be qualitatively the same as those of the primaries, a visual examination of the stellar images was made. For the brightest secondaries it was difficult to detect any difference in the profiles as compared to primaries of similar magnitude. However, it was noticed that except for the brightest secondaries the image density profiles were not saturated. This visual impression was supported by microdensitometer tracings of several secondary and primary images of the same standard (see Figure 3). The use of a linear relationship between magnitude and the square of the iris reading requires that the density profiles be saturated. Since this condition was not satisfied by most of the secondaries, it was concluded that they were unlikely

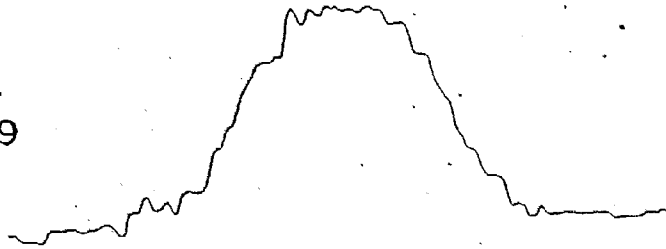
to be useful for extending the calibration relations.

The problems with the secondary images outlined above has important implications for the work of Pedreros *et al.* (1984). They used hand drawn curves to describe the calibration curves, which does not require the images to be saturated. However, if the density profiles of the secondaries and primaries are fundamentally different, a magnitude dependence of  $\Delta m$  may exist. This effect was not considered by Pedreros *et al.* (1984) and could introduce serious systematic errors into their data at faint magnitudes.

The secondaries were used to put limits on the extent to which the linear calibration relations defined by the primaries could be extrapolated. The limits were taken to be 0<sup>m</sup>2 brighter than the points at which it became apparent that the secondaries were deviating from a linear relationship. The brighter secondaries appeared to obey linear relationships (although not necessarily the same as for the primaries) as long as they had saturated profiles, and helped define the turnover points of the calibrations. The magnitude limits derived in this manner were 17<sup>m</sup>4 for the U and V plates and 18<sup>m</sup>0 for the B plate. (see Figs. 4a, b, and c). The brighter secondary images allowed the linear calibration relations derived from the primary images to be extrapolated with confidence to these limits.

Figure 3

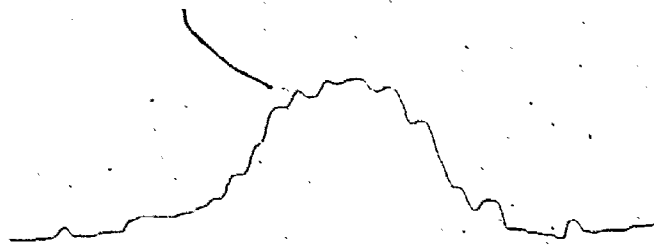
E  
V=12.79



Es  
V=17.51



N  
V=13.51

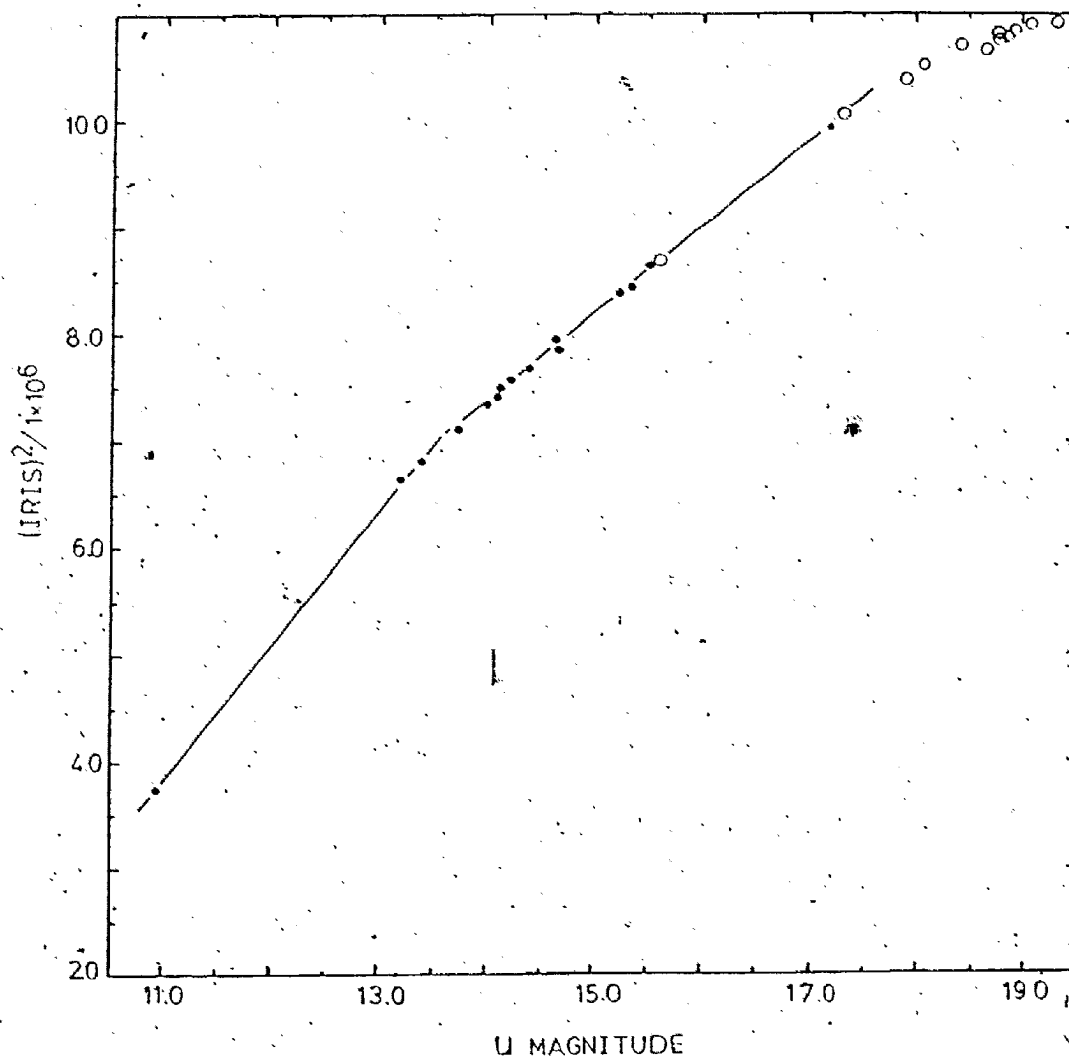


Ns  
V=18.23



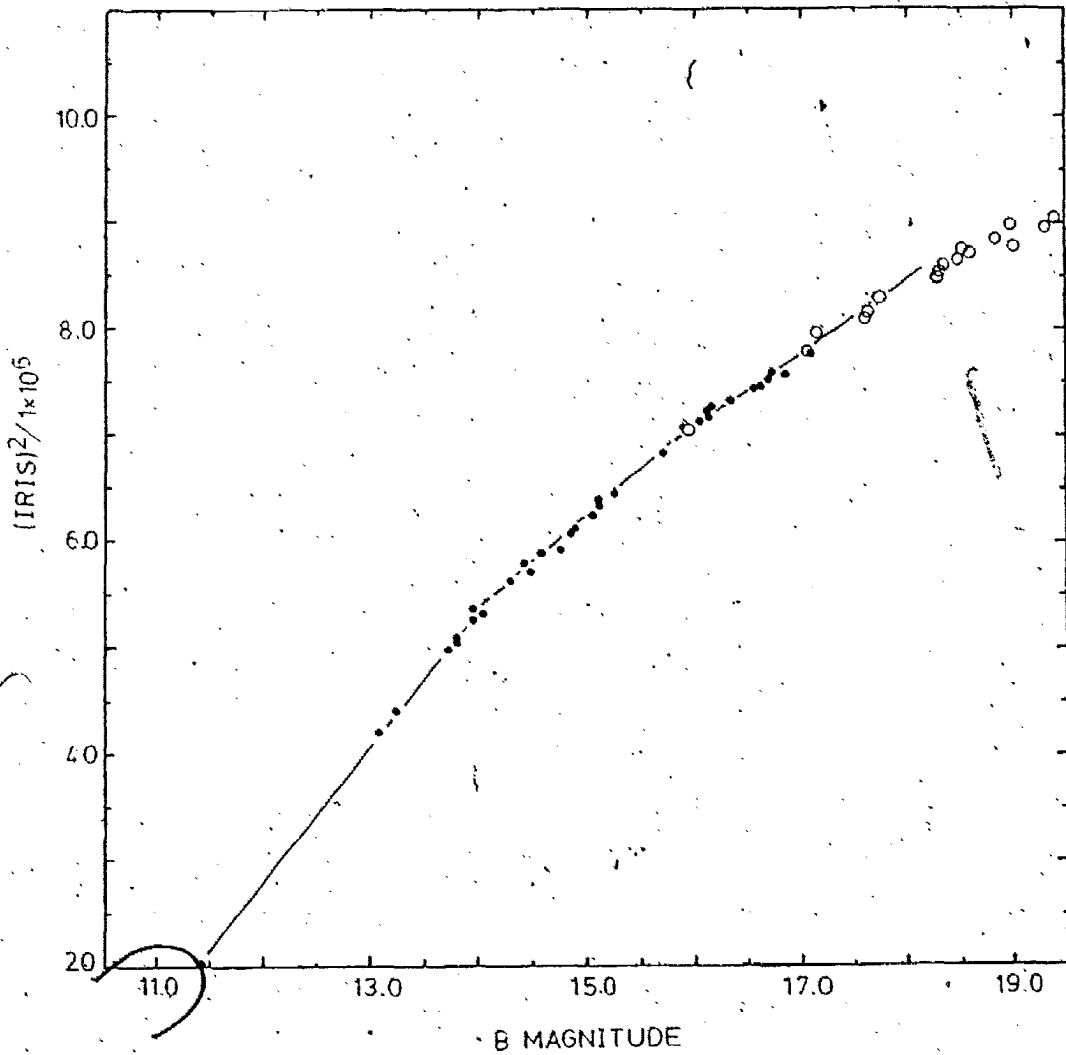
Microdensitometer tracings of two standard stars and their secondary images ("s") are displayed above. The secondary images were scanned perpendicular to the direction of displacement from the primary images. A magnitude shift of 4.74 was assumed for the secondary images. The profiles of the secondary images do not appear to be saturated Gaussians. A saturated Gaussian, as seen in the primary images of stars E and N, is characterized by a flat top or plateau. A stellar image with a saturated Gaussian profile corresponds to a well exposed image with a black core. The profiles must be saturated Gaussians to obey the linear calibration relations used in this study.

Figure 4a



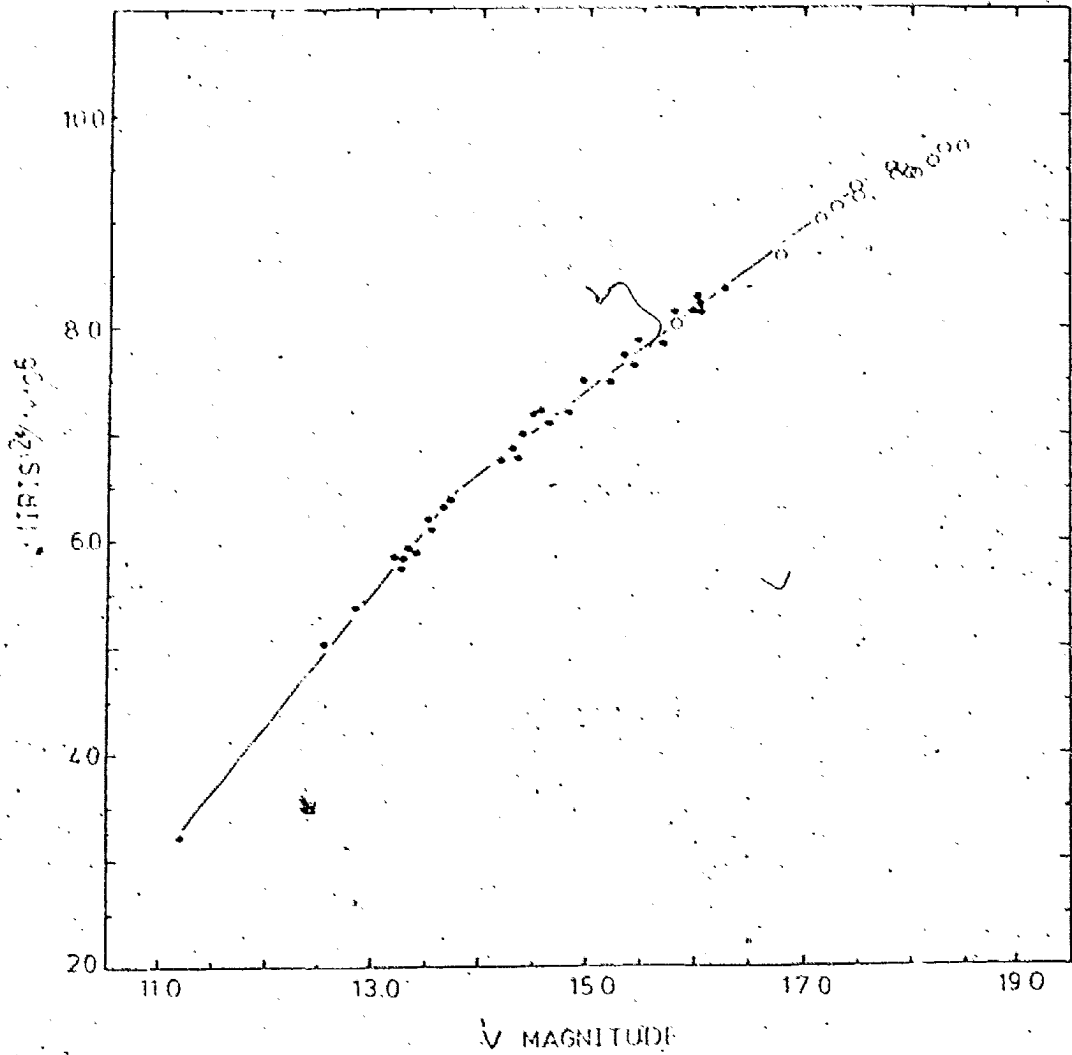
A plot of the calibration relation for plate 738a (U plate); the filled circles represent primary images and the open circles represent the secondary images. The secondary images have a magnitude shift of 4.74. The calibration fit has been extended to the approximate magnitude at which the secondary images no longer appear to obey the linear relation valid for brighter stars.

Figure 4b



A plot of the calibration relation for plate 734i (B plate); the filled circles represent primary images and the open circles represent the secondary images. The secondary images have a magnitude shift of 4.68. The calibration fit has been extended to the approximate magnitude at which the secondary images no longer appear to obey the linear relation valid for brighter stars.

Figure 4c



A plot of the calibration relation for plate 737b (V plate); the filled circles represent primary images and the open circles represent the secondary images. The secondary images have a magnitude shift of 4.72. The calibration fit has been extended to the approximate magnitude at which the secondary images no longer appear to obey the linear relation valid for brighter stars.

## Calibration Results

The internal accuracy of the measurements was investigated by comparing the average magnitudes obtained for stars on the same plate from two different measuring sessions. Comparing results from the same plate for two different measurers should reveal any systematic differences between them. Figure 5 shows that the results have a high level of internal accuracy and exhibit no trends between measurers. The student measures were also compared with those of the author and no trends were detected. This indicates that the iris photometry was done in a consistent fashion.

The results of the initial calibration relations were tested for trends using the program stars. This was considered important because the fits were extrapolated past the faintest standards. Plots were made of the differences between the average magnitude derived for each star from the measures on individual plates, versus its mean magnitude, with colour corrections applied. Trends were found in the reductions for the U and B plates (see Figs. 6a and 7a). The data were then reanalysed in the following manner. Program stars and their magnitudes from plates having well defined calibration relations were used as supplementary standards for the other calibration relations. These supplementary standards were given half-weight and new least squares fits were calculated. This refitting procedure was mostly successfully in removing the obvious trends in the residuals (see

Figs. 6b and 7b).

### Colour equations

To ensure standardization to the Johnson UBV system, colour equations were applied to the data. The equations were of the following form,

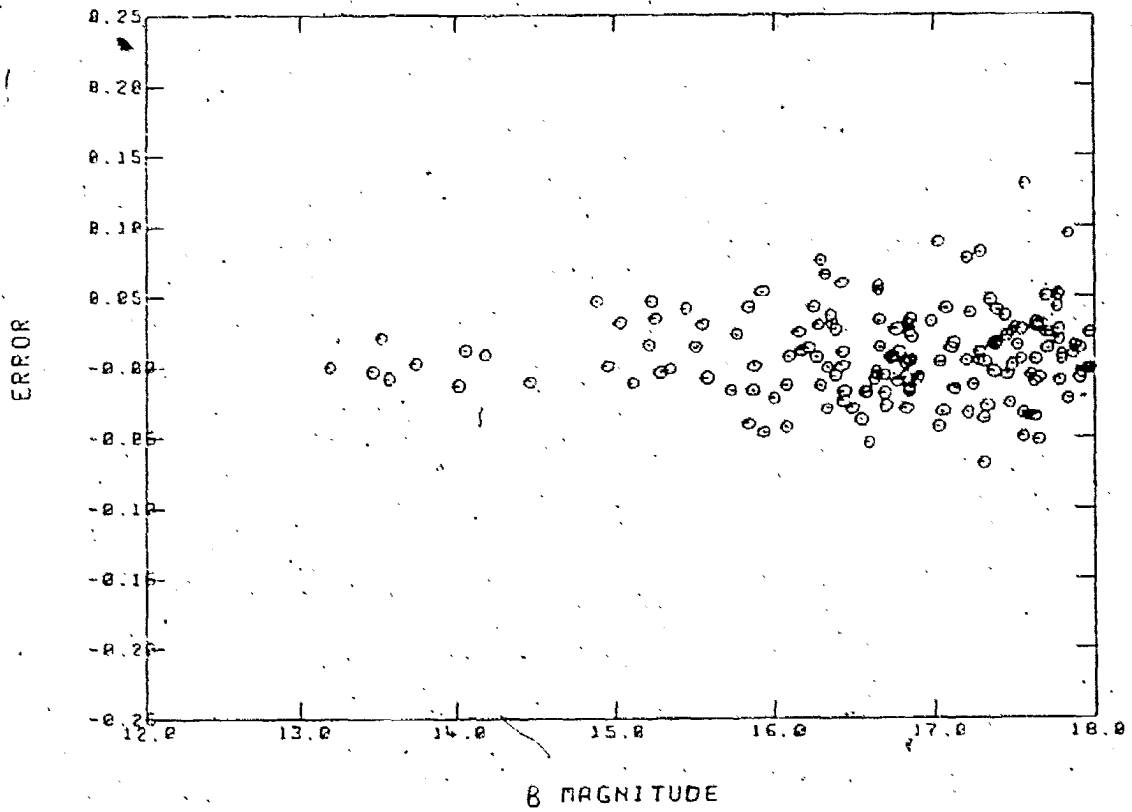
$$V_{pe} - V_{pg} = a_1 + b_1(B - V)_{pg} \quad (1)$$

$$(B - V)_{pe} = a_2 + b_2(B - V)_{pg} \quad (2)$$

$$(U - B)_{pe} = a_3 + b_3(U - B)_{pg} \quad (3),$$

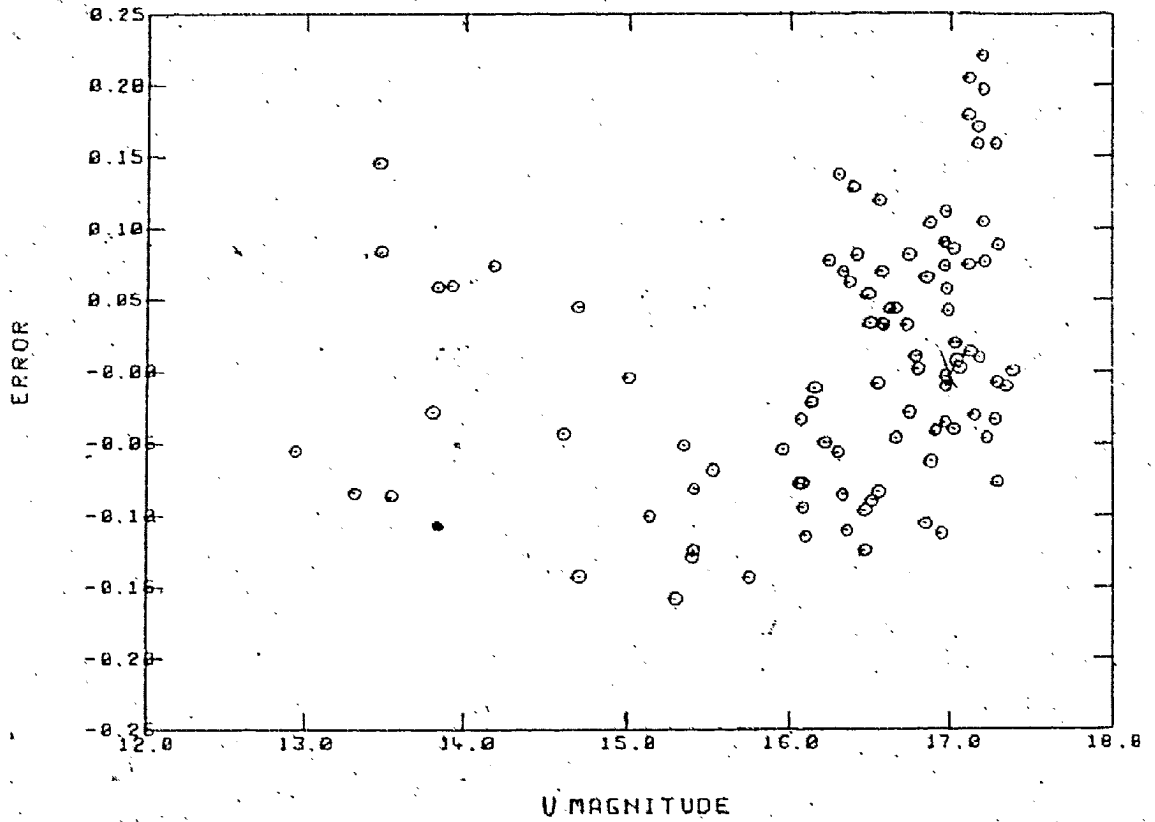
for simplicity of calculation. Simple least squares fits were performed, (Figs. 9a-c) on the data, and Table IV lists the resulting solutions. Strictly speaking, large errors exist in the photographic magnitudes and colours so that a least squares fit assuming no errors in the photographic data is not applicable. However, the photographic system is only marginally different from the standard Johnson UBV system. Equations (1) and (2) have slopes and intercepts just over the one sigma level from an exact match, while the parameters of equation (3) are within one sigma of an exact match. This indicates that colour corrections to most stars are quite small. The difference in the corrections between a least squares fit assuming no errors in the photographic data and a more sophisticated fitting procedure would be vanishingly small.

Figure 5



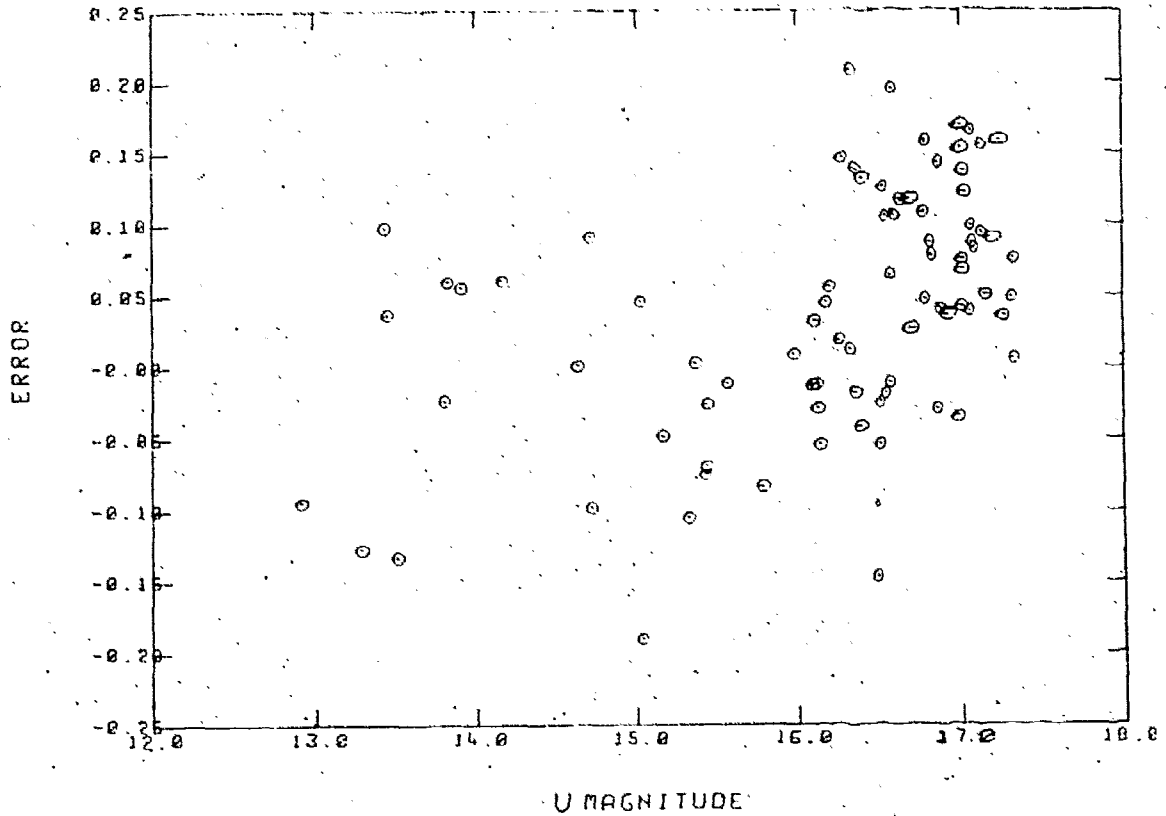
Comparison of the calculated B magnitudes (plate 737) between the two measurers. The error is in magnitudes. The errors increase as the limiting magnitude of the calibration relation is approached. No other trend is apparent.

Figure 6a



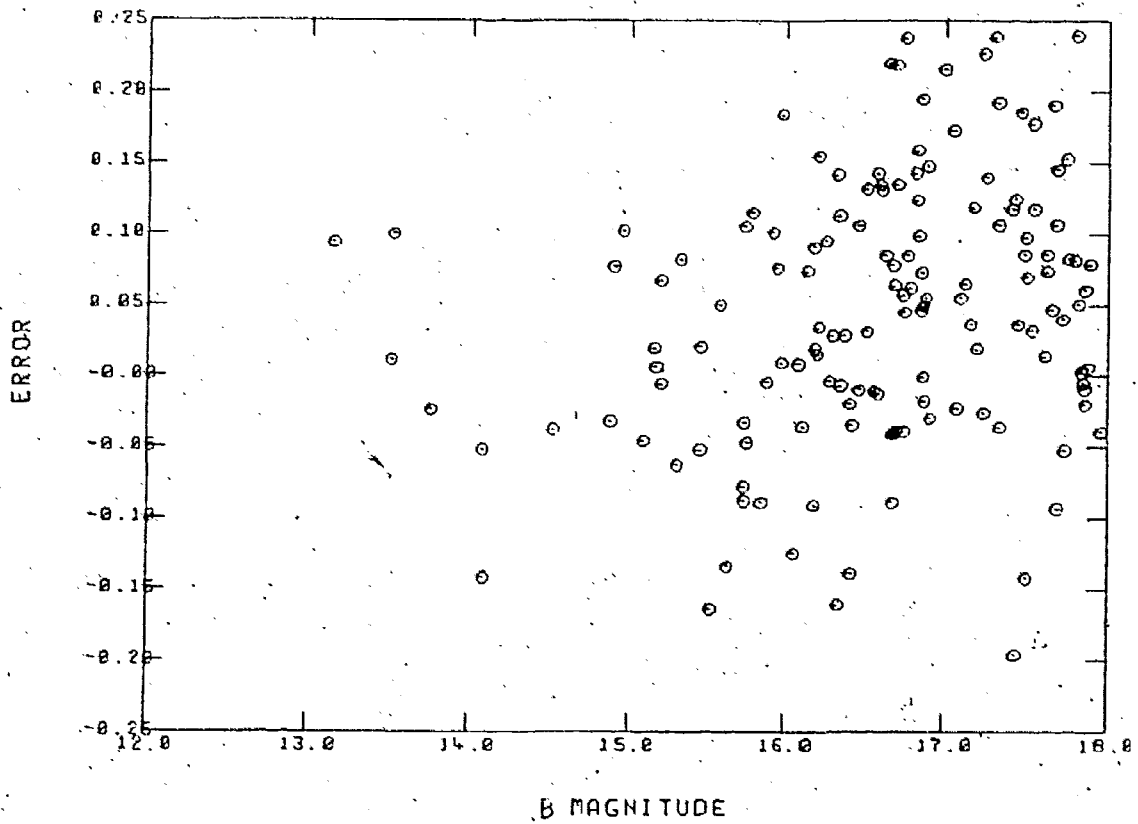
The plot shows a comparison of the calculated U magnitudes between the poor seeing and good seeing plates. The error is the difference between the magnitudes from stars on plate 714 (poor seeing plate) and the average magnitudes of the same stars on plates 738 and 739 (good seeing plates). The residuals appear to exhibit a trend with magnitude.

Figure 6b



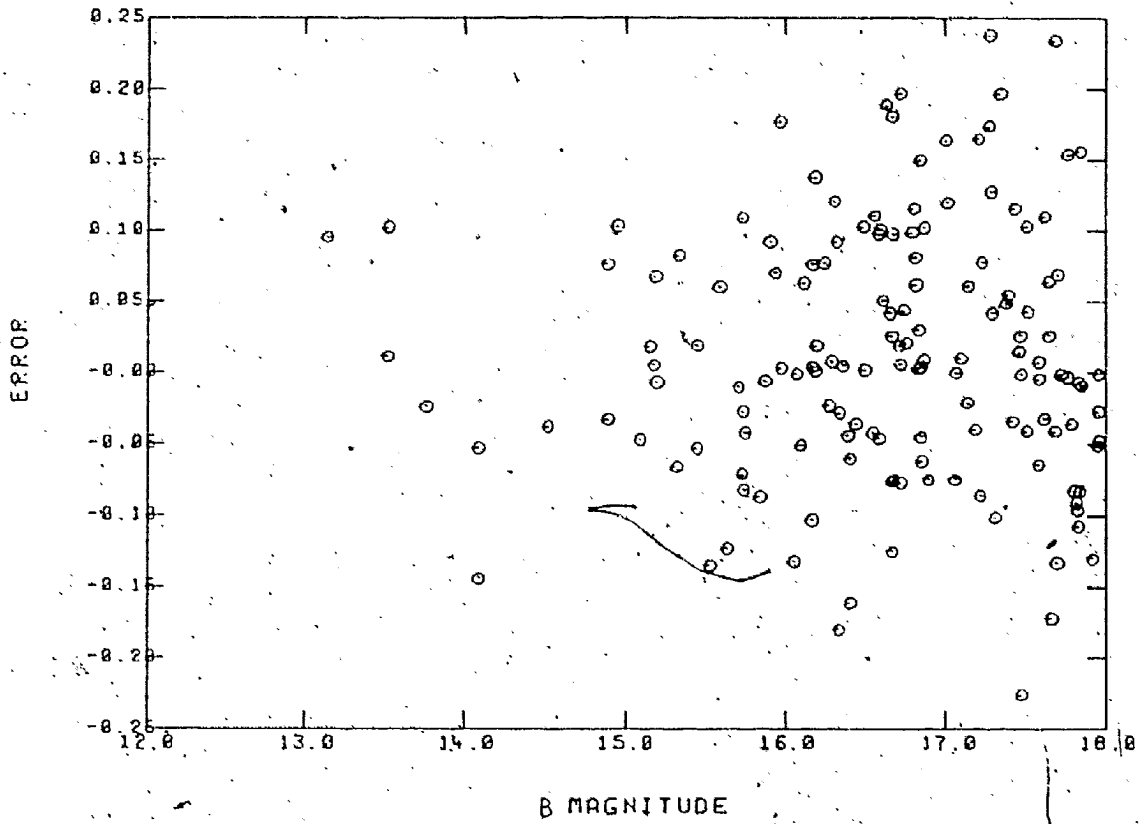
The plot shows a comparison of the calculated U magnitudes with the supplementary magnitudes used to calibrate the poor seeing plate. The trend that was originally present has been greatly diminished, if not eliminated, although a trend may still be present for the faintest stars.

Figure 7a



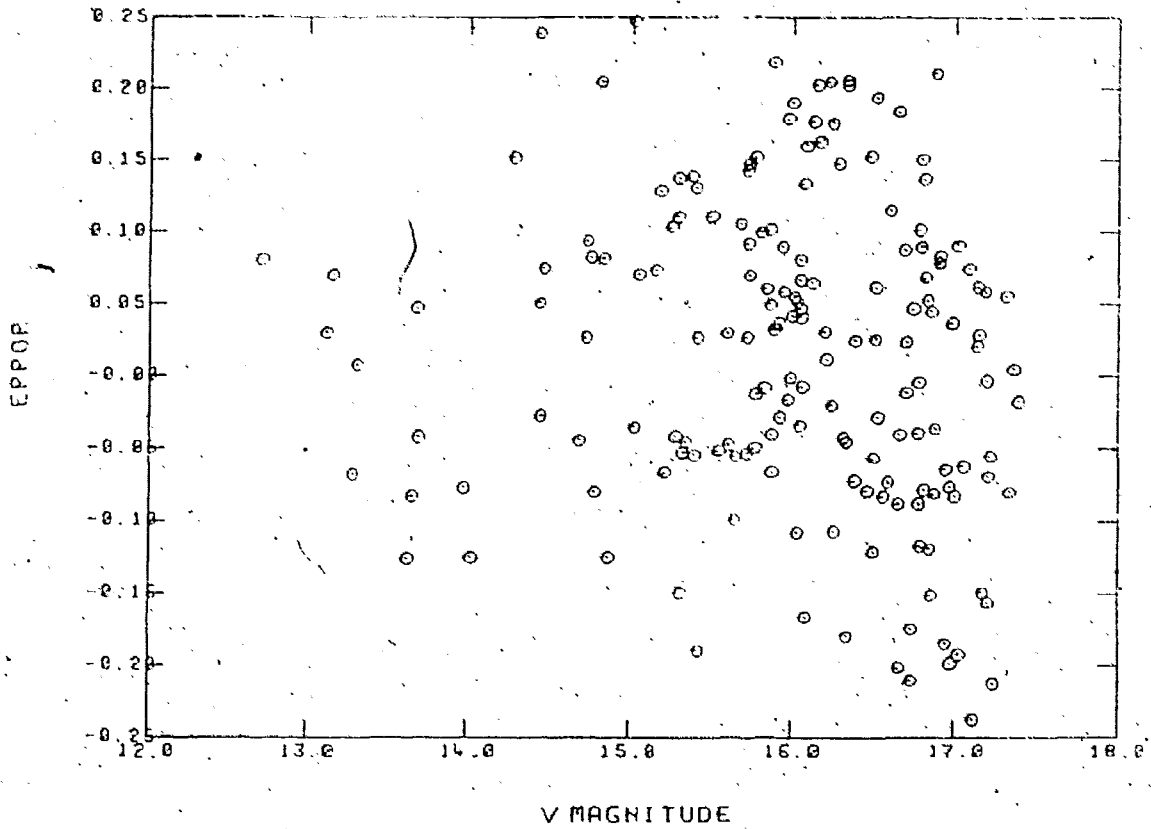
The plot shows a comparison of the calculated B magnitudes (plates 737 and 713). Note that the results for  $B \gtrsim 16^m5$  on plate 737 tend to be systematically fainter than those on plate 713. Plate 713 was considered to have the more reliable calibration relation because of its well defined kink and small scatter.

Figure 7b



The plot shows a comparison of the calculated B magnitudes with the trend between the two plates removed.

Figure 8



The plot shows a comparison of the V magnitudes. The errors appear to be randomly scattered.

Figure 9a

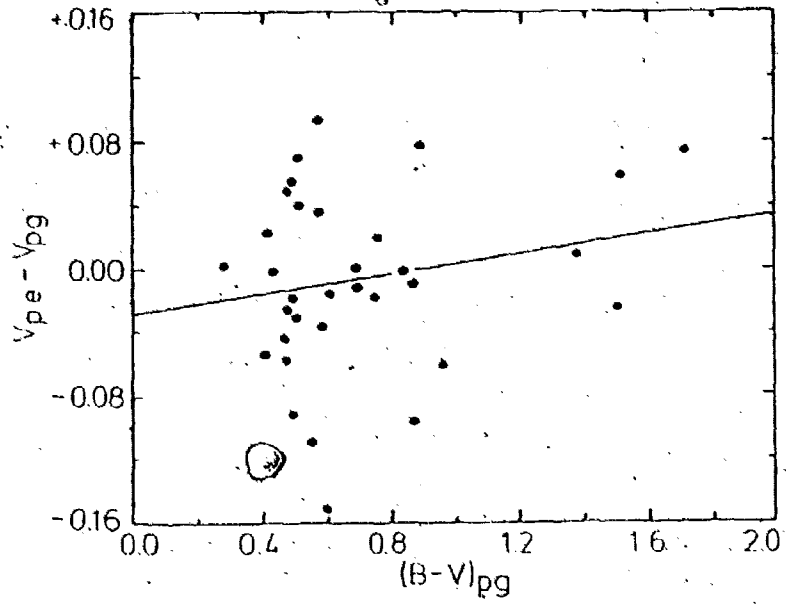


Figure 9b

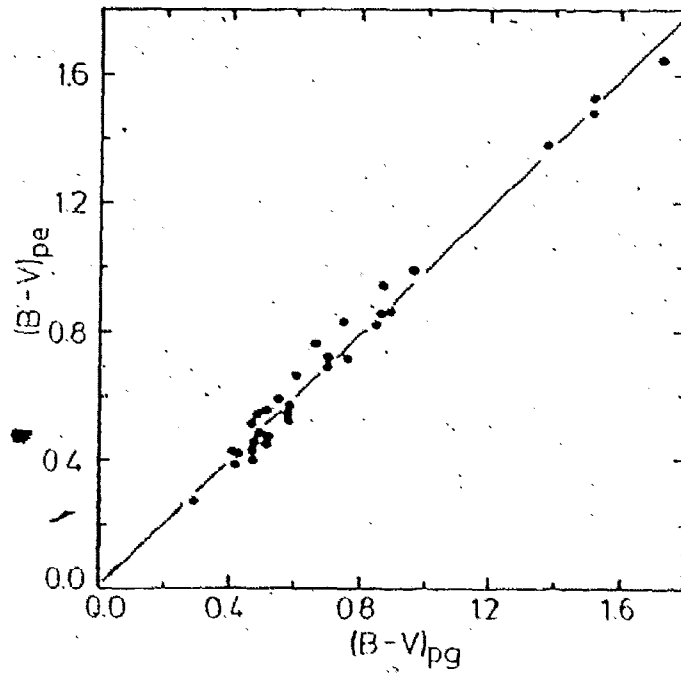
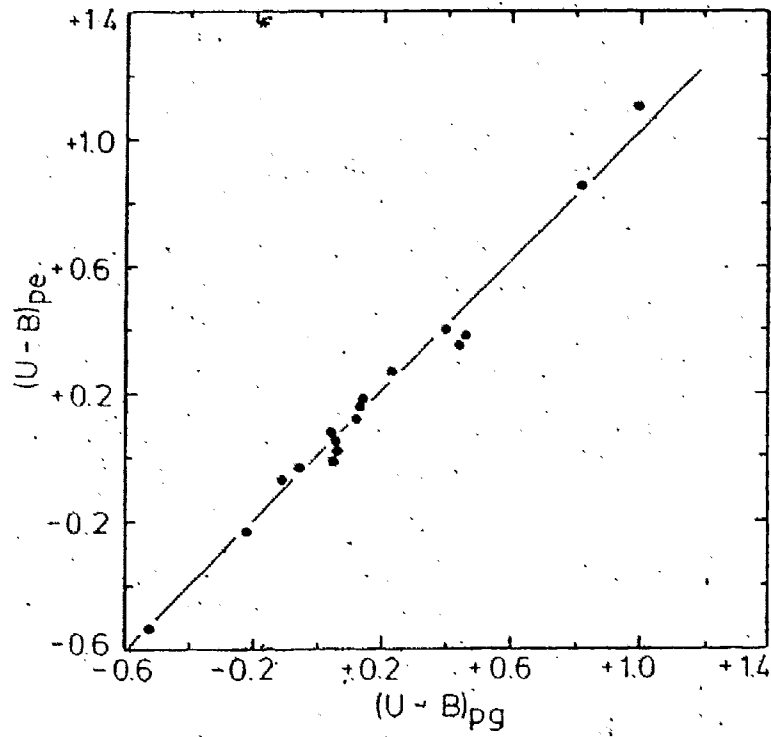


Figure 9c



Figures 9a, b, and c show the colour trends that are present in the photographic measurements of the standards. Least squares fits have been drawn through the data. It is apparent from the plots that the photographic system closely reproduces the standard Johnson UB system.

Table IV

Equation	a $\pm$ s.d.	b $\pm$ s.d.	rms	correlation coefficient
(1)	-0.029 $\pm$ 0.023	0.031 $\pm$ 0.029	0 <sup>m</sup> 057	0.180
(2)	0.027 $\pm$ 0.018	0.979 $\pm$ 0.023	0 <sup>m</sup> 045	0.991
(3)	-0.001 $\pm$ 0.012	1.021 $\pm$ 0.031	0 <sup>m</sup> 043	0.993

The uncertainty in the magnitudes and colours arising from the fits to equations 1 - 3 can be estimated from the errors of the fit parameters. From Table IV the errors are  $\Delta V = \pm 0^m 057$ ,  $\Delta(B - V) = \pm 0^m 045$ , and  $\Delta(U - B) = \pm 0^m 043$ , which are quite small for photographic data. The photoelectric standards have a wide range of colours. Thus, only program stars with extreme colour terms will lie outside the range over which the colour equations are applicable.

The uncertainties quoted from the errors in the colour equations are probably not realistic assessments of the errors in the program stars, which are magnitude dependent (see Figs. 5-8). Most of the program stars lie at the faint ends of the calibration sequences, and their uncertainties are best determined from a comparison of plate averages. The mean standard deviations for all program stars calculated in this manner are  $\Delta V = \pm 0^m 061$ ,  $\Delta B = \pm 0^m 046$  and  $\Delta U = \pm 0^m 058$ . These correspond to uncertainties in the colour terms of  $\Delta(B - V) = \pm 0^m 076$  and  $\Delta(U - B) = \pm 0^m 074$ . These errors are a more accurate reflection of the uncertainties in the measurements than the errors from the colour equations.

## Chapter Three

### Dereddening

The bane of astronomers that work in the optical region of the spectrum is interstellar extinction, the effects of which must be carefully taken into account in any optical study. Interstellar matter absorbs preferentially in the blue, hence making objects observed through it appear redder than their true colours. Quantitatively this "reddening" can be expressed as a ratio of colour excesses from different regions of the spectrum; the ratio for the Johnson UBV system is  $E_{U-B}/E_{B-V}$ . An average galactic value often quoted for this ratio or reddening slope is about  $0.72 + bE_{B-V}$ , where  $b \simeq 0.05$ . The second term of the relation is sometimes called the curvature term, and is usually negligible over small ranges of reddening. The total amount of visual extinction,  $A_v$ , is related to the colour excess by the relation  $A_v = R_v \times E_{B-V}$ , the value of  $R_v$  generally lying between 3.0 and 3.3. Turner (1985) found that the value of  $E_{U-B}/E_{B-V}$  varied from 0.62 to 0.80 in six different regions, with an average close to 0.72. Of these six regions in the galactic plane, only one was within one  $\sigma$  of the average. Although average values for interstellar absorption can act as a guide, individual regions of the sky should be treated as such.

It is possible to calculate the reddening slope for a region if photometric and spectroscopic data are available. For NGC 7790 the only spectroscopic observa-

tions are those of Kraft (1958), who observed seven B-type members. Owing to the difficulties of spectral classification for mid-to-late B-type stars (which have few spectral lines that are frequently "washed out" by rapid rotation) and the highly sensitive spectral type dependence of intrinsic UBV colours for these same stars, the prospects of reliably determining the reddening slope for the field of NGC 7790 from the data available for this cluster are poor.

The prospects improve if one is willing to examine the surrounding field of the cluster. Turner (private communication) obtained a reddening slope of 0.76 for the star field of Berkeley 58 using spectroscopic and photographic data for stars within a few degrees of the cluster centre. Berkeley 58 is an open cluster  $\sim 40'$  from NGC 7790, located at  $\alpha_{1950.0} = 23^{\text{h}}57^{\text{m}}6$ ,  $\delta_{1950.0} = +60^{\circ}41'$  (Ruprecht *et al.* 1981). The diameter of the field of study of NGC 7790 is about  $14'$ , placing Berkeley 58 only a few cluster diameters away. On the Palomar Sky Survey there is no obvious difference in the extinction between the two clusters (except for some patchy clouds in Berkeley 58), and the dust cloud responsible for the foreground reddening in this field is only about 500 pc distant (Lynds 1968). It therefore appears reasonable to adopt a reddening slope of 0.76 for NGC 7790, as indicated by stars in the field of the cluster. The curvature term of the reddening slope was assumed to be zero in this study. This is a reasonable approximation since the range of colour excesses for the stars in NGC 7790 is too small for the curvature in the ratio  $E_{U-B}/E_{B-V}$  to be important.

Stars observed in all three passbands were individually dereddened in this study. There were thirteen standard stars with no photoelectric U observations, which were analysed as follows. Colour corrected U, B, and V photographic magnitudes were calculated and the photographic U magnitudes were used with the photoelectric B magnitudes to obtain values for (U - B). For stars with poorly determined B and V magnitudes (i.e. one observation) and those standards that were consistently rejected from the U plate calibration relations, the photographic magnitudes were used. The magnitudes, colours and adopted reddening solutions are documented in Table V. The values for the reddening have been corrected to that expected for a B0 star using a relation obtained by Fernie (1963), namely

$$E_{B-V}(B0) = E_{B-V} / [(0.97 - 0.09(B - V))_0].$$

Table V

Star	V	(B - V)	(U - B)	(B - V) <sub>0</sub>	V - M <sub>v</sub>	E <sub>B-v</sub>
1	15.86	+0.51	+0.36	+0.18	13.47	0.35
2	14.46	+1.31	+0.78	—	—	—
3	15.71	+1.18	—	—	—	—
4	13.33	+1.59	+1.40	—	—	—
5	13.76	+1.53	+1.06	—	—	—
6	16.05	+0.82	+0.21	+0.52	11.70	0.33
7	15.94	+0.74	+0.41	+0.28	13.09	0.48
8	15.63	+0.56	+0.38	-0.02	14.21	0.60
9	15.36	+1.72	—	—	—	—
11	14.90	+1.70	—	—	—	—
12	15.77	+0.56	+0.33	+0.25	13.09	0.33
13	15.39	+0.49	+0.51	—	—	—
14	15.86	+0.63	+0.42	+0.22	13.33	0.44
18	15.42	+0.70	+0.38	+0.29	12.55	0.43
19	15.30	+0.46	+0.36	+0.04	13.57	0.43
23	14.81	+1.80	—	—	—	—
24	15.20	+0.56	+0.32	-0.04	13.98	0.62
26	15.71	+0.49	+0.48	—	—	—
27	16.04	+0.57	+0.37	+0.22	13.49	0.37
28	15.31	+0.58	+0.46	+0.12	13.17	0.48
29	15.82	+0.73	+0.43	+0.27	13.04	0.49
30	15.97	+0.72	+0.35	+0.32	12.91	0.42
31	16.03	+0.87	+0.28	+0.47	12.04	0.43
32	15.88	+0.69	+0.39	+0.27	13.08	0.44
33	15.90	+0.51	+0.44	—	—	—
34	15.59	+0.58	+0.38	+0.21	13.07	0.39
35	15.78	+1.02	+0.37	+0.52	11.43	0.54
36	13.68	+0.43	+0.05	-0.10	12.22	0.55
37	15.40	+0.55	+0.44	+0.04	13.65	0.53
38	14.72	+0.45	+0.17	-0.07	13.77	0.53
39	13.21	+0.16	+0.18	—	—	—
40	13.12	+0.35	-0.14	-0.15	13.15	0.51
41	12.52	+0.31	+0.00	-0.09	11.79	0.41
42	14.79	+0.96	+0.36	+0.60	9.97	0.39
43	14.66	+0.80	+0.32	+0.39	11.22	0.45
44	16.04	+0.81	+0.21	—	—	—
45	15.94	+0.82	+0.22	—	—	—
46	15.97	+0.88	+0.27	—	—	—
47	16.08	+0.78	—	—	—	—

Table V (continued)

Star	V	(B - V)	(U - B)	(B - V) <sub>0</sub>	V - M <sub>v</sub>	E <sub>B-V</sub>
48	15.29	+0.84	+0.24	—	—	—
49	15.84	+0.97	+0.22	—	—	—
50	14.49	+1.70	+1.10	—	—	—
51	14.74	+0.36	+0.26	+0.00	13.20	0.37
52	13.14	+0.38	-0.07	-0.13	12.91	0.52
53	15.73	+0.58	+0.26	+0.31	12.74	0.29
55	13.10	+0.42	-0.08	-0.15	13.09	0.57
56	15.37	+0.61	+0.26	+0.33	12.29	0.29
57	15.85	+0.58	+0.35	+0.25	13.18	0.36
58	15.87	+0.58	+0.52	—	—	—
59	14.11	+1.52	+0.88	—	—	—
60	15.49	+0.59	+0.42	+0.18	13.09	0.43
61	14.67	+0.54	-0.05	-0.17	14.96	0.72
62	13.27	+0.49	+0.06	-0.12	12.87	0.62
63	14.71	+0.49	+0.23	-0.06	13.65	0.56
64	13.65	+1.67	+1.44	—	—	—
65	15.72	+0.68	+0.44	+0.28	12.88	0.42
66	15.59	+0.75	+0.56	+0.17	13.23	0.61
67	16.15	+0.58	+0.43	+0.16	13.84	0.44
68	15.80	+0.62	+0.34	+0.29	12.93	0.35
69	15.68	+0.99	+0.31	—	—	—
70	16.06	+0.53	+0.36	+0.19	13.60	0.35
71	15.76	+0.53	+0.51	—	—	—
72	15.99	+0.62	+0.37	+0.25	13.32	0.39
73	16.01	+0.83	+0.46	+0.31	13.03	0.55
74	13.90	-0.25	+1.38	—	—	—
76	15.73	+0.94	+0.34	+0.59	10.69	0.38
77	15.04	+0.81	+0.32	+0.40	11.55	0.45
78	16.06	+0.67	+0.31	+0.32	13.01	0.37
79	16.04	+0.63	+0.29	+0.31	13.04	0.33
80	15.71	+0.54	+0.32	+0.24	13.07	0.31
81	15.17	+0.49	+0.31	-0.02	13.51	0.52
82	15.28	+0.47	+0.33	+0.18	12.89	0.31
83	16.13	+0.60	+0.37	+0.23	13.52	0.38
84	15.16	+0.90	+0.35	+0.42	11.48	0.52
85	14.81	+0.74	+0.60	—	—	—
86	14.02	+0.51	+0.09	-0.11	13.53	0.68
87	13.66	+0.44	-0.20	-0.15	14.32	0.64
88	15.00	+0.46	-0.03	-0.14	14.84	0.59

Table V (continued)

Star	V	(B - V)	(U - B)	(B - V) <sub>0</sub>	V - M <sub>v</sub>	E <sub>B-v</sub>
89	15.67	+0.68	+0.20	+0.41	12.11	0.29
90	14.24	+0.92	+0.22	—	—	—
91	14.27	+0.69	+0.48	+0.19	11.81	0.52
93	15.70	+0.58	+0.34	+0.25	13.01	0.35
94	15.27	+0.49	+0.39	+0.11	13.18	0.40
95	12.70	+0.44	-0.19	-0.19	13.35	0.64
96	15.05	+1.78	—	—	—	—
97	15.27	+1.58	—	—	—	—
98	14.07	+0.18	+0.48	—	—	—
99	13.04	+0.51	+0.26	-0.05	11.89	0.57
100	14.42	+0.48	+0.11	—	—	—
101	16.77	+1.00	—	—	—	—
102	16.50	+0.94	—	—	—	—
103	16.56	+1.18	—	—	—	—
104	16.45	+0.94	—	—	—	—
105	16.77	+1.10	—	—	—	—
106	16.78	+0.85	—	—	—	—
107	16.51	+0.81	—	—	—	—
108	16.82	+0.78	—	—	—	—
110	16.84	+0.76	—	—	—	—
112	16.88	+0.92	—	—	—	—
113	16.27	+0.75	+0.26	+0.40	12.76	0.38
114	15.41	+0.57	+0.34	-0.04	14.16	0.63
117	16.73	+0.87	—	—	—	—
119	16.38	+1.09	—	—	—	—
121	16.73	+0.96	—	—	—	—
122	16.80	+0.83	—	—	—	—
124	16.31	+0.77	+0.28	+0.40	12.79	0.40
125	17.03	+0.96	—	—	—	—
127	16.18	+0.67	+0.35	+0.29	13.28	0.40
128	16.98	+0.99	—	—	—	—
129	16.07	+1.61	—	—	—	—
130	16.65	+0.76	—	—	—	—
137	16.66	+1.19	—	—	—	—
138	16.20	+0.92	—	—	—	—
141	16.90	+0.95	—	—	—	—
143	16.66	+1.00	—	—	—	—
146	16.50	+0.98	—	—	—	—

Table V (continued)

Star	V	(B - V)	(U - B)	(B - V) <sub>0</sub>	V - M <sub>v</sub>	E <sub>B-V</sub>
148	16.35	+1.65	—	—	—	—
150	16.90	+0.81	—	—	—	—
156	16.99	+0.87	—	—	—	—
161	16.66	+0.76	—	—	—	—
165	16.33	+0.77	+0.29	+0.39	12.85	0.41
167	16.93	+1.00	—	—	—	—
168	15.56	+1.63	—	—	—	—
171	16.24	+1.12	—	—	—	—
174	16.69	+0.79	—	—	—	—
175	16.82	+1.04	—	—	—	—
176	16.03	+1.64	—	—	—	—
181	16.46	+0.69	—	—	—	—
183	16.50	+0.81	—	—	—	—
184	16.80	+1.02	—	—	—	—
185	16.18	+0.66	+0.31	+0.32	13.15	0.36
188	16.68	+0.83	—	—	—	—
190	15.72	+0.45	+0.37	+0.11	-13.63	0.36
202	16.58	+0.94	—	—	—	—
211	16.24	+0.99	—	—	—	—
212	17.05	+0.93	—	—	—	—
213	16.96	+0.81	—	—	—	—
214	16.13	+1.12	—	—	—	—
215	16.94	+0.90	—	—	—	—
221	16.33	+0.89	—	—	—	—
228	16.37	+1.15	—	—	—	—
230	16.13	+1.16	—	—	—	—
231	16.07	+1.22	—	—	—	—
232	16.88	+1.09	—	—	—	—
235	16.79	+0.93	—	—	—	—
236	16.59	+0.83	—	—	—	—
241	16.50	+0.74	—	—	—	—
244	16.80	+0.90	—	—	—	—
248	17.01	+0.92	—	—	—	—
255	16.84	+1.12	—	—	—	—
262	16.49	+0.81	—	—	—	—
267	16.24	+0.63	+0.37	+0.26	13.51	0.39
276	16.69	+0.83	—	—	—	—
277	16.00	+1.14	—	—	—	—
280	16.62	+1.24	—	—	—	—

Table V (continued)

Star	V	(B - V)	(U - B)	(B - V) <sub>0</sub>	V - M <sub>v</sub>	E <sub>B-V</sub>
286	16.08	+0.68	+0.42	+0.24	13.44	0.46
289	15.66	+1.36	—	—	—	—
290	16.79	+1.19	—	—	—	—
291	16.82	+1.03	—	—	—	—
292	15.54	+0.55	—	—	—	—
297	16.87	+0.95	—	—	—	—
10 <sup>†</sup>	16.03	+0.72	+0.42	+0.27	13.24	0.47
17 <sup>†</sup>	16.02	+0.55	+0.38	+0.19	13.59	0.38
16	15.33	+0.62	—	—	—	—
20 <sup>†</sup>	15.77	+1.00	+0.37	+0.57	11.12	0.47
21 <sup>†</sup>	15.98	+0.71	+0.46	+0.23	13.36	0.48
25 <sup>†</sup>	15.44	+0.68	+0.36	+0.29	12.55	0.41
100 <sup>†</sup>	14.39	+0.44	+0.11	-0.06	13.33	0.51
A	11.11	+0.28	-0.53	-0.26	13.01	0.54
B	12.18	+0.43	-0.02	-0.13	11.95	0.57
C	12.50	+0.58	+0.27	-0.07	11.55	0.66
D	12.63	+0.46	+0.32	-0.01	11.13	0.48
E	12.79	+0.43	-0.04	-0.14	12.63	0.57
F	12.87	+2.00	+2.06	—	—	—
G	13.18	+0.57	+0.38	-0.04	11.93	0.63
H	13.19	+0.53	+0.35	-0.02	11.77	0.57
I	13.22	+1.25	+0.85	—	—	—
J	13.24	+0.56	+0.38	-0.02	11.82	0.60
K <sup>†</sup>	13.23	+1.53	+1.34	—	—	—
L	13.30	+0.73	0.16	—	—	—
M	13.37	+0.39	-0.07	-0.07	12.42	0.47
N	13.51	+0.47	+0.07	-0.11	12.56	0.59
O	13.52	+0.43	-0.01	-0.12	13.16	0.56
P	13.63	+0.83	+0.17	—	—	—
Q	13.80	+0.48	+0.06	-0.11	13.35	0.60
R	14.17	+0.41	+0.02	-0.11	13.68	0.53
S	14.29	+0.53	-0.23	-0.22	15.46	0.76
T <sup>†</sup>	14.19	+0.83	+0.25	+0.50	9.97	0.38
U	14.51	+0.60	+0.40	-0.02	13.02	0.64
V <sup>†</sup>	14.55	+0.50	+0.25	-0.05	13.43	0.57

<sup>†</sup> UBV photographic magnitudes

<sup>‡</sup> U photographic magnitudes

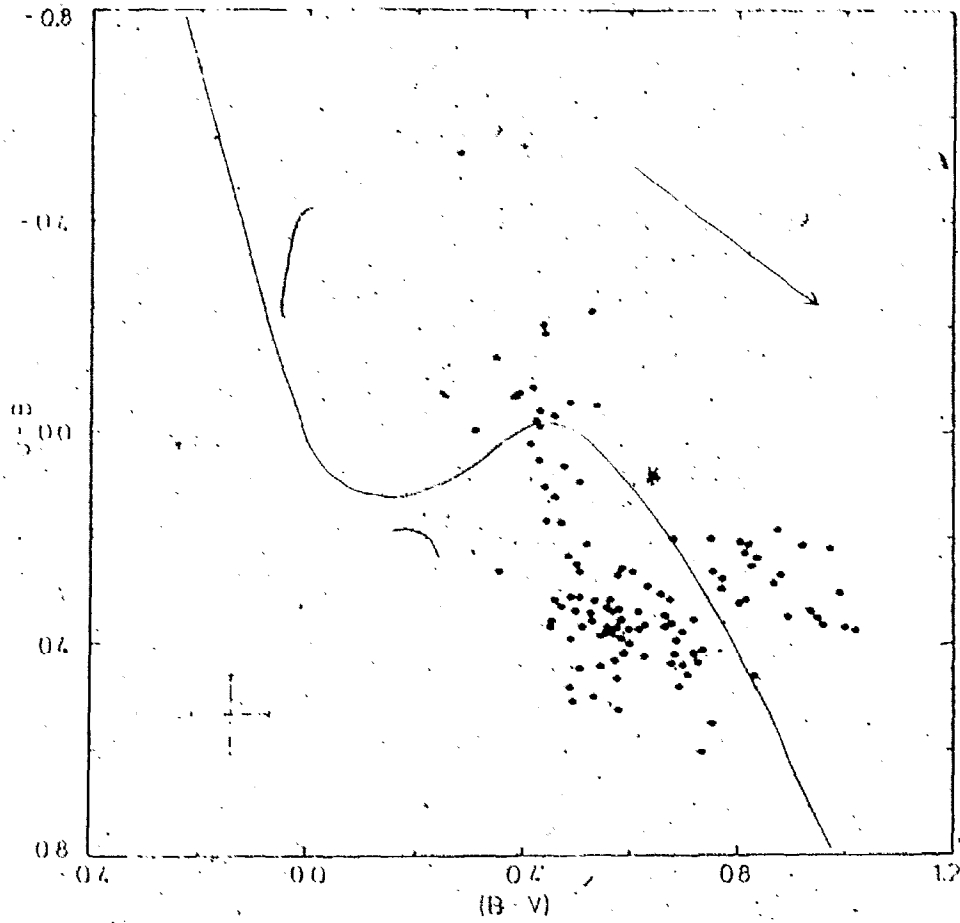
Table V (continued)

Star	V	(B - V)	(U - B)	(B - V) <sub>o</sub>	V - M <sub>v</sub>	E <sub>B-v</sub>
W	14.59	+1.49	+1.11	—	—	—
X	14.65	+0.46	+0.12	-0.09	13.92	0.56
Y <sup>†</sup>	14.75	+1.39	+0.84	—	—	—
Z <sup>†</sup>	14.73	+0.52	+0.21	-0.08	13.86	0.61
a <sup>†</sup>	15.01	+0.67	+0.37	+0.28	12.16	0.40
b <sup>†</sup>	15.14	+0.51	+0.31	-0.03	13.80	0.56
c <sup>†</sup>	15.42	+0.87	+0.16	—	—	—
d <sup>†</sup>	15.68	+0.95	+0.35	+0.45	11.84	0.43
e <sup>†</sup>	15.87	+0.50	+0.34	+0.19	13.44	0.32
f <sup>†</sup>	16.02	+0.75	+0.20	+0.46	12.06	0.32
g <sup>†</sup>	16.17	+0.89	+0.20	—	—	—

<sup>†</sup> UBV photographic magnitudes

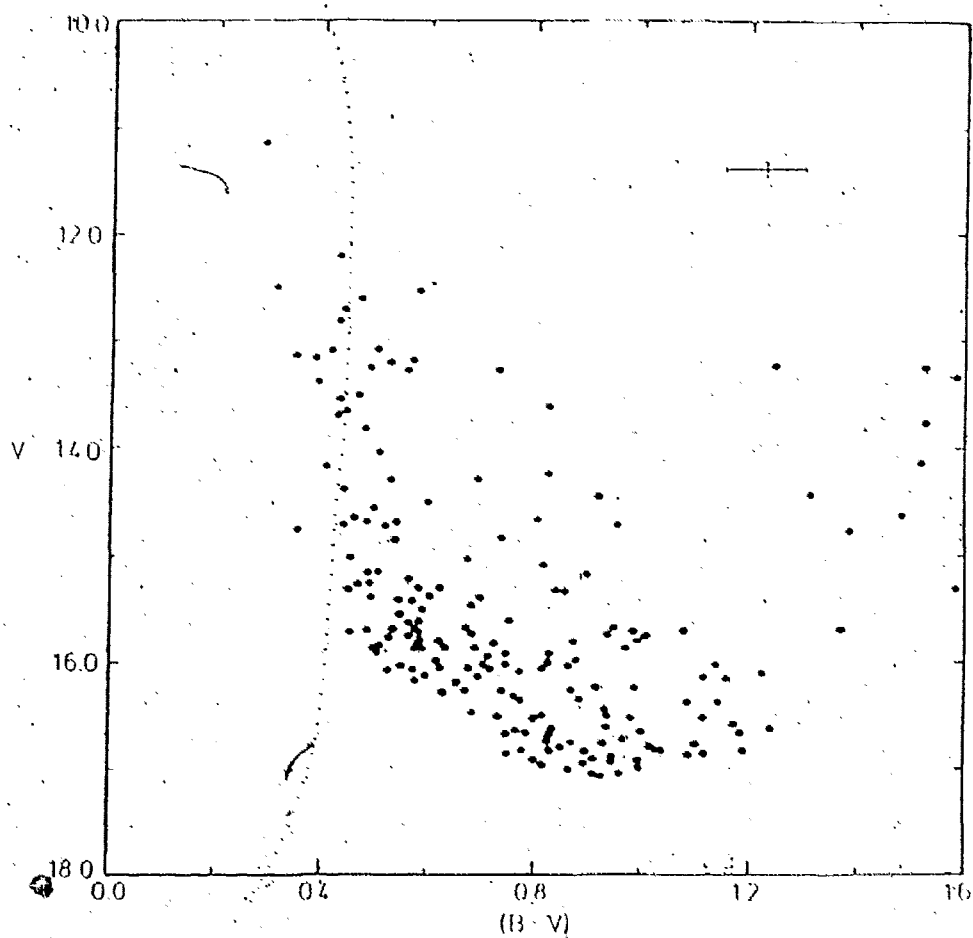
<sup>‡</sup> U photographic magnitudes

Figure 10



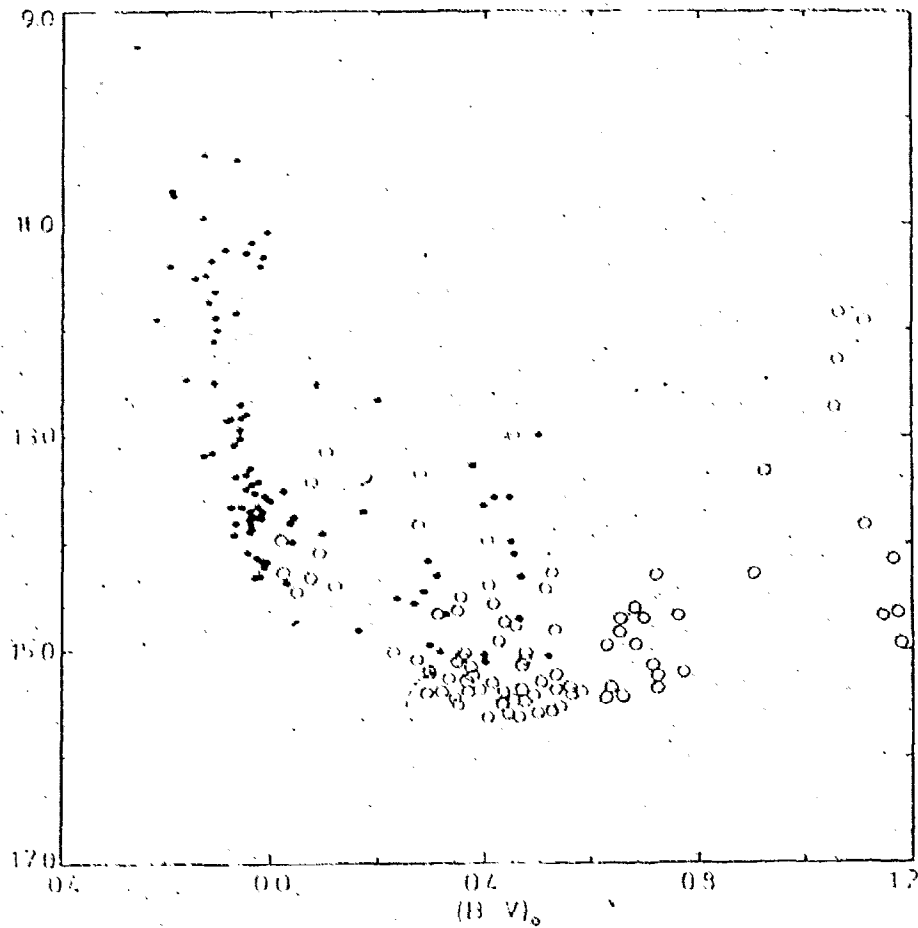
Two Colour Diagram of the stars in the field of NGC 7790. The intrinsic two colour relation and reddening slope used in the analysis have also been plotted. The error bars represent one sigma (see text for details).

Figure 11



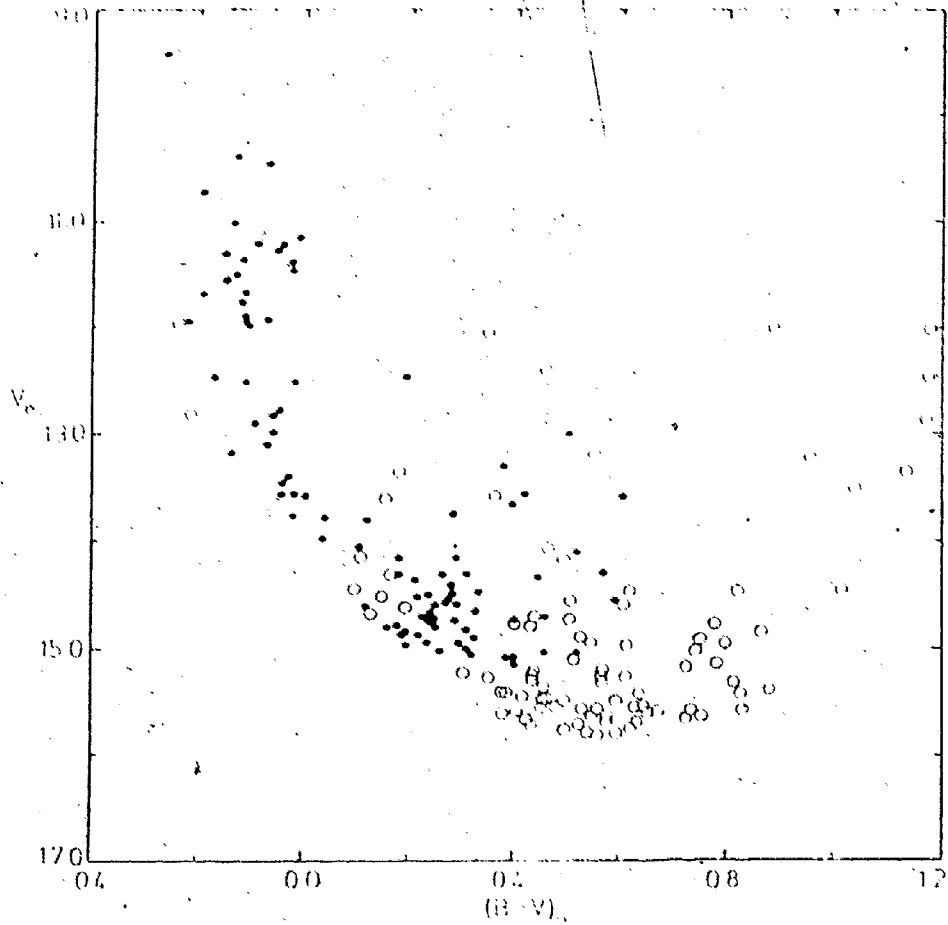
Colour Magnitude Diagram of the stars in the field of NGC 7790. The error bars represent one sigma (see text for details).

Figure 12



Intrinsic Colour Magnitude Diagram of NGC 7790 (filled circles represent individually dereddened stars and open circles represent stars dereddened with mean  $E_{B-V}$ ). The larger reddening solutions were used for most stars. Note the paucity of stars between  $(B - V)_0 = 0.10$  and  $(B - V)_0 = 0.20$ .

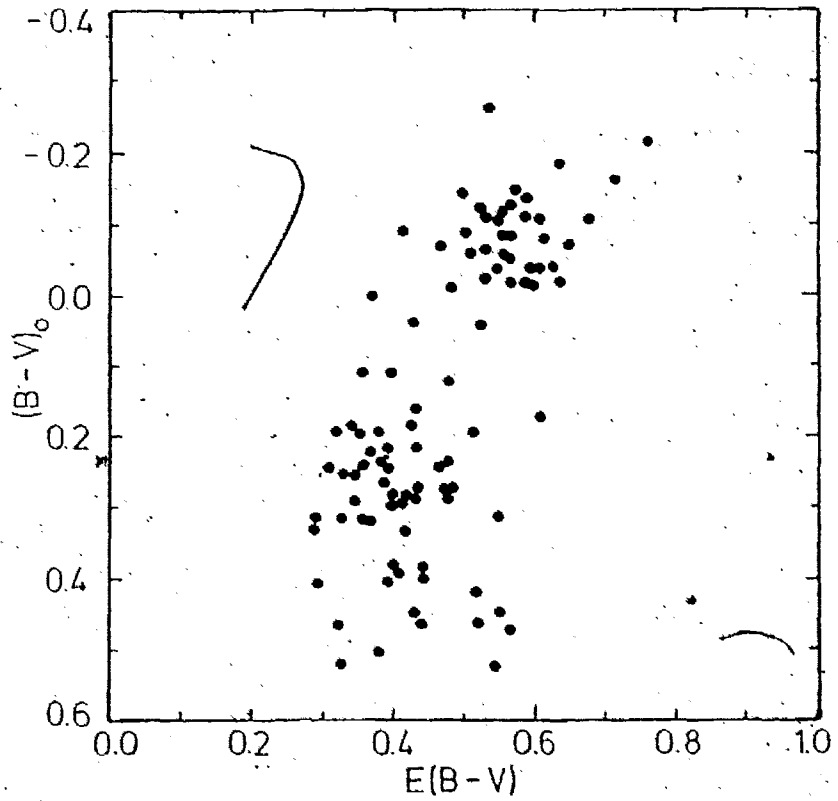
Figure 13



Intrinsic Colour Magnitude Diagram of NGC 7790 (filled circles represent individually dereddened stars and open circles represent stars dereddened with mean  $E_{B-V}$ ). The smaller reddening solutions were used for most stars. There appears to be a relatively smooth distribution of stars with respect to spectral type.



Figure 14



Intrinsic colour versus reddening plot. Note that stars with  $(B - V)_0 < 0.10$  tend to have larger reddenings than stars with  $(B - V)_0 > 0.10$ .

The data were dereddened to Johnson's (1966) intrinsic colour relation for main sequence stars, and multiple reddening solutions were noted. Figure 10 shows a two colour plot of the stars and the intrinsic colour relation used. In particular, some stars have unique reddening solutions, and these helped to describe the spatial variation of reddening across the field. The process of choosing the correct solution required careful consideration. Many stars in the BA star bump had two reasonable solutions. A colour magnitude diagram was plotted using both sets of reddening solutions. Ideally, the dereddening process should not introduce any peculiarities into the colour magnitude diagram that are not present in the original (see Fig. 11). Adopting the larger reddening solutions for many stars led to an artificial feature not seen in colour magnitude diagrams of open clusters, namely a gap in the main sequence around  $(B - V)_0 \sim 0.1$  (see Fig. 12). Systematically choosing the larger reddening solutions led to an undersampling of stars with  $(B - V)_0 \gtrsim 0.0$ . This undersampling was particularly noticeable for A-type stars. However, the plot with smaller reddening solutions does not exhibit this problem (see Fig. 13). Since a relatively smooth distribution of stars exists along the main sequence with the frequency of stars steadily increasing with later spectral type, the smaller reddening solutions for most stars near the BA star bump seem likely to be correct.

The intrinsic colour versus reddening plot clearly showed that late-type stars had systematically smaller reddenings than early-type stars (see Fig. 14). This

trend was also evident if the larger reddening solutions were adopted. A similar effect can be seen in several other clusters (Turner, private communication), and a possible explanation for this phenomenon (still only a working hypothesis) is circumstellar reddening. For stars with  $(B - V)_0 > 0.10$ ,  $\langle E_{B-V} \rangle = 0.40 \pm 0.06$ , while for stars with  $(B - V)_0 < 0.10$ ,  $\langle E_{B-V} \rangle = 0.57 \pm 0.07$ . This dispersion in reddening is identical to what is seen in other clusters (Turner, private communication). The overall mean reddening of the measured stars is 0.48. However, the trend found in the reddening makes the usefulness of a mean cluster reddening somewhat questionable. A similar trend was also found in  $(U - B)$  colour excesses. Stars with  $(U - B)_0 < -0.06$  had  $\langle E_{U-B} \rangle = 0.44 \pm 0.06$ , while stars with  $(U - B)_0 > -0.06$  had  $\langle E_{U-B} \rangle = 0.29 \pm 0.07$ . The trend in reddening for early-type stars cannot be explained by the evolution of these stars away from the ZAMS. Stars with  $(B - V)_0 \lesssim -0.10$  appear to have evolved away from the ZAMS (see Fig. 19). Although they will have slighter redder intrinsic colours than stars on the ZAMS, the difference is too small to account for the observed trend. Most authors have found  $\langle E_{B-V} \rangle > 0.50$  for NGC 7790 (Sandage 1958, Pedreros *et al.* 1984, Mateo and Madore 1988), but this clearly applies only to the cluster B stars. The trend found in the present study may explain some of the discrepancies in the published distance estimates for NGC 7790, since Zero Age Main Sequence (ZAMS) fits clearly depend upon the adopted reddenings of the faint stars which are heavily weighted in the fits.

Sandage (1958) calculated the reddening of NGC 7790 to be  $E_{B-V} = 0.52$ . His study had a strong selection effect favouring early-type stars because of its magnitude limit. The magnitude limit was particularly severe in the U passband, and restricted the number of stars that could be individually dereddened. Sandage therefore observed virtually no stars with  $(B - V)_0 > 0.0$ . Owing to the trend found in the reddening, one would expect him to obtain a larger mean reddening than that found in this study, but his results are affected by the systematically blue colours of his photoelectric photometry, which produces systematically small colour excesses. Pedreros *et al.* (1984) used essentially the same data and dereddened each star individually, yet arrived at a much larger value for the mean reddening; they found  $\langle E_{B-V} \rangle = 0.64$ . The large gap seen in their observed colour magnitude diagram for cluster members is some cause for concern and suggests a problem with the colours or with the adopted reddening solution (see Fig. 15 a,b). The gap is not present in their observed colour magnitude diagram, which hints at a problem with the dereddening technique adopted.

The value of  $\langle E_{B-V} \rangle$  for a cluster can depend on the method used to obtain it. One fast method still frequently used is to shift the two colour data for cluster stars to a best fit with the intrinsic relation. If emphasis is placed on matching stars in one particular spectral range, systematic trends in the reddening go unnoticed. A poor fit over a particular spectral range could easily be attributed to scatter in the data. It therefore seems desirable to individually deredden stars to ensure

that no such trends in the data are overlooked.

The above method of shifting the stars to an intrinsic two-colour relation was used by Mateo and Madore (1988) in their study; they obtained  $\langle E_{B-V} \rangle = 0.56$ . An examination of their two colour diagram reveals that the stars in the B to A spectral range fit the intrinsic relation quite well, while later type stars appear to lie systematically on the blue side of the relation (see Fig. 16). It would appear that a smaller reddening would be more appropriate for these stars as indicated by the present, more detailed, study. The reddening they found for stars that best fit the intrinsic two colour relation (i.e.  $(B - V)_0 < 0.10$ ) is in close agreement with the reddening found for similar stars by this author. The small difference of 0.01 in the values of  $\langle E_{B-V} \rangle$  can be explained by the different reddening slope used, which points out the need to adopt reddening relations valid for the region of the Galaxy being studied.

A comparison the two colour plots of this study and Mateo and Madore (1988) reveals a marked difference between the two sets of data (see Figs. 16a,b). The plot from this study shows that stars are systematically above the intrinsic relation. This difference is too large to be explained by the uncertainties in  $(B - V)$  and  $(U - B)$  in the present study. Similarly, systematic errors in the calibration relations large enough to explain the difference seem very unlikely. The source of the discrepancy between the two studies is not known.

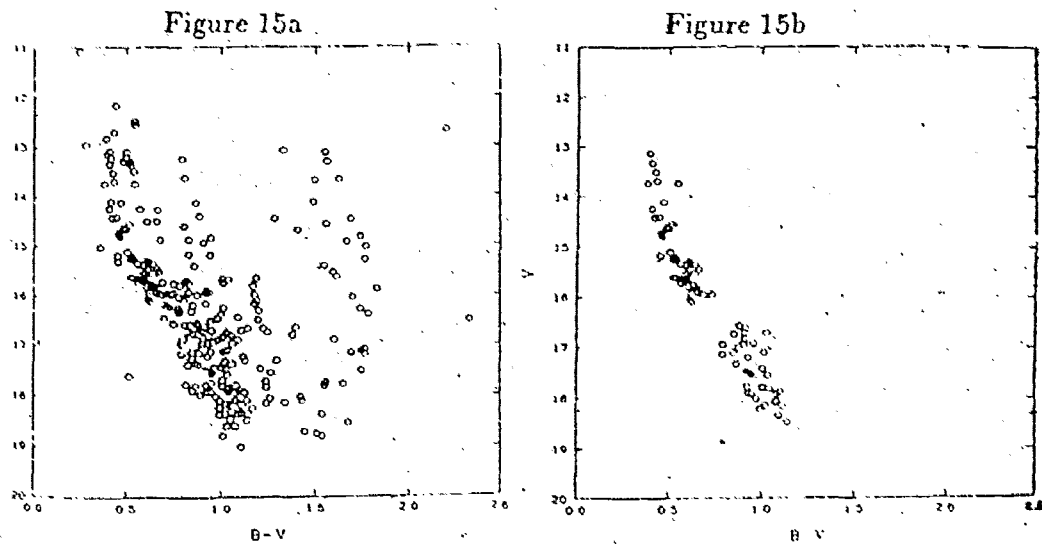
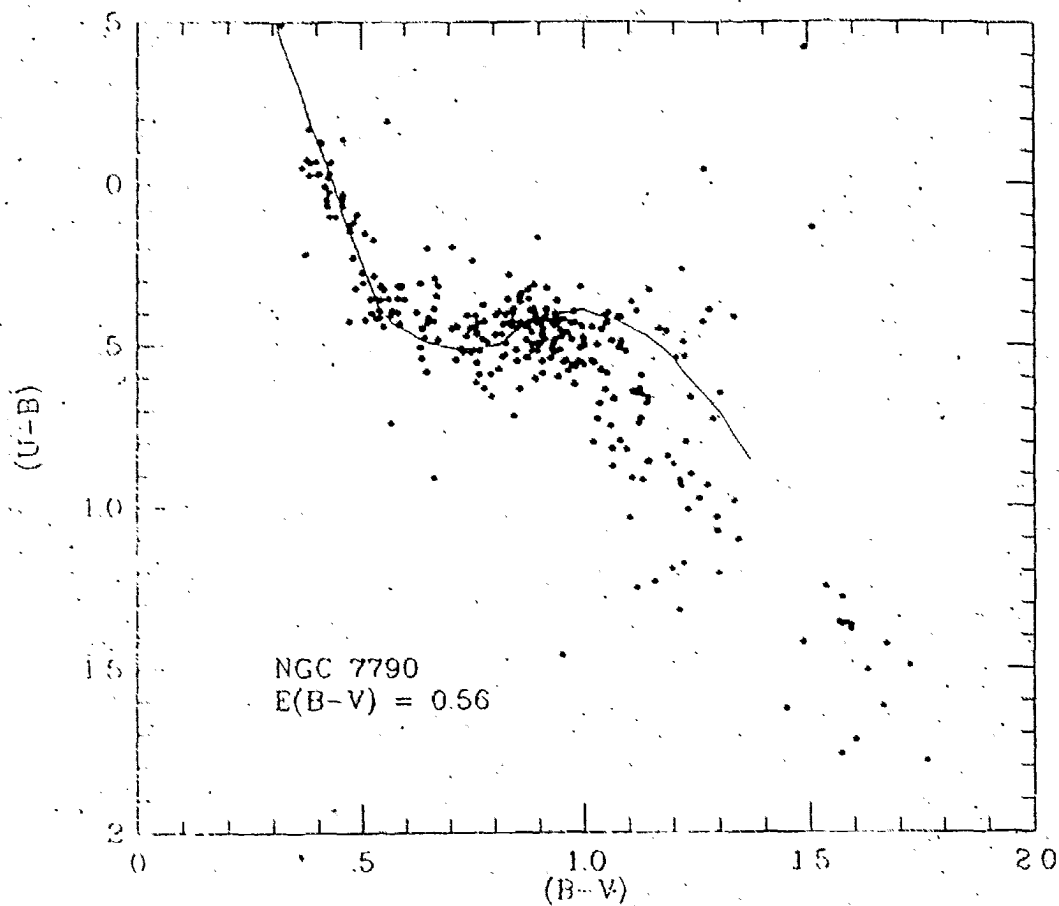


Figure 15a: Colour magnitude diagram from Pedreros *et al.* (1984) for stars in the field of NGC 7790.

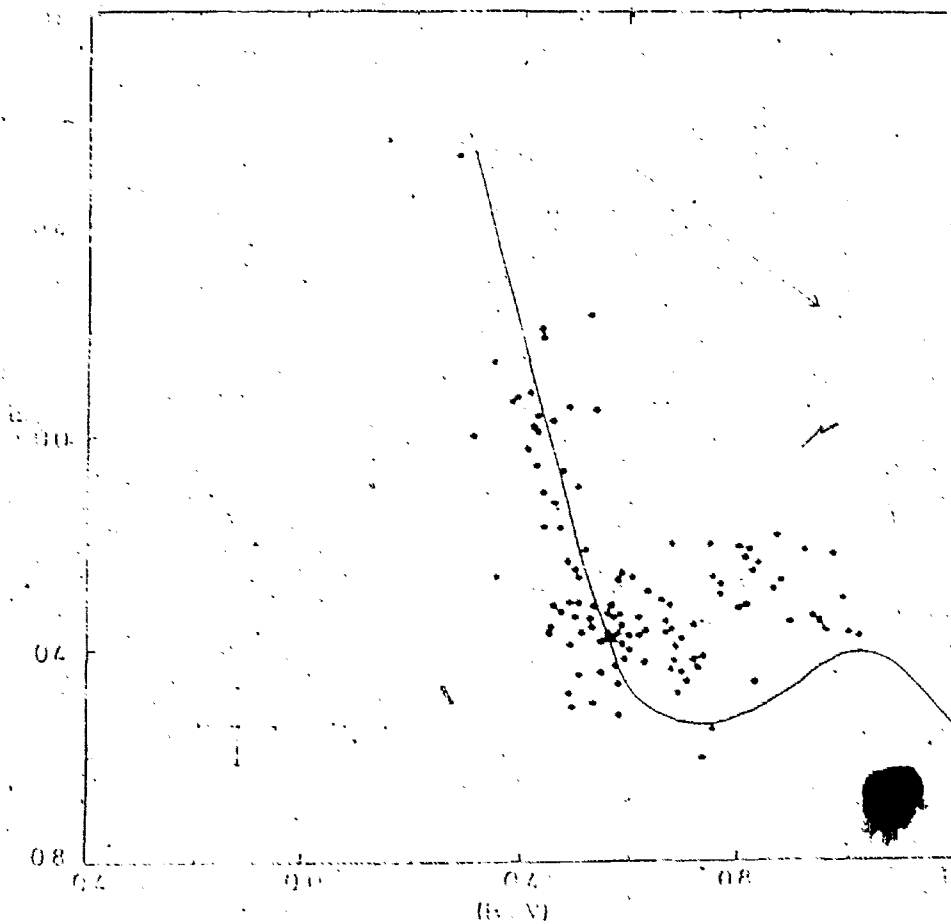
Figure 15b: Colour magnitude diagram of probable cluster members of NGC 7790 from Pedreros *et al.* (1984). Note the gap in the main sequence that is not present in Fig 15a.

Figure 16a



Two colour diagram of stars in the field of NGC 7790 from Mateo and Madore (1988). Note that the intrinsic colour relation fits stars of spectral class B and A, while stars later than A appear to be systematically on the blue side of the intrinsic colour relation.

Figure 16b



Two colour diagram of stars in the field of NGC 7790 from this study. The intrinsic relation has been shifted by  $E_{B-v} = 0.57$  along a reddening slope of 0.76. Note that stars after the BA hump appear to be systematically above the intrinsic relation. Compare with Fig. 16a.

The field of NGC 7790 was examined for any spatial correlations in the extinction. Since the early-type stars exhibited systematically larger colour excesses, possibly due to circumstellar reddening, the analysis was restricted to values of  $E_{B-V}$  for stars with  $(B - V)_0 > 0.10$  (see Fig. 17). A plot was also constructed that included all stars. There were no obvious spatial correlations in the colour excesses in either diagram although some trends were evident in the plot restricted to stars with  $(B - V)_0 > 0.10$ . The estimated error,  $\Delta E_{B-V} = 0^m02$ , is too small to explain the observed differences in reddening between stars in close proximity. This same result was found by other investigators (Sandage 1958, Pedreros *et al.* 1984). It appears that the dust obscuring NGC 7790 has a distinctly patchy distribution.

A variable extinction analysis was undertaken to determine  $R_v$ , the ratio of total to selective absorption. Since the stars in a cluster are at a common distance, the distance modulus of individual stars in the cluster should be the same except for variations due to extinction. The amount of total extinction,  $A_v$ , equals  $R_v \times E_{B-V}$ . Thus,

$$V - M_v = C + R_v \times E_{B-V}$$

where  $C$  equals  $5 \log d - 5$ . Hence, cluster stars on a  $V - M_v$  versus  $E_{B-V}$  plot should lie on a straight line with a slope of  $R_v$ . The values of  $M_v$  used in this analysis are obtained from the dereddened  $(B - V)_0$  colour, under the assumption that the star lies on the ZAMS.

Figure 17

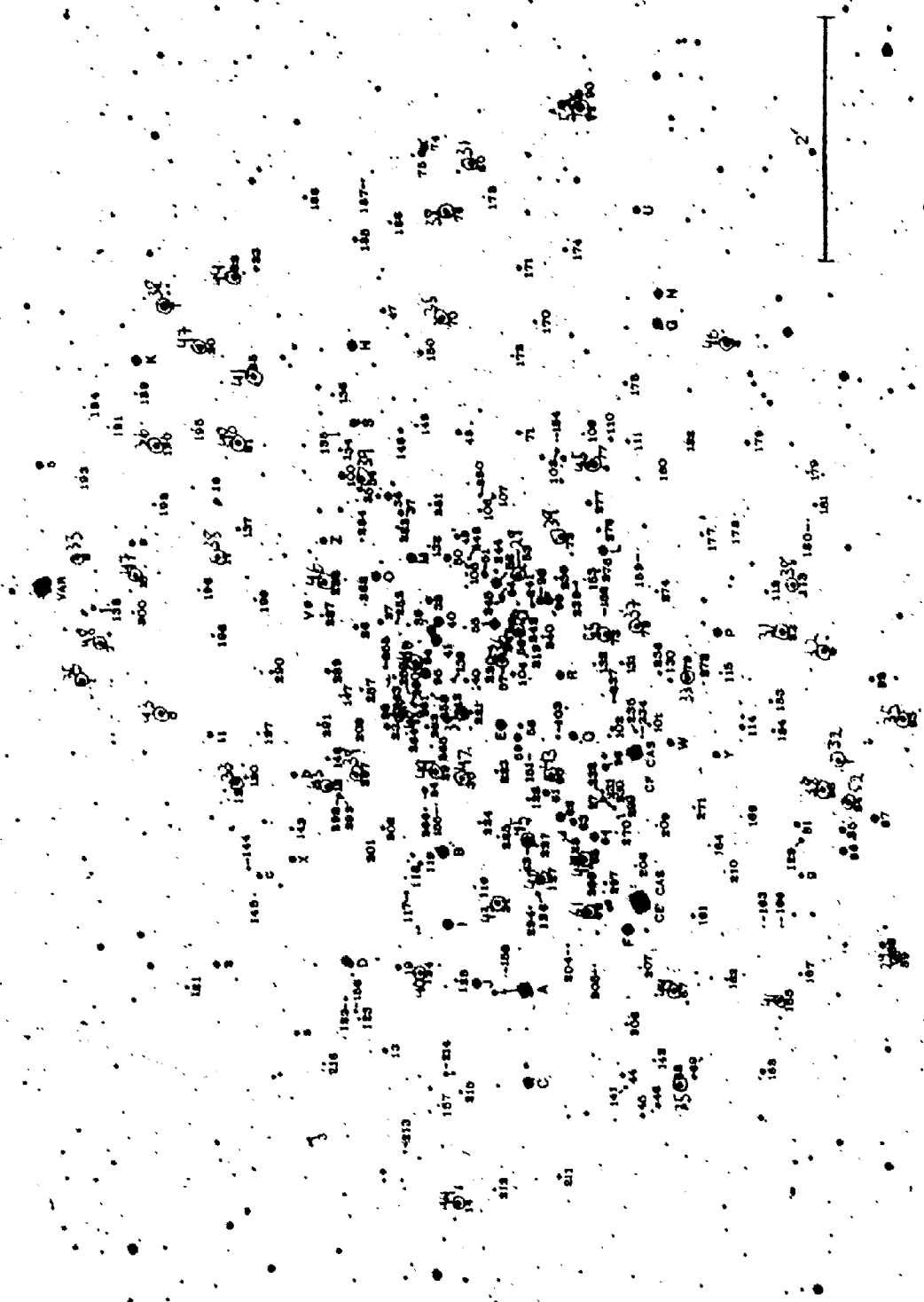
Field Reddening Chart of NGC 7790. The reddening values ( $\times 100$ ) have been plotted in red for stars with  $(B - V)_0 > 0.1$ . Stars in close proximity tend to have similar reddenings, however, numerous exceptions to this observation exist. The reddening across the field of NGC 7790 appears to be patchy.

THE QUALITY OF THIS MICROFICHE IS HEAVILY DEPENDENT UPON THE QUALITY OF THE THESIS SUBMITTED FOR MICROFILMING.

UNFORTUNATELY THE COLOURED ILLUSTRATIONS OF THIS THESIS CAN ONLY YIELD DIFFERENT TONES OF GREY.

LA QUALITE DE CETTE MICROFICHE DEPEND GRANDEMENT DE LA QUALITE DE LA THESE SOUMISE AU MICROFILMAGE.

MALHEUREUSEMENT, LES DIFFERENTES ILLUSTRATIONS EN COULEURS DE CETTE THESE NE PEUVENT DONNER QUE DES TEINTES DE GRIS.



This type of analysis is subject to various sources of error, and it is useful to review these to fully appreciate the limitations of the analysis. The process of dereddening causes random photometric errors in  $(B - V)$  and/or  $(U - B)$  for B and A stars to result in systematic scatter in the variable extinction diagram, producing artificially large values of  $R_v$  (Turner 1976). The use of a reddening line in the two colour plane to deredden stars leads to a correlation between the derived values of  $M_v$  and  $E_{B-V}$ . If  $E_{B-V}$  is underestimated then the derived value of  $M_v$  is too large ( $V - M_v$  is too small), while an overestimate of  $E_{B-V}$  leads to an underestimate of  $M_v$  ( $V - M_v$  too large). As noted by Danks (1987) this forces points to the upper left hand and lower right hand corners of the graph, respectively, thus increasing  $R_v$  above its true value. Contamination by field stars (foreground objects of small reddening or background stars of large reddening) also tends to lead to larger values of  $R_v$ . Binaries and evolved stars will have their absolute luminosities underestimated by assuming ZAMS values and hence will lie systematically away from the main sequence strip. To make use of realistic cluster data the slope of the relation must be determined from a lower envelope of stars.

The variable extinction plot was carefully examined to determine what stars were useful in calculating  $R_v$ . The main sequence was taken to be the lower envelope of stars. This envelope appeared to be approximately  $0^m80$  wide in  $V - M_v$ , if stars 88, 61 and S are rejected as likely background objects (see Fig. 18 a,b). The rejection of stars above this envelope was made in an attempt to

minimize the errors discussed above that result from the inclusion in the analysis of unresolved binaries, or evolved and foreground stars.  $H\beta$  indices measured by Schmidt (1981) were used to calculate  $M_v$  for a few evolved cluster members based on a correlation between absolute magnitude and the  $H\beta$  index. These calculations were added to the plot. Table VI lists the stars used in the calculation of  $R_v$ .

The determination of the slope of a data set requires some consideration of the errors present in the data. Due to the slope of the ZAMS relation a relatively small error in  $(B - V)_0$  leads to a much larger error in absolute magnitude. However, small errors in the colour terms do not result in a large uncertainty in the value of the reddening. Thus, most of the uncertainty in the data used to calculate  $R_v$  lies in the  $V - M_v$  term. Danks (1987) investigated this problem and estimated errors to be  $\Delta(V - M_v) = \pm 0^m39$  and  $\Delta E_{B-V} = \pm 0^m02$ . These errors were considered reasonable estimates for the errors in this study because of the similar reddening parameters, uncertainties in colour, and reddening values between the two studies.

Several methods of analysis were used to estimate the value of  $R_v$ . A least squares fit, assuming the reddening values to be error free, was initially used. Since,  $\Delta(V - M_v)$  is much greater than  $\Delta E_{B-V}$  this is a reasonable approximation. A least squares fit that used weights for the points according to the errors in each coordinate was also computed. A program developed by Reed (1988) was used to

Table VI

Star	$V - M_v$	$E_{B-v}$	Star	$V - M_v$	$E_{B-v}$
1	13.47	0.35	114	14.16	0.63
8	14.21	0.60	127	13.28	0.40
12	13.09	0.33	185	13.15	0.36
14	13.33	0.44	190	13.63	0.36
19	13.57	0.43	267	13.51	0.39
24	13.98	0.62	286	13.44	0.46
27	13.49	0.37	Z	13.86	0.61
34	13.07	0.39	b	13.80	0.56
37	13.64	0.53	d	13.44	0.32
38	13.77	0.53	17	13.59	0.38
51	13.20	0.37	21	13.37	0.48
53	12.74	0.29	R	13.68	0.53
57	13.18	0.36	X	13.92	0.56
63	13.65	0.56	A*	14.11	0.54
67	13.84	0.44	B*	13.35	0.57
68	12.93	0.35	E*	13.82	0.57
70	13.60	0.35	M*	13.66	0.47
72	13.33	0.39	N*	14.13	0.59
78	13.01	0.37	O*	14.34	0.56
79	13.04	0.33	Q*	14.43	0.60
80	13.07	0.31	36*	13.85	0.51
81	13.51	0.52	40*	14.18	0.50
82	12.89	0.31	52*	13.49	0.52
83	13.52	0.38	55*	13.26	0.57
93	13.01	0.35	62*	14.39	0.62
94	13.18	0.40	95*	14.16	0.64

\* $M_v$  from  $H\beta$  data

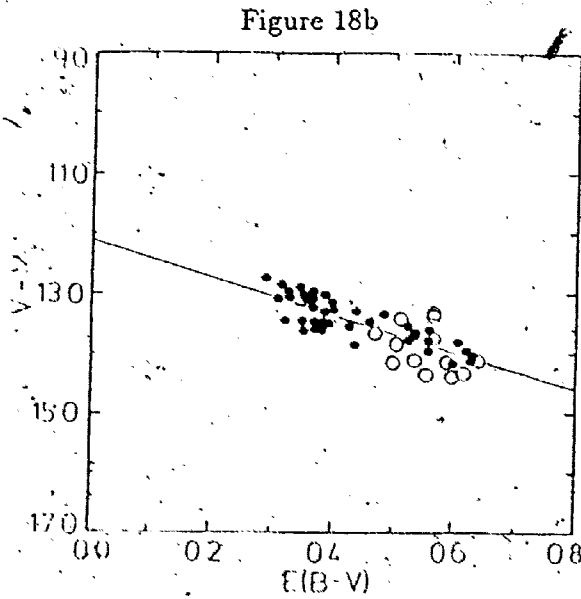
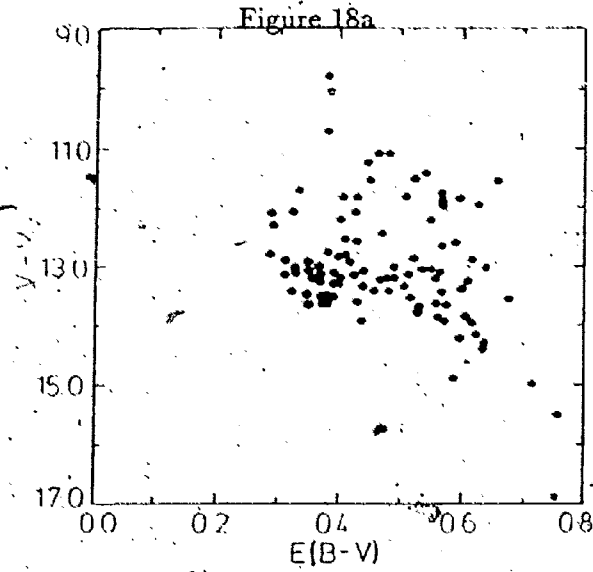


Figure 18a: Variable extinction plot for stars in the field of NGC 7790.

Figure 18b: Variable extinction plot of stars used to calculate  $R_v$  (filled circles represent  $M_v$  values from  $(B-V)_0$ ; open circles represent  $M_v$  values from  $H\beta$  index. A line with  $R_v = 3.1$  and  $V - M_v = 12.09$  has been drawn through the points.

perform this analysis, and error estimates from Danks (1987) were used to generate weights for the data. A least squares analysis can be skewed by points at either end of a fit. Although obviously erroneous points were excluded, the short range of reddening values makes the fits somewhat sensitive to the end point values. To minimize this problem a nonparametric fit was also made. This type of analysis calculates the slope between every pair of points and the median value is adopted as the best fit. A nonparametric fit is less affected by outlying points. The best fits were computed with and without the values from the  $H\beta$  study, and the results are listed in Table VII.

Table VII

Analysis	UBV Data	$H\beta$ & UBV Data
Least Squares (unweighted)	$R_v = 2.95 \pm 0.31$ $V_o - M_v = 12.18 \pm 0.14$	$R_v = 3.18 \pm 0.24$ $V_o - M_v = 12.10 \pm 0.11$
Least Squares (weighted)	$R_v = 2.98 \pm 0.31$ $V_o - M_v = 12.16 \pm 0.14$	$R_v = 3.23 \pm 0.24$ $V_o - M_v = 12.07 \pm 0.14$
Nonparametric	$R_v = 3.13 \pm 1.44$ $V_o - M_v = 12.03 \pm 0.63$	$R_v = 3.31 \pm 1.60$ $V_o - M_v = 12.00 \pm 0.73$

The different fits yield reasonably consistent results. The average values without regard to the errors of the fits are  $R_v = 3.13 \pm 0.14$  (s.d.) and  $V_o - M_v = 12.09 \pm 0.07$  (s.d.). The variable extinction analysis of the field of NGC 7790 indicates that the extinction slope is very close to the galactic average. A value of  $R_v = 3.1$  was adopted for the final reductions. The implications for the present value of the distance modulus will be discussed later.

## ZAMS Fitting

The process of distance determination through ZAMS fitting is a powerful method. However, there are inherent limitations and uncertainties with it. Schmidt (1984) discussed some of these problems. He concluded that overall the effect of the uncertainties will be to increase the distance modulus. Turner (1981) reviewed several important points to ensure that ZAMS fitting is done properly, namely: (1) The choice of a proper ZAMS is essential. This point is illustrated by the difference of  $0^m38$  in the distance modulus of NGC 7790 by Mateo and Madore (1988) using two different ZAMS relations (one observational and one theoretical). (2) The data must be tested to make sure they conform to the Johnson UBV system. Systematic errors are particularly likely to occur near the telescope limit. (3) If possible the method or choice of reddening should be confirmed. Spectroscopic data are very useful for this. (4) It is very important to do the ZAMS fit after the reddening corrections have been applied to the data. Every attempt was made to follow these points in this study.

It is worthwhile to briefly summarize how this present study adhered to these guidelines. The ZAMS used in this study is an empirical relation based upon the Pleiades cluster (Turner 1979) and is tied to a solar metallicity. It is outside the scope of this study to independently confirm the validity of the ZAMS used. However, in the absence of any evidence of metallicity differences between the two

clusters, the ZAMS for the Pleiades should be applicable. The data were carefully reduced to ensure they conformed to the Johnson UBV system and the final results were checked to remove any systematic trends. The plates were carefully examined to determine the useful limit of the stellar images. Some uncertainties existed in the dereddening process, such as in the choice of the reddening slope and the value of  $R_v$ . However, as much as the available data allowed, the reddening parameters for the field of NGC 7790 were calculated to reduce any errors introduced by relying solely on galactic averages.

An important part of any ZAMS fitting analysis is to obtain reliable data for as much of the main sequence as possible. This enables greater confidence to be placed in the fit to the main sequence. Most stars with magnitudes in all three passbands were individually dereddened. However, some stars had colours such that they fell below the intrinsic two colour relation when dereddened along the reddening slope; no individual reddening solutions were possible for these stars. Alternately, some stars had an anomalously large reddening solution because the extrapolated reddening line fell above the F star bump on the two colour relation. Instead of adopting a tangent point solution for these two cases, these stars were dereddened with a mean reddening appropriate for their colour i.e.  $E_{B-V} = 0.40$ . A number of stars had magnitudes in only the V and B passbands. To deredden these stars a mean  $E_{B-V}$  had to be used. The value adopted for  $(E_{B-V})$  was 0.40, which is the mean reddening for stars with  $(B - V)_0 > 0.10$ .

This was considered applicable because stars that were too faint to measure in U invariably had  $(B - V)_0 > 0.10$ . This mean value along with the extinction slope of 3.1 was used to deredden the stars. Table VIII lists the results for both dereddening procedures. The stars listed following the last photoelectric standard in Table VIII (i.e. star X) are those for which a mean reddening was used. Probable members are denoted by M, likely binary members by MB and nonmembers by NM.

Table VIII

Star	$V_0$	$(B - V)_0$	$(U - B)_0$	$V_0 - M_v$	Comment
1	14.79	+0.18	+0.11	12.40	M
6	15.03	+0.52	+0.00	10.68	NM
7	14.46	+0.28	+0.08	11.61	NM
8	13.76	-0.02	-0.07	12.34	M
10	14.56	+0.27	+0.08	11.77	NM
12	14.73	+0.25	+0.09	12.06	M
14	14.50	+0.22	+0.10	11.97	MB
17	14.85	+0.19	+0.11	12.42	M
18	14.08	+0.29	+0.07	11.21	NM
19	13.97	+0.04	+0.05	12.24	M
20	14.32	+0.57	+0.05	9.67	NM
21	14.49	+0.23	+0.10	11.87	NM
24	13.29	-0.04	-0.13	12.07	M
25	14.17	+0.29	+0.07	11.28	NM
27	14.89	+0.22	+0.10	12.34	M
28	13.82	+0.12	+0.11	11.68	NM
29	14.31	+0.27	+0.08	11.53	NM
30	14.66	+0.32	+0.05	11.61	NM
31	14.69	+0.47	-0.02	10.70	NM
32	14.52	+0.27	+0.08	11.73	NM
34	14.38	+0.21	+0.10	11.86	NM
35	14.11	+0.52	+0.00	9.76	NM
36	11.98	-0.10	-0.35	10.52	M
37	13.76	+0.04	+0.05	12.01	M
38	13.08	-0.07	-0.22	12.13	M
40	11.54	-0.15	-0.52	11.57	M
41	11.23	-0.09	-0.31	10.50	NM
42	13.57	+0.60	+0.09	8.75	NM
43	13.28	+0.39	+0.01	9.84	NM
51	13.59	+0.00	-0.01	12.05	M
52	11.51	-0.13	-0.46	11.28	M
53	14.84	+0.31	+0.06	11.84	MB
55	11.32	-0.15	-0.51	11.31	M
56	14.47	+0.33	+0.05	11.39	NM
57	14.74	+0.25	+0.09	12.07	M
60	14.16	+0.18	+0.11	11.76	NM
61	12.45	-0.17	-0.58	12.74	NM
62	11.35	-0.12	-0.40	10.95	M

Table VIII (continued)

Star	$V_0$	$(B - V)_0$	$(U - B)_0$	$V_0 - M_V$	Comment
63	12.97	-0.06	+0.28	11.91	M
65	14.41	+0.28	+0.08	11.57	NM
67	14.80	+0.16	+0.11	12.49	NM
68	14.72	+0.29	+0.07	11.85	MB
70	14.96	+0.19	+0.11	12.51	M
72	14.77	+0.25	+0.09	12.11	M
73	14.30	+0.31	+0.06	11.32	NM
76	14.55	+0.59	+0.08	9.51	NM
77	13.65	+0.40	+0.00	10.16	NM
78	14.90	+0.32	+0.05	11.85	MB
79	15.01	+0.31	+0.06	12.02	M
80	14.75	+0.24	+0.09	12.11	M
81	13.56	-0.02	-0.05	11.89	M
82	14.32	+0.18	+0.11	11.93	MB
83	14.96	+0.23	+0.10	12.34	M
84	13.56	+0.42	-0.01	9.88	NM
86	11.91	-0.11	-0.37	11.43	M
87	11.69	-0.19	-0.68	12.35	NM
88	13.17	-0.14	-0.47	13.01	NM
89	14.77	+0.41	+0.00	11.21	NM
91	12.65	+0.19	+0.11	10.19	NM
93	14.62	+0.25	+0.09	11.93	MB
94	14.03	+0.11	+0.11	11.94	M
95	10.72	-0.19	-0.67	11.37	M
99	11.27	-0.05	-0.16	10.12	NM
100	12.80	-0.06	-0.20	11.74	M
113	15.10	+0.40	+0.00	11.58	MB
114	13.46	-0.04	-0.12	12.21	M
124	15.08	+0.40	+0.00	11.56	MB
127	14.94	+0.29	+0.06	12.04	M
165	15.07	+0.39	+0.00	11.59	MB
185	15.06	+0.32	+0.05	12.03	M
190	14.61	+0.11	+0.11	12.52	M
267	15.03	+0.26	+0.09	12.31	M
286	14.64	+0.24	+0.09	12.00	M
T	13.01	+0.50	-0.01	8.79	NM
V	12.79	-0.05	-0.17	11.66	M
Z	12.83	-0.08	-0.25	11.96	M

Table VIII (continued)

Star	$V_0$	$(B - V)_0$	$(U - B)_0$	$V_0 - M_v$	Comment
a	13.76	+0.28	+0.07	10.91	NM
b	13.42	-0.03	-0.09	12.08	M
d	14.35	+0.45	-0.02	10.51	NM
e	14.87	+0.19	+0.11	12.44	M
f	15.03	+0.46	-0.02	11.07	NM
A	9.42	-0.26	-0.97	11.32	M
B	10.41	-0.13	-0.44	10.18	MB
C	10.47	-0.07	+0.22	9.52	M
D	11.13	-0.01	-0.04	9.63	MB
E	11.01	-0.14	-0.47	10.85	M
G	11.24	-0.04	-0.11	9.99	NM
H	11.44	-0.02	-0.07	10.02	NM
J	11.39	-0.02	-0.06	9.97	NM
M	11.91	-0.07	-0.46	10.96	M
N	11.67	-0.11	-0.37	10.72	NM
O	11.78	-0.12	-0.41	11.42	M
Q	11.93	-0.11	-0.39	11.48	M
R	12.52	-0.11	-0.37	12.03	M
S	11.94	-0.22	-0.77	13.11	NM
U	12.53	-0.02	-0.07	11.04	NM
X	12.91	-0.09	-0.30	12.18	M
2	13.21	+0.95	+0.49	—	NM
3	14.46	+0.828	—	—	NM
4	12.09	+1.24	+1.11	—	NM
5	12.43	+1.18	+0.76	—	NM
9	14.12	+1.38	—	—	NM
11	13.66	+1.36	—	—	NM
13	14.14	+0.11	+0.22	12.05	M
16	14.09	+0.24	—	11.45	NM
23	13.57	+1.46	—	—	NM
26	14.47	+0.10	+0.19	12.34	M
33	14.66	+0.12	+0.16	12.52	M
39	11.96	-0.23	-0.11	13.31	NM
44	14.80	+0.44	-0.08	10.98	NM
45	14.69	+0.44	-0.07	10.87	NM
46	14.73	+0.51	-0.02	10.44	NM
47	14.83	+0.40	—	11.31	NM
48	14.05	+0.47	-0.05	10.02	NM

Table VIII (continued)

Star	$V_0$	$(B - V)_0$	$(U - B)_0$	$V_0 - M_v$	Comment
49	14.60	+0.61	-0.07	—	NM
50	13.25	+1.36	+0.81	—	NM
58	14.63	+0.20	+0.23	12.15	M
59	12.86	+1.18	+0.59	—	NM
64	12.41	+1.33	+1.14	—	NM
69	14.44	+0.62	+0.02	—	NM
71	14.52	+0.15	+0.22	12.25	M
74	12.66	-0.66	+1.09	—	NM
85	13.57	+0.36	+0.31	9.31	NM
90	13.18	+0.55	-0.07	8.65	NM
92	14.56	+0.51	+0.10	10.27	NM
96	13.81	+1.44	—	—	NM
97	14.03	+1.24	—	—	NM
98	12.83	-0.21	+0.19	—	NM
101	15.53	+0.64	—	—	NM
102	15.26	+0.57	—	10.61	NM
103	15.32	+0.82	—	—	NM
104	15.21	+0.57	—	10.56	NM
105	15.53	+0.74	—	—	NM
106	15.54	+0.48	—	11.45	MB
107	15.27	+0.44	—	11.45	MB
108	15.58	+0.41	—	11.98	M
110	15.60	+0.38	—	12.21	M
112	15.64	+0.55	—	11.16	NM
117	15.48	+0.50	—	11.26	NM
119	15.14	+0.73	—	—	NM
121	15.49	+0.60	—	10.67	NM
122	15.56	+0.46	—	11.60	M
125	15.79	+0.60	—	10.97	NM
128	15.74	+0.62	—	—	NM
129	14.83	+1.27	—	—	NM
130	15.40	+0.38	—	12.01	M
137	15.41	+0.83	—	—	NM
138	14.96	+0.55	—	10.43	NM
141	15.66	+0.58	—	10.95	NM
143	15.41	+0.66	—	—	NM
146	15.25	+0.62	—	—	NM
148	15.11	+1.30	—	—	NM

Table VIII (continued)

Star	$V_0$	$(B - V)_0$	$(U - B)_0$	$V_0 - M_v$	Comment
150	15.66	+0.43	—	11.91	M
156	15.75	+0.50	—	11.53	M
161	15.41	+0.38	—	12.02	M
167	15.69	+0.64	—	—	NM
168	14.32	+1.29	—	—	NM
171	15.00	+0.71	—	—	NM
174	15.45	+0.42	—	11.81	M
175	15.57	+0.68	—	—	NM
176	14.79	+1.30	—	—	NM
181	15.22	+0.31	—	12.24	M
183	15.25	+0.44	—	11.43	MB
184	15.55	+0.65	—	—	NM
188	15.44	+0.46	—	11.48	MB
202	15.34	+0.57	—	10.69	NM
211	14.99	+0.62	—	—	NM
212	15.80	+0.56	—	11.21	NM
213	15.72	+0.43	—	11.97	M
214	14.88	+0.76	—	—	NM
215	15.69	+0.53	—	11.29	NM
221	15.09	+0.52	—	10.74	NM
228	15.13	+0.79	—	—	NM
230	14.89	+0.80	—	—	NM
231	14.83	+0.87	—	—	NM
232	15.64	+0.73	—	—	NM
235	15.54	+0.56	—	11.05	NM
236	15.35	+0.46	—	11.39	MB
241	15.26	+0.36	—	12.00	M
244	15.56	+0.53	—	11.15	NM
248	15.77	+0.55	—	11.24	NM
255	15.60	+0.76	—	—	NM
262	15.24	+0.46	—	11.43	NM
276	15.45	+0.46	—	11.49	M
277	14.76	+0.78	—	—	NM
280	15.37	+0.88	—	—	NM
289	14.42	+1.02	—	—	NM
290	15.55	+0.83	—	—	NM
291	15.58	+0.66	—	—	NM
292	14.29	+0.16	—	11.99	M

Table VIII (continued)

Star	$V_0$	$(B - V)_0$	$(U - B)_0$	$V_0 - M_v$	Comment
297	15.62	+0.58	—	—	NM
I	11.98	+0.89	+0.56	—	NM
K	11.99	+1.18	+1.05	—	NM
L	12.06	+0.35	-0.28	8.87	NM
P	12.39	+0.46	-0.27	9.67	NM
W	13.35	+1.14	+0.82	—	NM
Y	13.51	+1.04	+0.55	—	NM
c	14.17	+0.50	-0.13	9.95	NM
g	14.92	+0.52	-0.09	10.57	NM

The determination of membership for individual stars in a cluster based solely on photometric results cannot be considered conclusive. The lack of spectroscopic, radial velocity and proper motion data hampers the study of individual membership. Some proper motion data for NGC 7790 exist, but unfortunately are of little help. This will be discussed later. Statistical studies of the star fields can give guidelines on the number of expected members. Star counts by Turner (unpublished) indicate that to a magnitude limit of  $\approx 19$  on the red plate of the Palomar Sky Survey the ratio of members to nonmembers is 0.36. Star counts by Pedreros *et al.* (1984) on a U plate with a magnitude limit of  $\approx 20$  yielded a member to nonmember ratio of 0.29 which is consistent with the work of Turner. Since the magnitude limit of this study is only 17.4, the membership ratio could be higher.

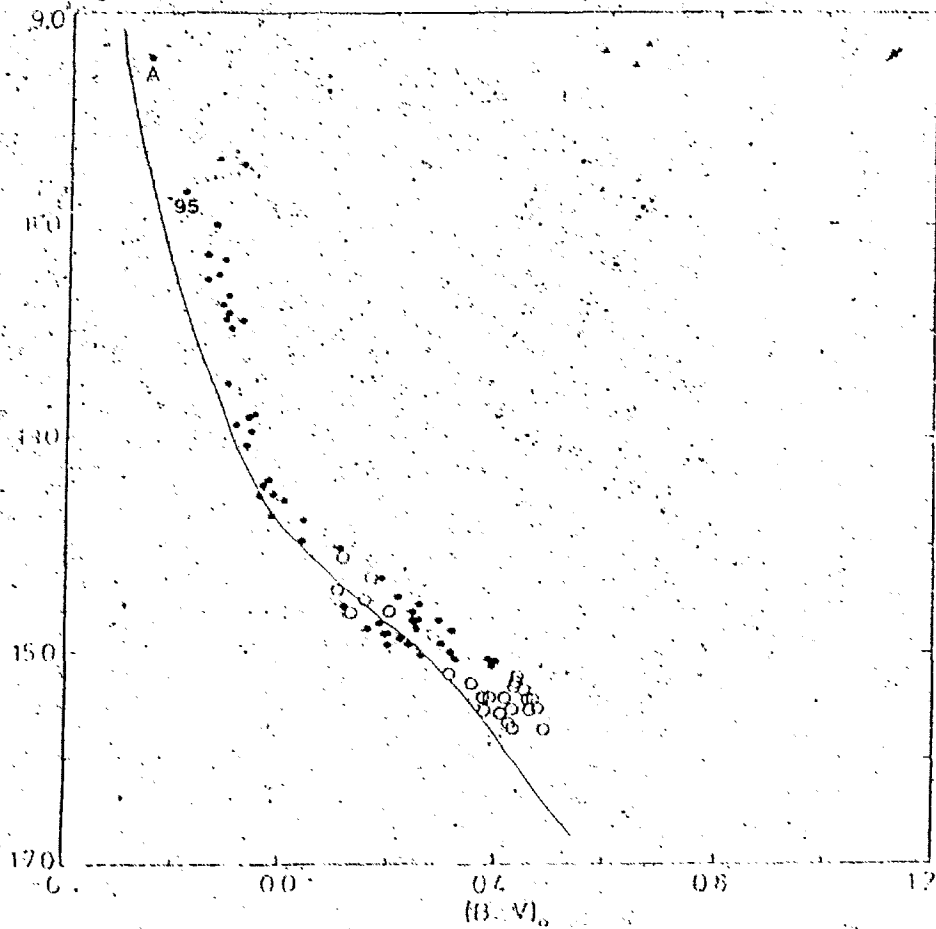
Membership was based here on a star's location in the dereddened colour magnitude diagram. The main sequence spread was assumed to be about  $0^m.5$ . The

sequence of evolved stars is very steep, and, although binaries will be scattered upward, they will still lie close to other cluster members. For this reason the membership strip tends to appear narrower for evolved stars than main sequence stars. Based on the colour magnitude diagram and a plot of  $V_0 - M_v$  vs.  $(B - V)$ , this study contains 120 probable nonmembers, 63 likely members and 16 stars that may be members, but are binaries. The corresponding ratio of members to nonmembers is 0.66. The brighter magnitude limit explains the larger ratio. A study to a fainter magnitude limit would likely contain a greater proportion of field stars due to the rapid increase in the luminosity function at fainter absolute magnitudes. Of course, it is also possible that we have been overly generous in our selection of likely cluster members. Somewhat tighter membership criteria could reduce the ratio to a value closer to 0.4.

A colour magnitude diagram was plotted for stars that were considered probable members of NGC 7790 (see Fig. 19). It is worth noting that stars A and 95 lie close to the ZAMS, but at significantly bluer colours (especially star A) than other cluster members. The distance moduli of these stars from the  $H\beta$  index are 12.42 and 12.18, respectively, which makes them likely cluster members. Their location in the colour magnitude diagram therefore suggests that they are blue stragglers.

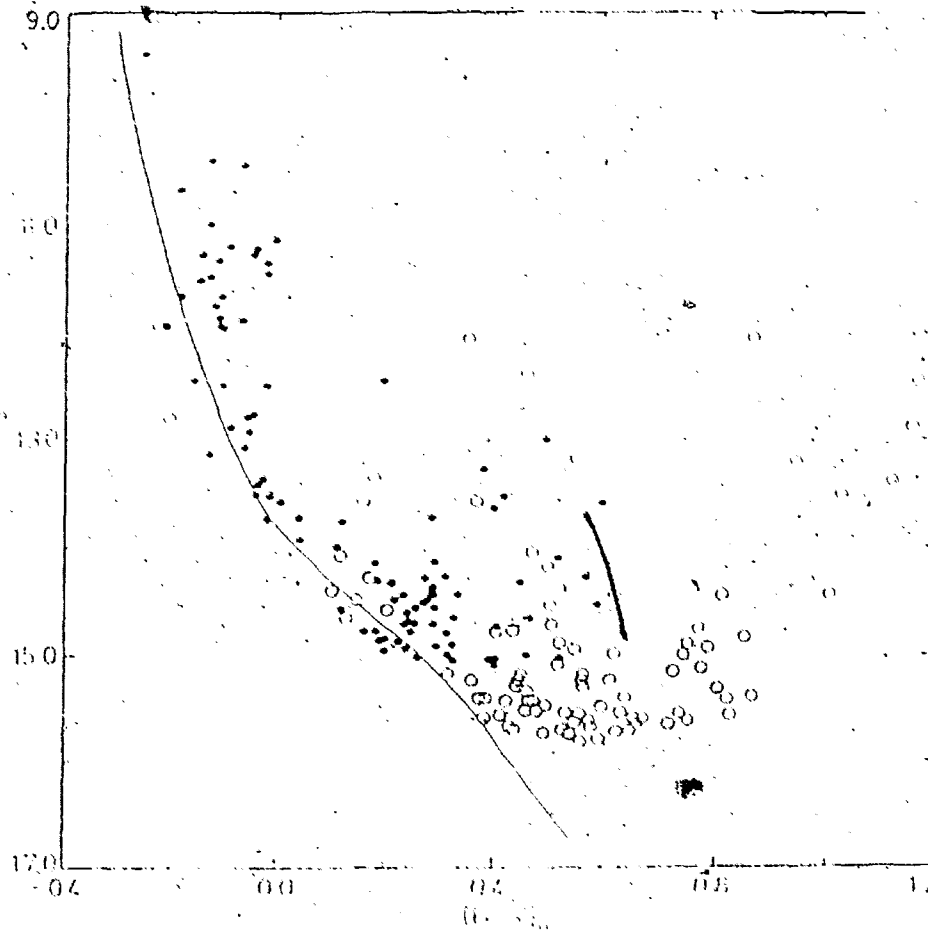
There are several possible methods of determining the distance modulus of

Figure 19



Intrinsic colour magnitude diagram for probable members of NGC 7790 (filled circles represent individually dereddened stars; open circles represent stars dereddened with mean  $E_{B-V}$ ; triangles represent Cepheids in NGC 7790). A ZAMS has been fit to the main sequence (see Fig. 20). Note that stars A and 95 lie close to the ZAMS, but are bluer than other probable cluster members. A ZAMS has been fit to the data yielding a distance modulus for the cluster of  $12.25 \pm 0.10$ . The error is an estimate of the uncertainty in the fit.

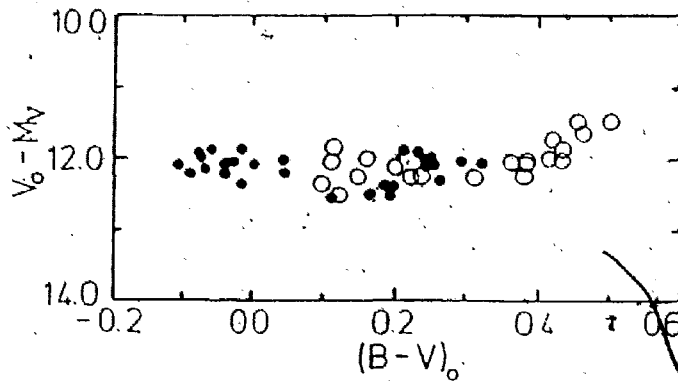
Figure 20



Intrinsic colour magnitude diagram for stars in the field of NGC 7790 (filled circles represent individually dereddened stars; open circles represent stars dereddened with mean  $E_{B-V}$ ). The ZAMS plotted assumes a distance modulus of 12.25.

NGC 7790. One approach is a sliding main sequence fit which yields a distance modulus of  $12.25 \pm 0.10$  (see Fig. 19). The error quoted is an estimate of the uncertainty in the fit. An alternative approach is to calculate the distance modulus of individual stars. The distance moduli for unevolved, single stars that were considered members on the basis of their position in the colour magnitude diagram were calculated and plotted against their intrinsic colours. This is essentially the same type of analysis as the variable extinction study. The plot of  $V_0 - M_v$  vs  $(B - V)_0$  shows that a trend exists for stars with  $(B - V)_0 > 0.40$  (see Fig. 21). There are several possible explanations for this trend. These stars lie close to the limits of the extrapolated calibration relations. The trend may result from problems with the calibrations at these faint magnitudes. A less likely possibility is that the pre-main sequence turn-on point has been detected. Finally, it should be noted that a mean reddening was used for these stars which may introduce some additional uncertainties in their distance moduli. Excluding stars with  $(B - V)_0 > 0.40$ , the average distance modulus was calculated to be  $12.15 \pm 0.20$ , where stars with a mean reddening were given a weight of 0.5. This result is consistent with the distance modulus found from the variable extinction analysis, and both analyses should be considered a lower limit because undetected binaries will tend to scatter stars upward in Figs. 18 and 21 and bias the results toward a systematically small value. The distance modulus from the sliding fit,  $V_0 - M_v = 12.25$ , which corresponds to a distance of  $2.82 \pm 0.13$  kpc, was adopted for the final solution.

Figure 21



Distance modulus versus intrinsic colour (filled circles represent individually dereddened stars; open circles represent stars dereddened with mean  $E_{B-V}$ ) for probable, unevolved, single cluster members. The distance moduli of stars with  $(B - V)_0 > 0.40$  appear to decrease with increasing  $(B - V)_0$ .

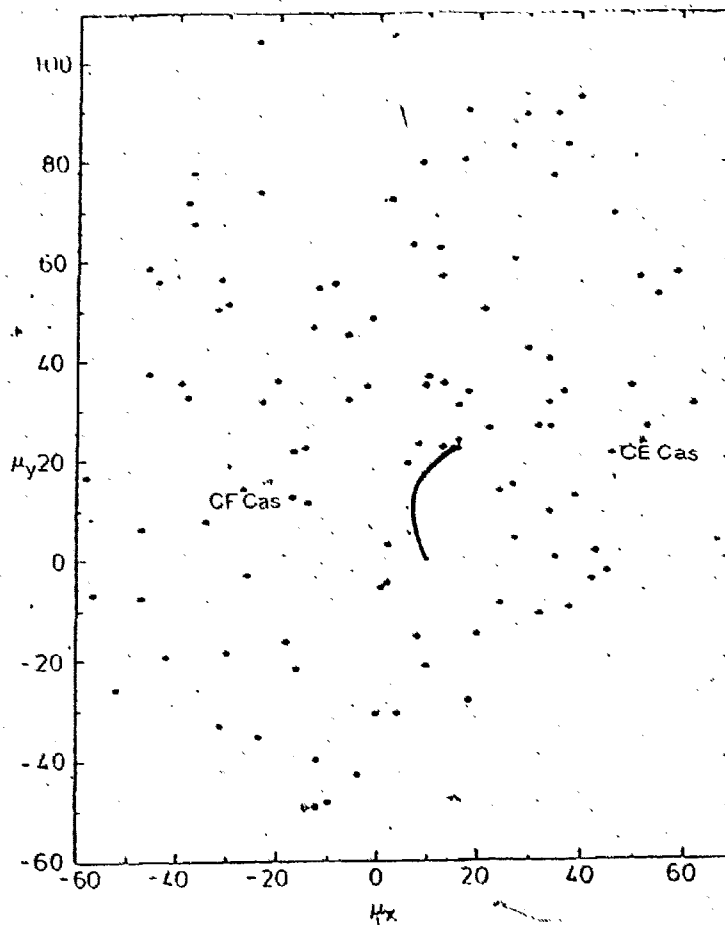
The distance modulus from this study lies at the lower end of the range of past estimates for the distance modulus of NGC 7790 (see Table I). It was noted earlier that Schmidt (1984) has found that errors inherent in the old ZAMS fitting technique tend to result in overestimated values for the distance modulus. The present results imply that these inherent uncertainties in the old ZAMS fitting process have been minimized in the present study. The distance found here for NGC 7790 is quite close to that of Mateo and Madore (1988). They found a distance modulus of 12.20 using the same ZAMS employed here. They also used a theoretical relation by Vandenberg and Bridges (1984) which gave  $V_0 - M_v = 12.58$ . Their final result was the average of the two. There are also several important differences in the details of their analysis compared with those employed here. For example, Mateo and Madore assumed  $E_{U-B}/E_{B-V} = 0.72$ , the value for the galactic average, while this study assumed  $E_{U-B}/E_{B-V} = 0.76$ , a result applica-

ble to the field of the cluster. More important are differences in the methods of dereddening cluster stars, (mean reddenings versus individual reddenings), which were discussed earlier. Despite these differences the distance moduli from the two studies are in remarkably close agreement.

### Proper Motion Study

The membership of CE Cas a and b and CF Cas in NGC 7790 is a well accepted fact in the literature. One of the tests for cluster membership is a common space motion with the cluster (proper motion, radial velocity). However, no proper motion studies of NGC 7790 exist other than those by Frolov (1977, 1979). This can be partly explained by the fact that NGC 7790 is  $\sim 2.8$  kpc distant and hence requires a considerable period of time before transverse motions become detectable. The initial plates were taken at the Tashkent Observatory between 1923 and 1925. Two sets of second epoch plates were taken, the first set at the Pulkovo Observatory in 1973 and the second set with a Schmidt telescope at the Engelhardt Astronomical Observatory. Both studies by Frolov had a magnitude limit of  $B = 16^m.5$ . The results from the two were combined and examined here. Frolov reported data for stars that were likely members of NGC 7790 based on their relative proper motions and position in a colour magnitude diagram. The proper motions of CF Cas and CE Cas a and b indicate they are probable members of NGC 7790. No radial velocity data have been published that would allow the

Figure 22



$\mu_x$  versus  $\mu_y$  (triangles represent Cepheids). The units of  $\mu_x$  and  $\mu_y$  are in  $10^{-4}$  arcsec per annum. CF Cas, CE Cas a and b appear to have similar relative proper motions as other probable members of NGC 7790.

membership determinations of Frolov (1977, 1979) to be confirmed.

## Chapter Four

### Discussion of Results

The purpose of this project is to accurately determine three calibrating points for the PL and PLC relations. The inferred luminosities of the Cepheids in NGC 7790 from the cluster distance and reddening determination of this study can be usefully compared with their predicted luminosities according to recently published PL and PLC relations. Published periods, apparent magnitudes and colours have been accurately determined for many galactic Cepheids. These values are needed in such a comparison. To calculate the absolute magnitude of an object from its apparent magnitude its reddening and distance must also be accurately known.

A major source of uncertainty in determining the absolute magnitudes of many Cepheids is their reddening. This is certainly the case for the Cepheids in NGC 7790. Ideally, the reddenings would be determined from the individual reddenings for cluster stars lying in close proximity to the Cepheids. However, due to the magnitude limit of this study there are few stars which satisfy this criterion. Furthermore, the reddening of NGC 7790 exhibits a trend with intrinsic colour with a range of  $\sim 0^m17$ . It is not clear what reddening value is physically meaningful for the Cepheids; the smaller value for stars of similar intrinsic colour or the larger value for stars at a closer evolutionary stage in their development. If the trend in reddening is due to circumstellar extinction, then the Cepheids may

also be affected by it. In either case the use of a mean reddening will be necessary, and due to the patchy nature of extinction across the field of NGC 7790, there is no guarantee that the adopted value will be applicable to the individual Cepheids.

Over the years several approaches have been made to calculate individual reddenings of Cepheids. Kraft (1961) calculated the reddening of CF Cas based upon a comparison of photometry and spectral classification at three different phases of the light curve, and obtained  $E_{B-V} = 0.54$ . He also calculated the Cepheid's space reddening by interpolation within isoreddening contours that were derived from the work of Sandage (1958) on NGC 7790, and obtained  $E_{B-V} = 0.57$ . However, problems with the photometry of Sandage (1958), discussed previously, make the usefulness of this last value questionable. Williams (1966) compared the break in the continuum across the G band with the  $(b - v)$  colour index to estimate the amount of interstellar reddening for galactic Cepheids. He found  $E_{B-V} = 0.54$  for CF Cas. Fernie (1967) noted that there is some uncertainty introduced into the reddening by the transformation to the standard Johnson UBV system from other systems. Fernie (1967) quotes a value of  $E_{B-V} = 0.52$  for CF Cas from the work of Williams (1966) using a slightly different transformation. Mianes (1963) used six colour photometry to calculate reddenings for Cepheids. Fernie (1967) quotes a value  $E_{B-V} = 0.54$  for CF Cas from this work. These reddenings, derived from different techniques, seem to be in excellent agreement with each other.

A note of caution is necessary at this point. The methods briefly discussed above are not independent from one other as might originally appear. The work of Williams (1966) serves to illustrate this point. His calibration of the break across the G band versus the  $(b - y)$  index was based upon five Cepheids, one of which was CF Cas. He adopted Kraft's (1961) reddening for CF Cas in his analysis. The close agreement of their reddening estimates for CF Cas is therefore not very surprising, and the fact that several different techniques are used to determine the reddening of Cepheids does not necessarily mean they are independent of each other.

More recent work on the reddening of Cepheids has confirmed the earlier findings for CF Cas. Parsons and Bouw (1971) calculated the colour excess of CF Cas to be 0.53 based on fitting UVBGR photometry with model atmosphere fluxes. Parsons (1971) calibrated the intrinsic colours using a cluster supergiant  $\alpha$  Per that has a reasonably well-established reddening. Parsons and Bell (1975) reexamined the problem with improved model atmosphere calculations and calculated  $E_{B-V} = 0.48$  for CF Cas. Fernie (1982) determined a reddening relation based on BVRI photometry for yellow supergiants that is applicable to Cepheids with a phase correction. The relation is,  $E_{B-V} = -0.255 + 1.727(R - I) - 0.475(B - V) + 1.2A(0.045 - 0.133\phi - 0.13\phi^2 + 0.263\phi^3)$ , where  $A$  is the visual amplitude of the light curve and  $\phi$  is the phase of the observations. Fernie (1982) estimates the uncertainty in  $E_{B-V}$  to be  $0^m04$ . This equation

along with the photoelectric observations from Moffett and Barnes (1984) of CF Cas was used to calculate its reddening. The average reddening from 31 different points on the light curve of CF Cas was calculated to be  $0.60 \pm 0.03$  s.d.. Caldwell and Coulson (1987) (CC hereafter) have found Fernie's relation yields reddenings systematically larger than those of Parsons and Bell (1975), Pei (1978) and Dean, Warren and Cousins (1978). CC found a shift of  $-0^m04$  was required to bring Fernie's results into agreement with the others. Applying this shift to the value from Fernie's relation results in a reddening of 0.56 for CF Cas. The results of individual reddening determinations of CF Cas are summarized in Table IX.

Table IX

$E_{B-V}$	Reference
0.54	Kraft 1961
0.54	Mianes 1963
0.52	Williams 1966
0.53	Parsons and Bouw 1971
0.48	Parsons and Bell 1975
0.56	Fernie 1982 and Moffett and Barnes 1984

The results of various determinations of the reddening of CF Cas are reasonably consistent with an average value of  $\langle E_{B-V} \rangle = 0.528 \pm 0.027$  s.d.. This result indicates that CF Cas has a significantly larger reddening than stars of a similar intrinsic colour ( $\langle E_{B-V} \rangle = 0.40 \pm 0.06$  s.d. for stars with  $(B - V)_0 > 0.10$ ). Stars with  $(B - V)_0 < 0.10$  have an average reddening of  $0.57 \pm 0.07$  s.d., which is in closer agreement with the value for CF Cas. The reddening value adopted for

this study was based on individual determinations for CF Cas, i.e.  $E_{B-V} = 0.528$ .

There are no independent reddening determinations for CE Cas a or CE Cas b, since the small separation (2.3" Opal *et al.* 1987) of the two objects makes photoelectric photometry of the individual Cepheids very difficult. CE Cas a and b were assumed to have the same reddening as CF Cas. It does not seem likely that these Cepheids have the same reddening as stars of similar intrinsic colour, according to the results for CF Cas. Since the mean reddening of early-type stars and the average value from the photometric studies of CF Cas are quite close, the error introduced by using this value for CE Cas a and b should be small.

The PL relation and the PLC relation continue to be reevaluated as new data for Cepheid calibrators become available. Feast and Walker (1987) (FW hereafter) and CC have recently published new calibrations for the relations. Both sets of relations yield essentially the same results, which is not surprising since FW used a PL relation slope derived from earlier work of CC on Cepheids in the Magellanic Clouds. The work of CC will be used here to compare the inferred luminosity of the Cepheids in NGC 7790 with values predicted by the PL and PLC relations. CC derived the following relations:

$$\langle M_v \rangle = -3.116 \log P - 3.77$$

$$\langle M_v \rangle = -4.026 \log P + 2.136 \langle \delta(BV_0) \rangle - 3.74$$

where  $\delta \log P = \log P - 0.9$  and  $\delta \langle (BV_0) \rangle = \langle (B_0) \rangle - \langle (V_0) \rangle - 0.7$ .

CC used 23 Cepheids in clusters and associations for their calibration. Cepheids in clusters were given a weight of 1.0, while those in associations were given a weight of 0.5. The PL relation had a sigma of  $\pm 0^m13$  and the PLC relation a sigma of  $\pm 0^m15$ . Any Cepheids that deviated from the solution by  $\pm 0^m40$  or greater were excluded. This criterion eliminated BB Sgr, WZ Sgr and SZ Tau from the solutions. The three Cepheids in NGC 7790 were all given a weight of 1.0. Since the distance determinations to these Cepheids are not independent, an alternative would have been to give each a weight of 1/3.

The values of  $\langle V \rangle$ ,  $\langle B \rangle$ , and  $\log P$  from CC were adopted for the comparison. As stated above,  $E_{B-V}$  was assumed to be 0.528 for all the Cepheids in the cluster. The distance modulus for NGC 7790 of 12.25 from the present study was used, and  $R_V$  was assumed to be 3.1. Table X lists the relevant data from CC, while Table XI lists the results of the comparison. Note that  $\Delta M_V^{PL} = M_V(\text{present}) - M_V^{PL}$ .

Table X

Object	$\langle V \rangle$	$\langle B \rangle$	$\log P$	$E_{B-V}$
CF Cas	11.136	12.312	0.6880	0.528
CE Cas a	10.916	12.115	0.7111	0.528
CE Cas b	10.988	12.106	0.6512	0.528

Table XI

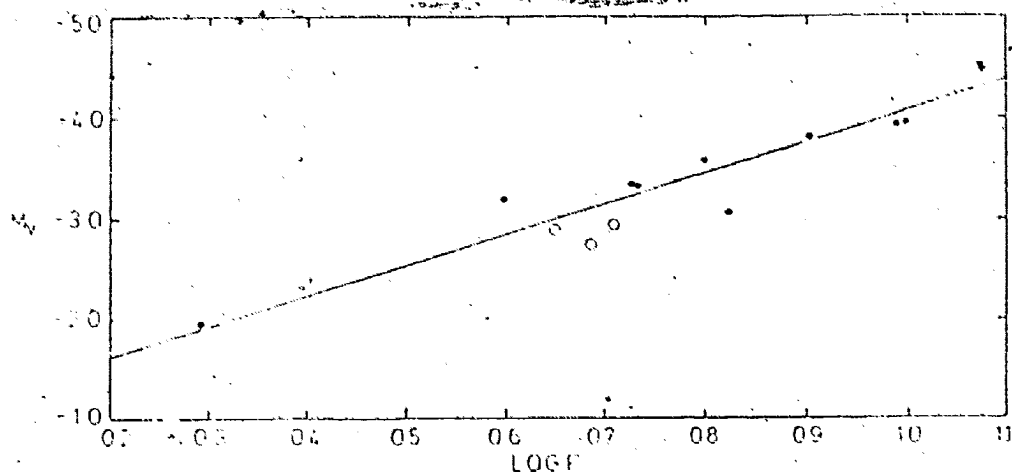
Object	$M_V$	$M_V^{PL}$	$M_V^{PLC}$	$\Delta M_V^{PL}$	$\Delta M_V^{PLC}$
CF Cas	-2.751	-3.111	-2.998	+0.360	+0.247
CE Cas a	-2.968	-3.183	-3.049	+0.215	+0.081
CE Cas b	-2.899	-2.996	-2.974	+0.097	+0.097

These results show that the current distance estimate for NGC 7790 yields luminosities for its Cepheids that are systematically fainter than predicted by the PL and PLC relations. However, the differences are within the limits used by CC for their relations. The differences can be partly explained by the fact that the current distance modulus for NGC 7790 is smaller than that used by CC. A comparison of absolute magnitudes of the three Cepheids with recently determined values for Cepheids of similar period (Turner private communication) shows good agreement (see Fig. 23). Schmidt (1984) argues that the current PL and PLC relations yield absolute magnitudes that are too bright by  $0^m.4$  to  $0^m.6$ . The current results are indeed fainter than the values predicted by PL and PLC relations, but by less than half the amount claimed by Schmidt. The reddenings for the Cepheids of NGC 7790 would have to be smaller by  $\sim 0^m.1$  for discrepancies in the absolute magnitude determinations to agree with the predictions of Schmidt. This seems unlikely based on the reddening determinations for CF Cas. If the mean reddening of B stars is used to calculate the absolute magnitude of the Cepheids they become brighter by  $0^m.13$ . This would bring them into closer agreement with values predicted by the PL and PLC relations of CC.

#### Age of NGC 7790 and Associated Cepheids

Theoretical and empirical relations exist to predict the age of both clusters and Cepheids. Independent estimates for the ages of NGC 7790 and the three Cepheids

Figure 23



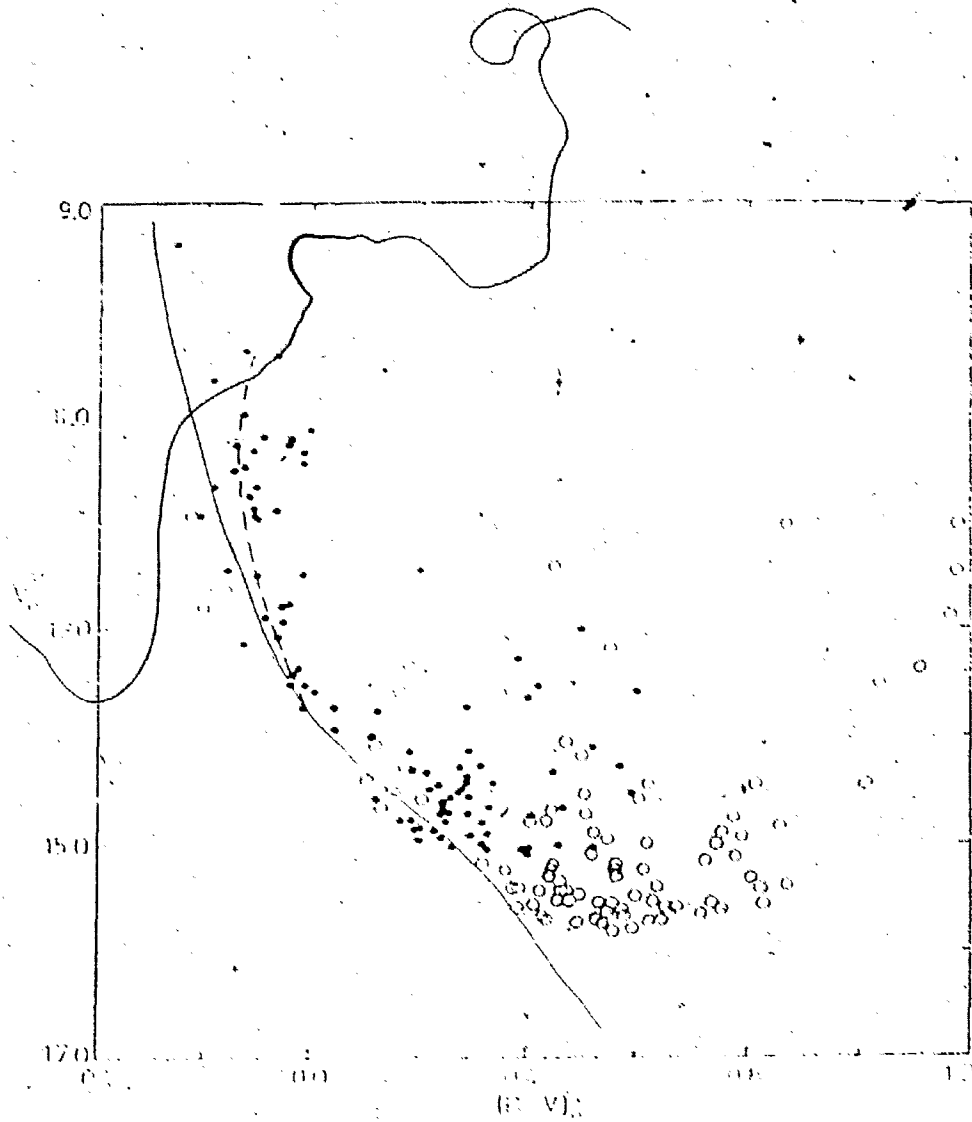
$M_v$  versus  $\log P$  for Cepheids (open circles: Cepheids in NGC 7790). The line drawn through the data is the PL relation from CC. A reddening of 0.528 was used to calculate the absolute magnitudes of the Cepheids in NGC 7790. The absolute magnitudes of the Cepheids in NGC 7790 appear to have a similar scatter about the PL relation as other cluster Cepheids.

associated with it should be approximately the same if they are physically associated (as appears likely). The age of clusters can be predicted from their turn-off points. The turn-off point for NGC 7790 was estimated to lie at  $(B - V)_0 = -0.15$  from the dereddened colour magnitude diagram. Figure 24 shows the colour magnitude diagram with evolution of the stars away from the main sequence drawn in schematically. The turn-off point was taken to be the minimum value of  $(B - V)_0$  for the cluster. Theoretical isochrones from Maeder and Mermilliod (1981) imply that this turnoff for NGC 7790 corresponds to an age of  $\sim 1.0 \pm 0.1 \times 10^8$  yr. An unpublished relation by Turner predicts a similar result. This relation,

$$\log(\text{age}) = 9.19 + 8.20 \times (B - V)_0,$$

yields an age of  $9.1 \times 10^7$  yr. Barbaro *et al.* (1969) estimated the age of NGC 7790 to

Figure 24



Intrinsic colour magnitude diagram of NGC 7790. The dashed line represents the evolution of the stars away from the main sequence. The turn-off point occurs at  $(B - V)_0 = -0.15$ .

be  $\sim 7 \times 10^7$  yr, but this is based upon older evolutionary models. Kippenhahn and Smith (1969) have investigated the correlation between the age of Cepheids and their periods using similar older evolutionary models. Based upon their relation including mass loss, the mean age of the three Cepheids is  $7.1 \pm 0.3 \times 10^7$  yr, which agrees with Barbaro *et al.*'s age estimate for NGC 7790. The small difference between  $7 \times 10^7$  yrs and  $9 \times 10^7$  yrs for the age of NGC 7790 can be explained by differences between current evolutionary models and older results. Thus, the age of NGC 7790 is consistent with the ages of its Cepheids. They are therefore almost certain to be physical members of NGC 7790.

#### Conclusions

Cepheids are important distance indicators in both galactic and extragalactic work. Cepheids in galactic clusters play a vital role in calibrating the PL and PLC relations that are used to establish the distances to external galaxies. This study has been successful in determining an accurate distance and reddening for NGC 7790, an open cluster that contains three Cepheids. However, this success does not directly translate into three accurate calibrating points for the PL and PLC relations, since problems exist with the accurate determination of the reddenings for the individual Cepheids in the cluster.

The difficulty in determining the reddening of the Cepheids in NGC 7790 has its origins in two features of the interstellar extinction in the cluster. The

first problem is the patchy distribution of the extinction in the field of NGC 7790. This problem is compounded by the fact that few individual reddening determinations were possible for stars near the Cepheids. Thus, a value based on an assumed space reddening near the Cepheids would be very uncertain. The second problem, a potentially more serious one, is the trend in reddening with intrinsic colour exhibited by stars in NGC 7790. The physical nature of this trend must be established before its effects on the reddening of the Cepheids can be properly assessed.

Other limitations exist to the accurate determination of the reddening for the Cepheids of NGC 7790. Uncertainties in the reddening parameters are a common feature of many studies of galactic clusters. The reddening slope,  $E_{U-B}/E_{B-V}$ , used in this study was not determined specifically for the field of NGC 7790, but rather from a large region surrounding NGC 7790 centred on the nearby cluster Berkeley 58. Although it is likely that this value is also valid for NGC 7790, the reddening slope should be determined for the field of interest. The extinction slope,  $R_v$ , was determined for the field of NGC 7790 to be  $3.1 \pm 0.1$ . Since the reddening for NGC 7790 is moderate, small uncertainties in  $R_v$  will result in small errors in distance, but will have little effect on the estimated luminosities for the Cepheids. Ultimately, uncertainties in the reddening parameters affect the accuracy of the distance determination for the cluster.

The problems discussed above serve to point out several aspects of this study that could benefit from new observational data. Spectra of cluster members of both early and late-type stars would be very useful. Spectra of cluster members are needed to confirm the values for the reddening and extinction slopes. Radial velocity measurements from spectra would also be helpful for membership discrimination. Spectra would be invaluable for investigating the nature of the trend observed in reddening. The magnitude limit of the photoelectric standards, particularly U passband standards, prevented individual reddening determinations for many stars in the field of NGC 7790. Also, the faint end of the calibration relations for the U passband were defined by relatively few stars, which is a cause for some concern. Any future photographic study of NGC 7790 would benefit from fainter photoelectric standards in the cluster field. Spectroscopic and photoelectric observations have been routinely carried out for decades, yet the distance and reddening of NGC 7790 could be more firmly established with a concentration of these routine observations upon the stars in NGC 7790.

From a procedural point of view this study has illustrated some important points in work of this nature. The dangers of using secondary images to extend a calibration relation is one example. A considerable amount of effort was expended investigating the secondary images to determine their limits in extending the calibration relations. The importance of individually dereddening stars was reaffirmed by this study. The trend seen in the reddening would not have been

detected if a mean reddening shift was used for the cluster.

The present determination of the distance modulus and reddening has inherent uncertainties. They include the choice of the reddening parameters and the ZAMS relation. The determination of the ZAMS relation is dependent on the distance to the Hyades cluster. Also, any differences in metallicity between NGC 7790 and the Pleiades will have a systematic affect on the distance derived for the cluster. This study has been able to determine the distance to NGC 7790 only to within the limits of these more fundamental parameters.

## References

- Alter, G., Ruprecht, J., Vanýsek 1970, *Catalogue of Star Clusters and Associations, Second Edition*, edited by G. Alter, B. Balázás, J. Ruprecht (Akadémiai Kiadó, Budapest), 617
- Baade, W. 1952, *Trans. I.A.U.*, **8**, 397
- Baloña, L.A., Shobbrock, R.R. 1984, *Mon. Not. R. astr. Soc.*, **211**, 375
- Barbaro, G., Dallaporta, N., Fabris, G. 1969, *Astrophys. Sp. Sc.*, **3**, 123
- Bevington, P.R. 1969, *Data Reduction and Error Analysis For the Physical Sciences*, (McGraw Hill Book Company), 104
- Blanco, V.M. 1982, *Pub. A.S.P.*, **94**, 201
- Bottlinger, K.F., Schneller, H. 1930, *Zs. f. Ap.*, **1**, 339
- Caldwell, J.A.R., Coulson, I.M. 1986, *Mon. Not. R. Astron. Soc.*, **218**, 223
- Caldwell, J.A.R., Coulson, I.M. 1987, *Astron. J.*, **93**, 1090
- Christian, C.A., Racine, R. 1983, *Pub. A.S.P.*, **95**, 457
- Christian, C.A., Adams, M., Barnes, J.V., Butcher, H., Hayes, D.S., Mould, J.R., Siegel, M. 1985, *Pub. A.S.P.*, **97**, 363
- Danks, T.A. 1987, M.Sc. Thesis, Saint Mary's University.
- Dean, J.F., Warren, P.R., Cousins, A.W.J. 1978, *Mon. Not. R. Astron. Soc.*, **183**, 569
- Doig, P. 1925, *J.B.A.A.*, **35**, 202
- Doig, P. 1926, *J.B.A.A.*, **36**, 113
- Feast, M.W., Walker, A.R. 1987, *Ann. Rev. Astron. Astrophys. 1987*, **25**, 345

- Fernie, J.D. 1963, *Astron. J.*, **68**, 780
- Fernie, J.D. 1967, *Astron. J.*, **72**, 422
- Fernie, J.D. 1969, *Pub. A.S.P.*, **81**, 707
- Fernie, J.D. 1982, *Astrophys. J.*, **257**, 193
- Frolov, V.N. 1977, *Izv. Glav. Astro. Obs. Pulkovo*, **195**, 80
- Frolov, V.N. 1979, *Izv. Glav. Astro. Obs. Pulkovo*, **196**, 69
- Hertzprung, E. 1913, *Zeit. für Wiss. Phot.*, **5**, 94, 107
- Irwin, J.B. 1955, *Mon. Notes R. Astron. Soc. South Africa*, **14**, 38
- Janes, K.A., and Adler, D. 1982, *Astrophys. J. Supp.*, **49**, 425
- Johnson, H.L. 1966, *Ann. Rev. Astron. Astrophys.* 1966, **4**, 193
- Kholopov, P.N. 1956, *Peremennye Zvezdy*, **11**, 325
- Kippenhahn, R., Smith, L. 1969, *Astron. Astrophys.*, **1**, 142
- Kukarkin, B.W. 1937, *Astr. Zhurnal U.S.S.R.*, **14**, 125
- Kukarkin, B.W. 1949, *Peremennye Zvezdy*, **7**, 69
- Kraft, R.P. 1958, *Astrophys. J.*, **128**, 161
- Kraft, R.P. 1961, *Astrophys. J.*, **134**, 616
- Lundemark, K. 1931, *Medd. Lund. Obs. Ser. 2*, **6**(No. 60)
- Lynds, B.T. 1968, *Nebulae and Interstellar Matter* ed. B.M. Middlehurst, L.H. Aller, University of Chicago Press 1968, Chapt. 3
- Mateo, M., Madore, B.F. 1988, preprint

- Mianes P. 1963, *Ann. Astrophys.* **26**, 1
- Mineur, H. 1944, *Ann. Astrophys.*, **7**, 160
- Maeder, A., Mermilloid J.C. 1981, *Astron. Astrophys.*, **93**, 136
- Moffett, T.J., Barnes III, T.G. 1984, *Ap. J. Suppl.*, **55**, 389
- Opal, C.B., Krist, J.E., Barnes, T.G., Moffett, T.J. 1987, *Bull. A.A.S.*, **19**, 1052
- Parsons, S.B. 1971, *Mon. Not. R. Astron. Soc.*, **152**, 121
- Parsons, S.B., Bell, R.A. 1975, *Dudley Observatory Reports*, **9**, 73
- Parsons, S.B., Bouw, G.D. 1971, *Mon. Not. R. Astron. Soc.*, **152**, 133
- Pedreras, M., Madore, B.F., Freedman, W.L. 1984, *Ap.J.*, **286**, 563
- Pel, J.W. 1978, *Astron. Astrophys.*, **62**, 75
- Pickering, E.C. 1912, *Harvard Circ.*, No. 173
- Reed, B.C., Turner, D.G., Scrimger, J.N. 1986, *J. Roy. Astron. Soc. Can.*, **80**, 203
- Reed, B.C. 1988, *Am. J. Phys.*, **57**, in press
- Ruprecht, J. 1966, *BAC*, **17**, 34
- Ruprecht, J., Balázs, B., White, R.E. 1981; *Catalogue of Star Clusters and Associations Suppl. 1*, ed. B. Balázs (Akadémiai Kiadó, Bucharest, Hungary), p.62
- Sandage, A. 1958, *Astrophys. J.*, **128**, 150
- Schaeffer, B.E. 1981, *Pub. A.S.P.*, **93**, 253
- Schmidt, E.G. 1981, *Astrophys. J.*, **86**, 242
- Schmidt, E.G. 1984, *Astrophys. J.*, **285**, 501

- Shapley, H. 1918, *Astrophys. J.*, **48**, 89
- Trumpler, R.J. 1930, *Lick Obs. Bull.*, **14**, 154 (No. 420)
- Turner, D.G. 1976, *Astron. J.*, **81**, 97
- Turner, D.G. 1979, *Pub. A.S.P.*, **91**, 642
- Turner, D.G. 1981, *Astron. J.*, **86**, 222
- Turner, D.G. 1985, *IAU Coll. 82, Cepheids: Theory and Observations*, ed. B. F. Madore (Cambridge University Press), p. 206
- Turner, D.G. 1986, *Astron. J.*, **92**, 111
- Vandenberg, S., Bridges 1984, *Astrophys. J.*, **278**, 679
- Walker, A.R. 1985, *Mon. Not. R. Astron. Soc.*, **209**, 83
- Williams J.A. 1966, *Astron. J.*, **71**, 615

## Curriculum Vitae

**Name:** John M. Takala

**Birthplace:** Toronto, Ontario

**Birthday:** Feb. 20 1963

**Education:** University of Toronto, Toronto Ontario  
B.Sc. 1986

Saint Mary's University, Halifax Nova Scotia  
M.Sc. 1988  
"A UBV Study of the Field of NGC 7790"

McMaster University, Hamilton Ontario  
1988 -

**Awards:** H.S. Robertson Scholarship  
University of Toronto 1984-85

Saint Mary's Graduate Fellowship  
Burke Gaffney Memorial Scholarship  
Saint Mary's University 1987-88